UNIVERSITY of CALIFORNIA

SANTA CRUZ

SYMMETRY OF PLANTS

A dissertation submitted in partial satisfaction of the
requirements for the degree of

DOCTOR OF PHILOSOPHY

in

MATHEMATICS

by

Scott G. Hotton

December 1999

The dissertation of Scott G. Hotton is approved:

_____

Professor Richard Montgomery, Chair

_____

Professor Christophe Golé

_____

Professor Ralph Abraham

_____

Dean of Graduate Studies

Abstract

Symmetry of Plants

by

Scott G. Hotton

It is fairly well known that Fibonacci numbers appear frequently in plants. This has resulted in many applications of Mathematics to plant patterns such as spiral phyllotaxis. More recently improvements in experimental techniques has increased our understanding of plant development. Also high speed computers have given us a better understanding of the complexities involved in the developmental process. Furthermore the field of dynamical systems has developed powerful techniques for understanding complex processes. In this thesis we define and investigate two families of dynamical systems that model meristematic plant development. We use Hyperbolic geometry to strengthen the "Fundamental Theorem of Phyllotaxis". We determine the fixed points of the first family of dynamical systems and prove their stability. Finally we compare the second family of dynamical systems to the first and show that we expect the same qualitative behavior from both models

Contents

List of Figures

Dedicated to my parents

Acknowledgements

I wish to thank Christophe Golé, Pau Atela, and Junko Hoshi for their support and sharing their research with me.

Chapter 1

Modeling Plant Development

1.1 Meristematic Plant Development

Phyllotaxis is the study of plant patterns. Despite their diversity similar patterns are observed in many different types of plants. A common eye catching pattern consists of two sets of spirals forming a lattice. This can be seen in the stamens and carpels of flowers, the florets of compound flowers (e.g. the Daisy shown in figure 1.1), the scales of pine cones, cycads, and seed ferns. This pattern is known as Spiral Phyllotaxis

The tip of a plant shoot is known as the apex. The apex contains meristematic tissue, i.e. a region containing undifferentiated stem cells. This region is called the apical meristem. The apical meristem is responsible for the production of plant organs such as leaves, thorns, tendrils, sepals, petals, etc. Near the boundary of the meristem is a region called the apical ring. Its in this region that new plant organs are formed. It usually takes a microscope to observe the process. Plant organs begin when cells in a spot along the apical ring undergo extensive cell divisions resulting in a bump, called a primordium, on the side of the apical ring (see figure 1.2). The phyllotactic pattern exhibited by the primordia is preserved as they develop into the various plant organs. Therefore with a good model of meristematic development we can account for the phyllotactic patterns found
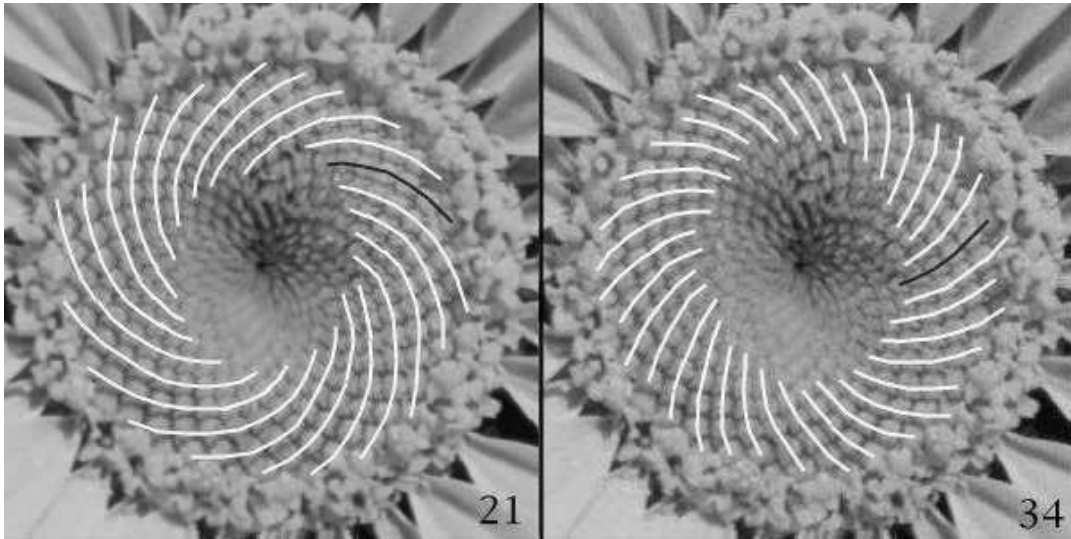
Figure 1.1: Capitulum of a Daisy displaying Fibonacci numbers

in plants.

This thesis defines and analyzes two closely related families of Dynamical Systems that model meristematic development. The Dynamical Systems approach goes beyond merely providing a mathematical framework for describing the patterns observed in plants and can be used to make testable predictions about the developmental process.

Around the turn of the 18th century the well known Astronomer Johanne Kepler observed that the Fibonacci numbers are common in plants. And around 1790 Bonnet [7] made this observation more precise by pointing out that in spiral phyllotaxis the number of spirals going clockwise and counter-clockwise were frequently two successive Fibonacci numbers. For example the Daisy shown above has 21 spirals going in one direction and 34 spirals going in the other direction. The pair of (21,34) is called the phyllotactic numbers of the flower.

One consequence of the Dynamical Systems approach is that the Fibonacci numbers appear naturally. There is no need to assume the plants are attempting to achieve any number theoretic goal. Many earlier explanations [8, 9, 37] for the prevalence of the Fibonacci numbers assumed that certain number theoretic conditions promoted the survival of plants. The prevalence of the Fibonacci
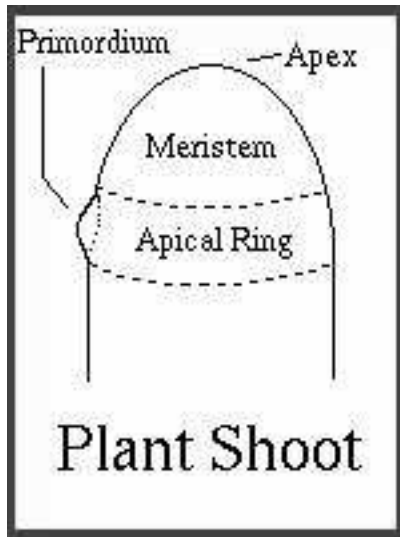
Figure 1.2: Schematic diagram of Meristematic Development

numbers was then seen as a consequence of Darwinian evolution in which the fittest survive. On the other hand the Dynamical Systems approach suggests that the prevalence of the Fibonacci numbers is due to the fact that plants follow the same pathways during their early stages of development. The pattern established early in development is then preserved in the adult plant. This does not contradict the theory of evolution of course. Rather it suggests that natural selection is acting to promote certain types of developmental processes. This view relieves botanists from having to determine the function that the Fibonacci numbers serve in a mature plant.

The Dynamical Systems approach also shows the existence of behavior (see section 3.5) that has received little recognition in the field of Phyllotaxis but which has in fact been observed. Part of the difficulty has been a lack of any mathematical theory for incorporating this observation into the field of Phyllotaxis. Consequently the Dynamical Systems approach gives an unprecedented unity to the field of Phyllotaxis.

At the cellular level there are two important processes in plant growth: cell division and cell expansion. Together these two processes change the shape and size of a plant and its various organs. There is no simple causal relationship between these two processes. Plant cells manufacture

many compounds but they expand mainly by taking in water. Plant cell division generally consists of the duplication of the nucleus and the building of a cell wall to separate the two new nuclei. The two new cells are usually half the size of the parent cell and together they occupy about the same region of space as the parent cell had occupied.

A plant shoot is approximately a cylinder so it is convenient to use a cylindrical coordinate system to indicate position on a shoot. Cell division is classified into three types according to the orientation of the new cell wall with respect to the three mutually orthogonal directions of the cylindrical coordinate system. In transverse cell division the new cell wall is roughly orthogonal to the axis of the shoot, in periclinal cell division the new cell wall is parallel to the surface of the plant, and in anticlinal cell division the new wall is contained in a plane passing through the axis of the shoot.
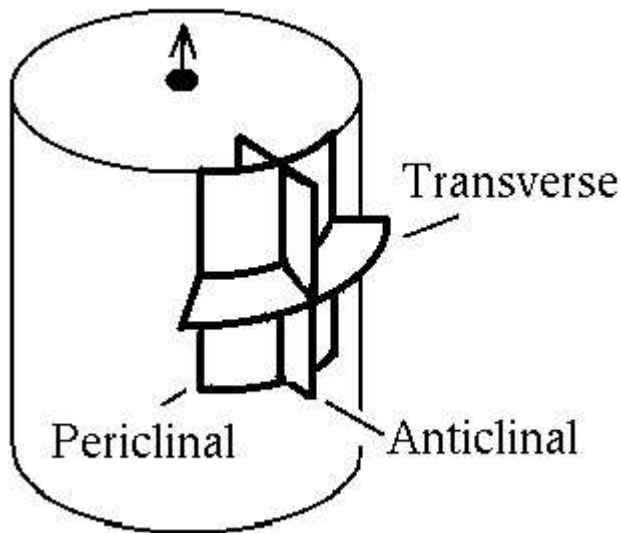
Figure 1.3: The three types of cell division

There are two basic types of development in plants: Embryonic and Meristematic. Embryonic development occurs after pollination and results is a seed or spore. After a period of dormancy a seed begins to absorb water, its cells undergo expansion, and a new plant bursts out. This is

commonly known as germination. After germination, if all goes well, the seedling has a root growing down into the ground and a shoot growing up from the ground. The line formed by the root and shoot form the main axis of the plant.

In this thesis we are mainly interested in Meristematic development. In some species of plants the meristems are present before germination while in other species the meristems form after germination. Thus depending on the plant there may or may not be a clear boundary between Embryonic and Meristematic development. Regardless we can focus on the development which occurs after germination which is strictly meristematic.

When a stem cell divides it can produce one new stem cell and one new cell which begins to differentiate. From this process the different types of cells needed by the plant are left behind in the "wake" of the meristem as the tips grow. Plant organs begin when cells in a spot along the apical ring undergo extensive periclinal division resulting in a primordium. Primordia tend to form periodically over time. Within a primordium the cells expand, divide, and differentiate. As the primordium grows its develops into an entire plant organ. The early stages of primordia formation are basically the same regardless of what organ that primordium will develop into. The type of cells that develop is not completely determined until after the formation of the primordium. A variety of factors both environmental and genetic contribute in determining which type of plant organ develops.

1.2 Applying Topology to Biology

Despite its long history number theoretic observations in plants have received little attention from botanists. Part of the problem has been the variability of plant growth. Precise numerical modeling of the type seen in celestial mechanics has seemed unrealistic in Botany. Biology has been labeled as a soft science. Modern Biology has managed to overcome this label to a large extent but there are still branches within Biology that have been unable to shake off this stigma. Unfortunately many biologists have become alienated from Mathematics as a result.
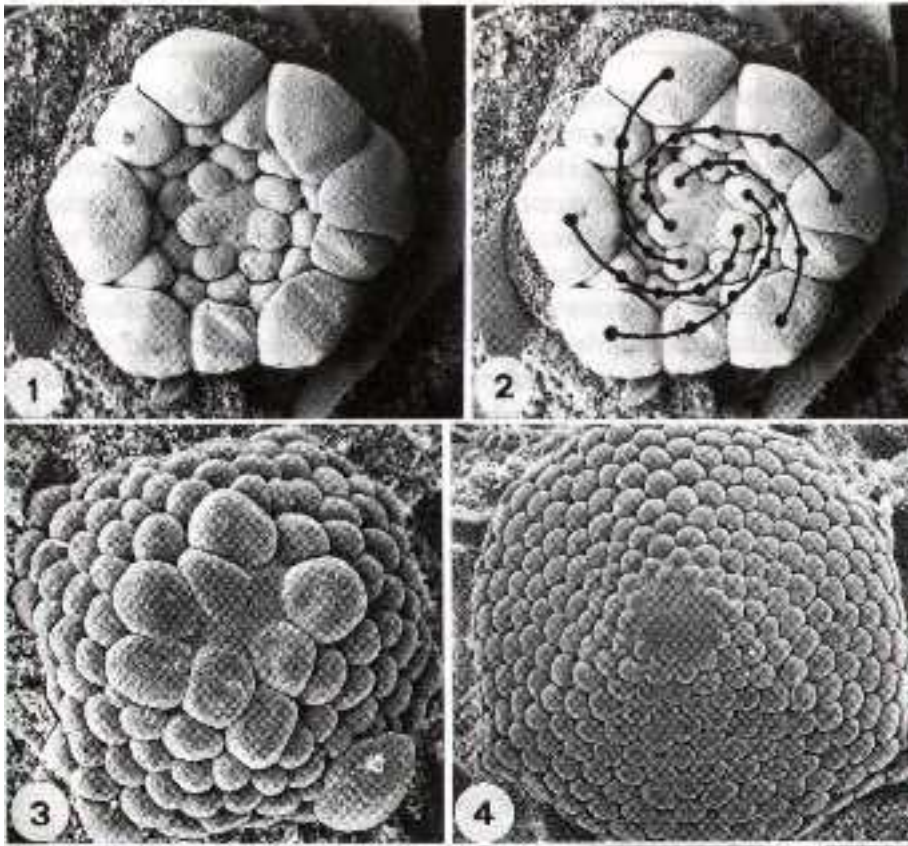
Figure 1.4: Photos of primordium (from Endress [12])

However there are ways to make mathematically rigorous assertions without relying on the repeatability of numerical measurements. Amongst other things the field of Topology in Mathematics is full of rigorously established theorems on objects sitting in space that make no reference whatsoever as to the size of the objects or the distance between the points in the object. A famous example is the Königsberg Bridges problem solved by Euler in the 18th century. The town of Königsberg is broken into several parts by rivers. The different parts of the town were connected by seven bridges. Euler showed that it was impossible to take a walk over all seven bridges without crossing some bridge twice. This fact had little to do with the precise position of the bridges. Each of the bridges could have been built in different places, but so long as they still connected the same parts of town to each other no path could cross every bridge without crossing some bridge twice.
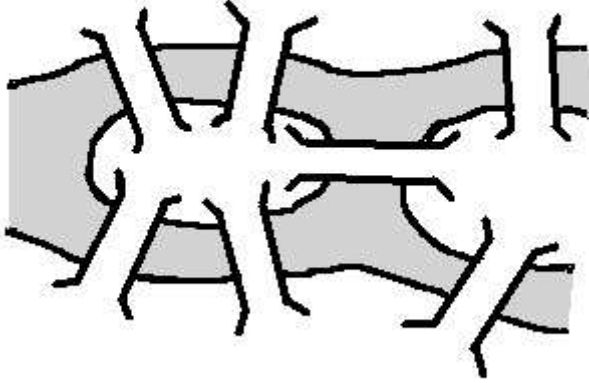
Figure 1.5: Königsberg Bridges

This is an example of a Topological theorem. The field of Topology has grown immensely since the days of Euler. Topology has already been successfully applied in many diverse fields such as heart disease and circuit design. There is even an enzyme, Topoisomerase, that is named after its function of changing the topology of DNA strands. In particular Topology is an important tool in Dynamical Systems Theory that we shall make use of.

One could say that Biology has had a reputation as a soft science in part because the systems studied in Biology are soft. Being soft they are easily deformed by external perturbations. They are essentially open systems exposed to their environment. Even when they sit in a lab they are sensitive to varying conditions and like snowflakes one almost never sees two individuals develop in precisely the same way.

Yet despite the wide variety of shapes and sizes of organisms some order is apparent. Tasks such as the classification of different types of organisms can be safely performed without insisting that Taxonomists find traits that have a precise characteristic size of shape for each taxon. In particular the individuals within a species often have similar topological features. In using the number of legs as

a distinguishing characteristic between insects and arachnids we are implicitly assuming that there is enough similarity between their legs that we can ignore the difference between individual legs and treat them all as different versions of the same basic organ. This assessment is done heuristically. It is a skill that most people can easily perform. Indeed that is one reason why the number of legs is a useful taxonomic characteristic.

The study of symmetry is usually seen as the study of objects that remain invariant under a group of rigid motions. Under ideal conditions such symmetry can be found in plants. For example flower petals often display 5-fold symmetry. In a symmetrical flower each petal is virtually the same size so we can rotate the flower one fifth of a turn and it will appear as if has not been rotated at all such as the Jasmine in figure 1.6

Figure 1.6: A Jasmine blossom on the left and a Geranium blossom on the right

Sometimes however the petals of a flower are not all the same size like the Geranium blossom in figure 1.6. Those petals pointing away from the axis of the plant are smaller than those pointing towards the axis. None-the-less each of the petals is morphologically the same. The petals are roughly scaled copies of one another. A rigid motion of the flower will not map one petal onto another. But if we scale each petal individually as we rotate then we can map the petals onto each other. This is a bit more abstract because while we can physically rotate a flower we cannot shrink

or stretch the petals. So we are forced to only imagine performing this motion. The symmetry in the flower is still easy enough to see. We can quickly recognize that there are five nearly identical petals. We wouldn't want to assert this flower lacks any symmetry simply because the petals are no longer the same size.

The type of motion that leaves the Geranium flower invariant is called a homeomorphism. Homeomorphisms have been extensively studied in Topology and much is known about them. So we can expand the usual notion of symmetry to include the study of objects that remain invariant under a group of homeomorphisms. With this notion of symmetry we can see that plants are full of symmetry.

This applies in particular to spiral phyllotaxis. Just as a space lattice is a useful idealization of crystalline structure so a spiral lattice is a useful idealization of spiral phyllotaxis. While crystals are rigid structures and plants are soft this simply means that we need to use this more general notion of symmetry with spiral phyllotaxis. It doesn't necessarily mean there is a sacrifice in mathematical rigor.

1.3   Types of Phyllotaxis

To completely study the symmetry of plants we should consider an entire individual plant including the half that is typically underground. But of course this is much more difficult than merely studying the half that is exposed to observation. The vast majority of data on plant symmetry involves those parts of the plant that grows above ground. It is not difficult to see that there is a vast difference between the half that is above ground and the half that is below. Although growth in the two halves are coupled and their relative sizes must remain within bounds.

It is fairly well known that the arrangement of plant organs, i.e. phyllotaxis, assumes only a few basic forms. Unfortunately the effort at classifying phyllotactic forms has resulted in a proliferation of terminology e.g. bipinnate, orthodistichy, spirodistichy, spirodecussation, etc. Despite the large vocabulary used to describe phyllotaxis there is an underlying topological commonality

among phyllotactic forms. We shall find a small subset of the terminology to be sufficient.

One of the simplest types of phyllotaxis is called "alternate" or "distichous". In this type of phyllotaxis the primordia develop one at a time on opposite sides of the apex. The resulting structure is approximately planar with the plant organs alternating in direction along the stem. A closely related type of phyllotaxis is called "spiral". The primordia still develop one at a time in the apical ring. Each primordium forms at a fixed angle from the previous primordium. This is known as the divergence angle. As the plant grows the plant organs tend to form a spiral helix about the stem. One could say that alternate phyllotaxis is a special case of spiral phyllotaxis where the divergence angle is 180°.
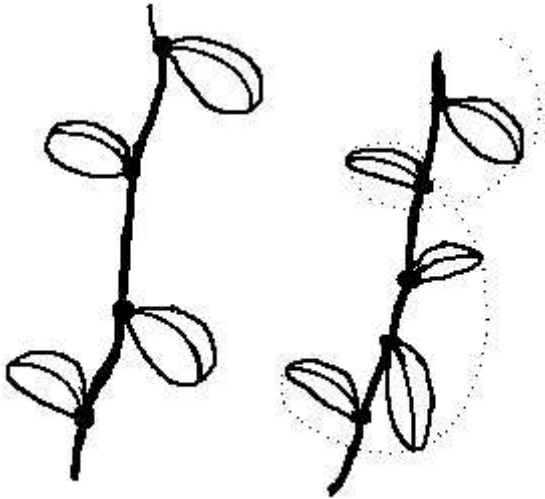
Figure 1.7: Alternate and Spiral phyllotaxis

The places where the plant organs are attached to the plant are called the "nodes" of the plant. When primordia formation is periodic the nodes are equally spaced from each other.

When more than one primordia forms at a time the plant is said to form a "whorl". Whorls composed of two primordia are called dimerous, whorls with three primordia are called "trimerous" and so on. The primordia in a whorl are often assumed to be equally space along the apical ring.

When successive layers of dimerous whorls form at 90° with respect to each other we get what is known as "opposite" or "decussate" phyllotaxis. We can also have "tricussate" phyllotaxis in which trimerous whorls form at 60° with respect to each other. In fact there are types of phyllotaxis which form four, five, etc primordia at a time with the primordia in each successive layer developing exactly halfway between the primordia in the previous layer.

Occasionally successive layers of whorls do not form exactly halfway between the previous layers. This is called "multijugate" phyllotaxis. Multijugate phyllotaxis with dimerous whorls is called "bijugate", and with trimerous whorls it is called "trijugate" and so on. One could say that multicussate phyllotaxis is a special case of multijugate phyllotaxis.
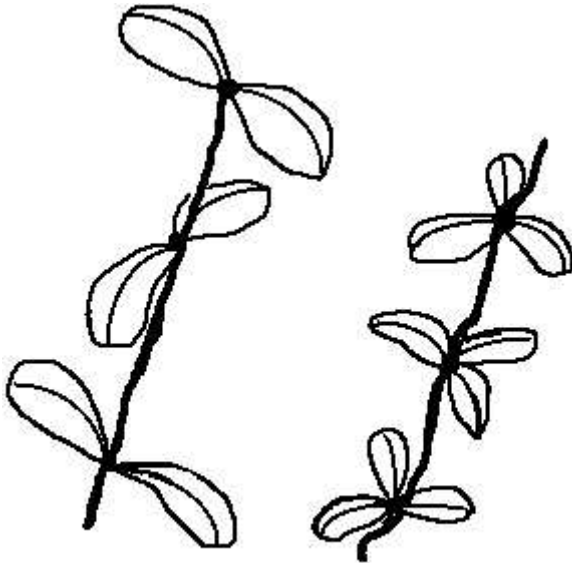
Figure 1.8: Decussate, Tricussate Phyllotaxis

Slowing the developmental process down by lowering the temperature caused primordia that normally would have formed simultaneously in a whorl to form one at a time instead. This suggests that whorled phyllotaxis and spiral phyllotaxis are closely related. [42, 30]

All of these forms are present in primitive plants and not infrequently many of them are present in a single species. Sometimes one type of phyllotaxis is exhibited in the juvenile stage of a

plant while another type is exhibited in the adult stage, e.g. eucalyptus. Environmental factors can also play a role. Phyllotactic patterns are only loosely related to taxonomy.

1.4   Reductionism and Holism

The invention of the microscope has opened a wonderful view of the world to Biology. The information that it provides us has explained so many facts that it has become a fundamental research tool in Biology and in particular Phyllotaxis. The microscopes success stimulated new directions to research and helped fuel the rise of reductionism in Biology. The cell emerged as a fundamental biological unit. For many species the individuals are just single cells. For other organisms like plants and animals the individuals are multi-cellular. Multi-cellular organisms have been studied by determining what types of cells they were composed of and how the cells interacted with each other. Eventually even the cells themselves were studied by looking at the molecules that make up the cells. This lead to the discovery of the genetic material DNA.

The process of development in a multi-cellular organism has been seen as a problem of gene expression. Different genes are expressed in the various cells that become the different parts of an organism. All of the cells of an organism are the descendents of a single cell and all of the cells share the same DNA. The differentiation of cells corresponds to different sets of genes being turned off or on in the various cell types as the organism develops.

Genetic studies, particularly on *Arabidopsis thaliana*, have demonstrated the existence of homeotic genes in plants. Homeotic genes influence which of the other genes are turned off or on in a cell. A mutation in a homeotic gene can result in a completely different plant organ developing from a primordium than would normally occur. In particular there is a set of homeotic mutations in *Arabidopsis thaliana* that turn all the floral organs into leaves producing, of course, a sterile plant.

In 1790 Goethe proposed that all floral organs are modifications of a basic leaf pattern. Angiosperms in particular seem to have a knack for modifying their leaves into floral organs. The Christmas poinsettia is a good example. It attracts pollinators to its tiny flowers by making the

large subtending leaves bright red or white. These leaves are very similar morphologically to the rest of the leaves on the plant except for the color. They are not quite as modified from their original leaf form as other subtending organs like bracts and sepals. Bracts and sepals in turn are less modified than petals.

Figure 1.9: Bougainvillea flower growing from leaf

Another good example is Bougainvillea shown in figure 1.9. Here we have a triplet of red leaves. Other Bougainvilleas can have purple or yellow leaves. The colored leaves resemble the green leaves but emerging from the center of each red leaf is a small flower with five white petals. The triplet of leaves has the appearance of a single flower with three red petals. It even functions like a flower attracting pollinators with its symmetrical appearance and bright color. Furthermore the red leaves help protect the sex organs while at the same time provide a place for pollinators to land on. It appears that as angiosperms evolve back and forth from animal to wind pollination they can add on successive layers of subtending organs resulting in a great diversity of flower forms [50].

The question arises as to how genes get turned on or off in plant development. Certain details of the molecular mechanism have been revealed but what remains to be understood is how

the cells can know which genes to turn on or off so that it can fit in with the rest of the organism. This is seen as a problem of understanding how the cells communicate. We tend to think of the cell walls as fundamental boundaries so that the collective behavior of the cells depends on information being exchanged across these boundaries. In Botany this question has turned up a plethora of plant hormones which have a variety of effects on plants. It would seem as though these could act as signals but no mechanism has emerged to explain plant development and their role in plants remains controversial.

The problem may be that it is the wrong question to ask. We know that a system of molecules can engage in collective behavior when the system can exchange energy with its environment and reach a state far from thermodynamic equilibrium. This is known as a dissipative system. For example a layer of fluid heated from below will tend to form convection cells. The molecules in these convection cells don't so much talk with each other as they respond to the forces they experience. They don't negotiate with each other and reach an agreement to form a pattern of convection cells. The impact of the heat energy creates pressure on the system as a whole which acts as a whole in response. Individual molecules may buck the induced flow but most molecules will participate in it to prevent pressure from building up. In this way collective behavior emerges without individual molecules playing the role of transmitters and receivers of signals that tell them what to do.

Similarly some aspects of the collective behavior of cells in a multi-cellular organism might be best understood without emphasizing the role of communication between cells. Early in the Earth's history there were no multi-cellular organisms, only single-celled organisms. In that time Natural Selection acted on individual cells and encouraged the evolution of cells that promoted their own survival. But with multi-cellular organisms Natural Selection acts on collections of cells. There is no longer the selective pressure for individual cells in an organism to promote their own survival. In a multi-cellular organism the most highly specialized cells often have very short life spans in comparison to the life span of the organism. Multi-cellular organisms are always shedding dead cells. The continued presence of highly specialized cells in the organism is due to the continued
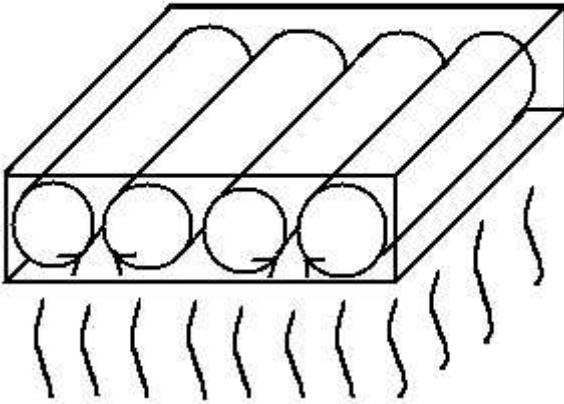
Figure 1.10: Convection rolls in a layer of fluid

presence of less differentiated cells which reproduce and differentiate in order to replace the dead cells. So it is reasonable to think that cells could loose some degree of individuality in a multi-cellular organism and that they could respond in a passive manner to internal stresses and chemical flows within the plant.

As an analogy consider an electric wire. It is clear that an electric current going into the wire must match that leaving the wire otherwise an electric charge would build up. Now suppose that instead of the wire being a thin continuous tube of metal that its is broken up into a bunch of cylindrical segments stacked next to each other like cells in a filament of algae.

The conductivity of the wire may go down but it will still be the case that the current going into the wire must equal that coming out. We don't ask how each segment knows how to pass this much current. Each segment of the wire is merely a piece of metal. The segments don't send or receive specific messages with each other and agree on what the current is going to be. It is obvious that the same principle that applies to the continuous wire also applies to the segmented wire. A charge would build up if the in and out currents don't match. Technically one could say
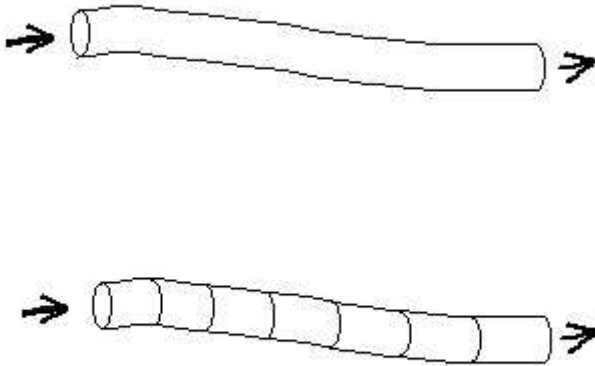
Figure 1.11:

that the act of passing an electric current between the segments is a form of communication but this observation would only serve to obscure the simplicity of the process. Whether the wire is continuous or segmented has little effect on the current flowing through it. Similarly the demarcation of cell walls in a plant might not represent a fundamental division in the plant.

Plants are descendents of algae and there are large plant sized single cell algae (e.g. members of the genus *Acetabularia*) that undergo a similar type of development as plants. The algae even produce sexual organelles at the end of their stalks. This type of development occurs at about the same spatial scale in both plants and algae suggesting a common physical mechanism in the developmental process (see Goodwin [15]). For example in figure 1.12 we see on the left the pistil primordia developing in a strawberry blossom. The primordia are approximately 30 μm in diameter which is several times the size of the individual cells that it is composed of. On the right of figure 1.12 we see a single celled *Acetabularia Mediterranea* with its developing organelles which have a diameter of approximately 20 μm. A region of plant or algae membrane undergoes similar physical changes during development regardless if that region is small relative to the size of a cell or if that region

contains numerous cells. To focus on how the cells communicate during the process of meristematic development may lead to a misunderstanding of the physical aspect of the process which occurs at about the same spatial scale regardless of the size of the cells.
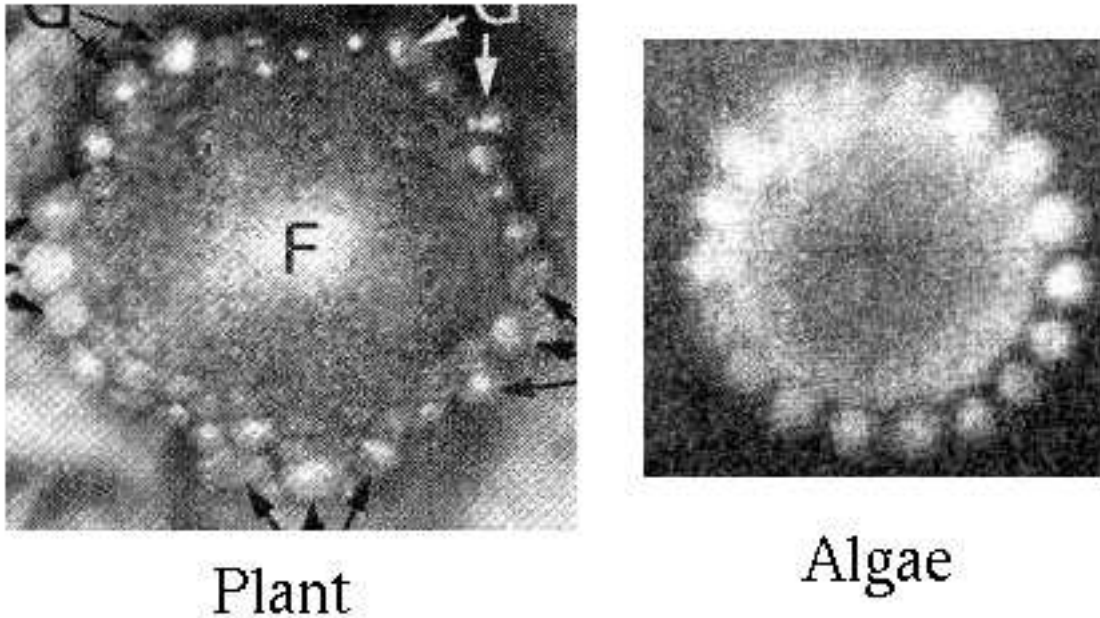
Figure 1.12: Developing tips of a Strawberry blossom (from Sattler [42]) and a single celled algae (from Harrison, *et. al.* [20])

Consequently a more holistic viewpoint may be called for. A model of the developmental process that operates at the scale of the primordia can be developed using Dynamical Systems theory.

1.5   Applying Dynamical Systems Theory to Phyllotaxis

1.5.1   Hofmeister's Hypothesis

In 1868 the botanist Hofmeister [22] began observing meristematic development under the microscope. From his observations he proposed several hypothesis on primordia formation. He assumed that the apical ring is circularly symmetric, that primordia form periodically over time,

and that new primordia form in the apical ring where the largest available space has been left by the previous primordia. These hypothesis constitute one of the earliest attempts to model meristematic development. Unfortunately the consequences of these hypothesis were not explored in detail until recently.

A fairly straight forward consequence is that if the period between primordia formation is small then many primordia will be near the apical ring. Whereas if the period is large then only a few primordia will be near the apical ring. In particular if the period is very large only one primordium will be near the apical ring so that the new primordium will form 180° from the previous primordium just as in alternate phyllotaxis. More generally we expect to see a correlation between the timing of primordia formation and the location of new primordia. This is indeed observed in meristematic development. In particular the work of Schwabe [49] has shown a fairly consistent correlation that is independent of whether the change in timing is genetic or environmental.

In 1992 the physicists Douady and Couder constructed a physical device and performed computer simulations to study the consequences of Hofmeister's hypothesis. They made the hypothesis more precise by representing the primordia by a configuration of point particles. Each particle produced a repulsive potential and the new particle appeared on a circle where the potential achieved its absolute minimum. Their experiments and simulations indicated that regular spiral patterns are in fact stable. (see also the systems proposed by Schwabe [47], Koch, Bernasconi and Rothen [31]).

1.5.2 Preview of Thesis Results

In this thesis we define two families of discrete dynamical systems whose iterates model the evolution of primordia arrangement. The plant surface is represented as a cylinder for the phyllotaxis of plant stems or as a plane for the phyllotaxis of compound flowers like Daisies. Naturally other geometries can be used as well. We focus on the cylindrical case in this thesis. The primordia are represented by particles. One particle is positioned on each member of a sequence of parallel circles on the cylinder. The angular displacement between the particles represents the divergence angles.

The state of the system is given by a sequence of divergence angles. At each iteration of the map the existing particles are shifted down to the next circle to represents the growth of the apex. A new particle is added to first circle represent the formation of a new primordium. This new particle chooses the location on the circle which minimizes a repulsive potential energy function generated by the other particles. This potential function represents an inhibition generated by the older primordia on the formation of the new primordium.

These families of Dynamical Systems offer a bridge to number theory. Spiral lattices appear as stable fixed points which explains the convergence to regular spiral patterns in plants from a wide range of initial conditions. The topology of the bifurcation diagram of the fixed points accounts for the prevalence of successive Fibonacci numbers in these regular spirals as well as the rarer cases in which the parastichy numbers are consecutive Generalized Fibonacci numbers (e.g. the Lucas sequence $1, 3, 4, 7, \ldots$).

We prove that this diagram is a truncated version of van Iterson's diagram [53] and that its topology is fairly simple. The structure of the diagram is succinctly revealed using the geometry of a flat cylinder. In this case partitioning the space of spiral lattices into regions of constant parastichy numbers gives a Hyperbolic tessellation.

To each particle we associate a central potential energy function $U(d)$. This is a positive decreasing function that goes to zero as d increases without bound e.g. $U(d) = d^{-s}$ for $s > 1$. There are two main ways to generate a potential energy field on the plane.

$$X(\zeta) \quad = \max_k U(||\lambda_k - \zeta||)$$
$$W(\zeta) \quad = \sum_k U(||\lambda_k - \zeta||)$$

where λ_k is the position of the particle on the kth circle and ζ is the position of a test particle. These potential energy fields reflect two extreme cases. With the X potential a test particle only "feels" the contribution of the closest particle to it while with the W potential a test particle "feels" the contribution of all the particles. The reality is somewhere in between.

However, generically, as the stiffness of the potential U (e.g. s in $U(d) = d^{-s}$) goes to

infinity the ratio $W(\zeta)/X(\zeta)$ goes to 1. The distinction between X and W becomes less significant as the stiffness is increased. Minimizing X gives rise to the following minimax principle: the incipient primordia chooses the location on the unit circle where the minimum distance to all primordia is maximized. This answers a question of Adler [5] as to the connection between his "minimax" principle (set in the more restrictive context of regular spiral configurations), and the model of Douady and Couder: the minimax principle of incipient primordia location is a stiff limit of Douady and Couder's principle of energy minimization. Hence with the field X the actual form of U is less relevant and the choice of location for the incipient primordia is geometric.

It is worth noting here that, although Douady and Couder and others have used the terminology of dynamical systems, this conceptual step had not been performed before[1]. The methods employed here can be thought of as a synthesis of Douady and Couder's simulations with Levitov's work [34, 35]. He recognized (via a thought experiment involving flux vortices in a superconducting media) that Hyperbolic tessellations could have a rule to play in Phyllotaxis. In this thesis we have made use of Hyperbolic tessellations to make rigorous statements about a dynamical model of plant development.

---

[1]A notable exception to this is the work of Kunz (Kunz' thesis [32] who independently came across a similar dynamical system and performed a (local) analysis of the linear stability of the fixed points.

Chapter 2

The Flat Cylinder and its lattices

2.1 Lattices

In the following chapters we will see that the fixed points of the dynamical system form half spiral lattices while the periodic orbits form regular point sets. We review relevant facts about lattices here and return to regular point sets later. We begin with a fairly general definition of a lattice. It is not the most general definition of a lattice but it includes everything we shall need.

Definition 2.1.1. A *lattice* is a finitely generated subgroup of a Lie group. A lattice in a plane is called a *planar lattice*, a lattice in a cylinder is called a *cylindrical lattice*, and a *spiral lattice* is a cylindrical lattice that is isomorphic to $\mathbb{Z}$.

This definition of lattices does include subgroups that are dense in the Lie group even though we are mainly interested in discrete subgroups. From now on in this thesis the term "cylinder" will refer to the usual two dimensional cylinder which is topologically $\mathbb{S}^1 \times \mathbb{R}$.

The universal covering space of a cylinder is $\mathbb{R}^2$. We can imagine rolling a cylinder across a plane impressing a lattice in the plane like a printing press. Conversely given a planar lattice we can cut out a strip with an appropriate width and glue the two edges together to obtain a cylindrical lattice.

It is useful to study cylindrical lattices by going to the covering space $\mathbb{R}^2$. This is in fact quite common in the field of Phyllotaxis. It is also useful to endow $\mathbb{R}^2$ with the Euclidean metric. This metric can be projected down to the cylinder. The resulting geometric object is called the flat cylinder, which we denote by $\mathcal{C}$. The flat cylinder provides an ideal geometry for studying spiral lattices for two reasons. First because it simplifies the analysis and second because the flat cylinder is isomorphic to any ruled cylinder such as the right circular cylinder which is a good approximation of the shape of plant stems.

2.2 Lattices in $\mathbb{R}^n$

In the 19th century the field of Crystallography motivated the study of lattices. This paralleled the development of Group Theory which became a very useful tool for studying lattices. Indeed this success was a source of inspiration for Klein's Erlangen program. This section follows this approach to geometry. The group of linear maps that preserves the Euclidean metric is $O(n)$. We outline a classification procedure for lattices using their invariance under the action of $O(n)$.

2.2.1 The Space of Lattices, $\mathcal{L}_n$

The standard lattice in $\mathbb{R}^n$ is $\mathbb{Z}^n$ which is generated by the standard basis of $\mathbb{R}^n$. Given $U \in M(n, \mathbb{R})$ we can construct a new lattice $L = U\mathbb{Z}^n$ where we think of the elements of $\mathbb{Z}^n$ as column vectors. The lattice, L, is all of the integer combinations of the columns of U. Any lattice in $\mathbb{R}^n$ with n (not necessarily distinct) generators is the image of $\mathbb{Z}^n$ under some $U \in M(n, \mathbb{R})$. For $L = \mathbb{Z}^n$ we can use the identity matrix. We can identify the space $\mathbb{R}^n \times \ldots \times \mathbb{R}^n$ of n ordered vectors from $\mathbb{R}^n$ with the space of matrices $M(n, \mathbb{R})$. An immediate consequence is

$$U \in GL(n, \mathbb{R}) \Leftrightarrow U\mathbb{Z}^n \quad \text{is discrete with rank } n$$

The space of lattices in $\mathbb{R}^n$ can be obtained from $M(n, \mathbb{R})$ by identifying those ordered generators that generate the same lattice. The automorphisms of $\mathbb{Z}^n$ form the group $GL(n, \mathbb{Z})$.

When $U \in GL(n, \mathbb{R})$ the automorphisms of $L = U\mathbb{Z}$ form the conjugate group $U\,GL(n, \mathbb{Z})U^{-1}$. Every ordered basis for L has the form UG for some $G \in GL(n, \mathbb{Z})$. Since $GL(n, \mathbb{Z})$ is a subgroup of $GL(n, \mathbb{R})$ the set $UGL(n, \mathbb{Z}) = \{UG : G \in GL(n, \mathbb{Z})\}$ is a left coset of $GL(n, \mathbb{Z})$ in $GL(n, \mathbb{R})$. Denote the space of discrete rank n lattices in $\mathbb{R}^n$ by $\mathcal{L}_n$. Consequently we can identify $\mathcal{L}_n$ with the collection of left cosets of $GL(n, \mathbb{Z})$ in $GL(n, \mathbb{R})$.

$$\mathcal{L}_n = GL(n, \mathbb{R})/GL(n, \mathbb{Z})$$

The orbit space $\mathcal{L}_n$ is not a quotient group for $n > 1$, since $GL(n, \mathbb{Z})$ is not normal in $GL(n, \mathbb{R})$.

Even when U is non-invertible UG generates the same lattice as U. Denote the collection of sets with the form $U\,GL(n, \mathbb{Z})$ for any $U \in M(n, \mathbb{R})$ by $M(n, \mathbb{R})/GL(n, \mathbb{Z})$. We can extend the quotient map $GL(n, \mathbb{R}) \to GL(n, \mathbb{R})/GL(n, \mathbb{Z})$ to a map $M(n, \mathbb{R}) \to M(n, \mathbb{R})/GL(n, \mathbb{Z})$ using the equivalence relation $U \sim V \Leftrightarrow V \in U\,GL(n, \mathbb{Z})$. Denote the set of lattices in $\mathbb{R}^n$ by $\tilde{\mathcal{L}}_n$ and identify it with the collection of equivalence classes.

$$\tilde{\mathcal{L}}_n = M(n, \mathbb{R})/GL(n, \mathbb{Z})$$

The case $n = 1$ is trivial, $\mathcal{L}_1 = GL(1, \mathbb{R})/GL(1, \mathbb{Z}) = \mathbb{R}^*/\{\pm 1\} \cong \mathbb{R}^+$. We identify a lattice in $\mathcal{L}_1$ with the element in $\mathbb{R}^+$ that generates it. And $\tilde{\mathcal{L}}_1 = \mathcal{L}_1 \cup \{0\}$ since $M(1, \mathbb{R})\backslash GL(1, \mathbb{R}) = \{0\}$. We identify $\tilde{\mathcal{L}}_1$ with the non-negative reals.

2.2.2 The Space of Homothety classes of lattices, $\mathcal{N}_n$

We want to classify lattices geometrically. There are three equivalence relations that we will consider. They form a fine, coarse, and intermediate stratification of $\mathcal{L}_n$. The first equivalence relation is "homothety", we say two lattices are equivalent if one is a scaled copy of the other up to rotation and reflection.

Definition 2.2.1. $L, L' \in \mathcal{L}_n$ are *homothetic* $\Leftrightarrow$ there are $k \in \mathbb{R}^*$ and $Q \in O(n)$ such that $L' = kQL$. Denote the space of homothety classes of lattices by $\mathcal{N}_n$.

If L, L' are homothetic then an ordered bases which generates L is homothetic to a ordered bases which generates L'. Conversely given two homothetic n-tuples of vectors the lattices they generate must be homothetic. To get the homothety classes of lattices we can either identify the ordered bases which generate the same lattice and then identify those that are homothetic, or we can identify those ordered bases that are homothetic and then identify those homothety classes that generate homothetic lattices.

The group of homotheties is $O(n)\mathbb{R}^+$ where $\mathbb{R}^+$ is short for $\{kI_n \mid k \in \mathbb{R}^+\}$. The ordered basis $U, V \in GL(n, \mathbb{R})$ are homothetic if there is $T \in O(n)\mathbb{R}^+$ such that $V = TU$. The set $\{TU \mid T \in O(n)\mathbb{R}^+\}$ is a right coset of $O(n)\mathbb{R}^+$ in $GL(n, \mathbb{R})$. The space of homothety classes of ordered basis is the collection of right cosets of $O(n)\mathbb{R}^+$ in $GL(n, \mathbb{R})$, denote this collection by $\mathcal{M}_n$. This equivalence relation can be extended to all of $M(n, \mathbb{R})$ like before, denote this collection by $\tilde{\mathcal{M}}_n$.

Let $U, V \in GL(n, \mathbb{R})$, U, V generate homothetic lattices if there are $T \in O(n)\mathbb{R}^+$ and $G \in GL(n, \mathbb{Z})$ such that $V = TUG$. There are two ways to obtain $\mathcal{N}_n$. We can form the left cosets $U\, GL(n, \mathbb{Z})$ and act on them by $O(n)\mathbb{R}^+$ or we can form the right cosets $O(n)\mathbb{R}^+U$ and act on them by $GL(n, \mathbb{Z})$.

Thus to obtain $\tilde{\mathcal{N}}_n$ it is not necessary to determine the space of lattices $\tilde{\mathcal{L}}_n$. We can obtain $\tilde{\mathcal{M}}_n$ instead.

2.2.3   Bravais Classes of Lattices

The second equivalence relation is called "holohedry" and it is based on the symmetry of the lattice. The translational symmetry of any $L \in \mathcal{L}_n$ is L itself which is always isomorphic to $\mathbb{Z}^n$. Thus the translational symmetries of L gives us no new information about L and are not very helpful for classifying the members of $\mathcal{L}_n$. We are only interested in the linear isometries of L. (the other isometries of $\mathbb{R}^n$ play a more interesting role with regular point sets).

Definition 2.2.2. The holohedral group of a lattice in $\mathbb{R}^n$ is the linear isometries that map the lattice to itself: $\mathcal{H}_L = O(n) \cap Aut(L)$. The only rescaling of a lattice in $\mathbb{R}^n$ to itself is the identity so
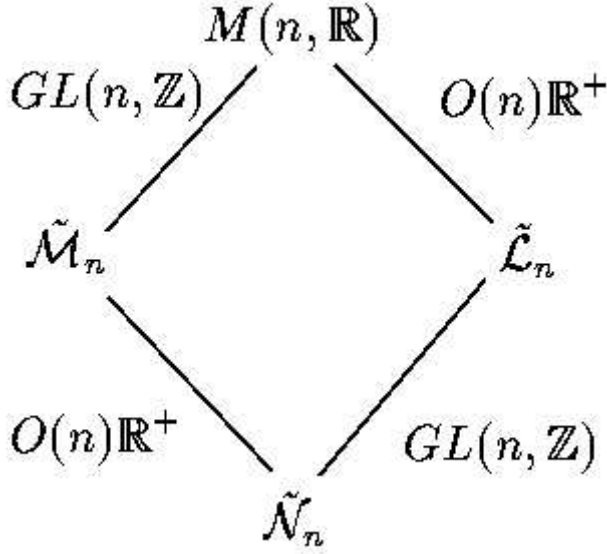
Figure 2.1: Two projections to $\tilde{\mathcal{N}}_n$

we could alternatively define $\mathcal{H}_L = O(n)\mathbb{R}^+ \cap Aut(L)$. The following propositions are easily proved.

Proposition 2.2.1. *For any lattice, $L \in \mathcal{L}_n$, the set, $\{\pm I_n\}$, is a subgroup of $\mathcal{H}_L$*

Proposition 2.2.2. *For any lattice, $L \in \mathcal{L}_n$, the group $\mathcal{H}_L$ is finite.*

Proposition 2.2.3. *If $k \in \mathbb{R}^*$ then $\mathcal{H}_{kL} = \mathcal{H}_L$. If $Q \in O(n)$ then $\mathcal{H}_{QL} = Q\mathcal{H}_L Q^{-1}$.*

Corollary 2.2.4. *If $L, L' \in \mathcal{L}_n$ are homothetic then $\mathcal{H}_L, \mathcal{H}_{L'}$ are conjugate in $O(n)$.*

Definition 2.2.3. *$L, L' \in \mathcal{L}_n$ are of the same *holohedry* type if $\mathcal{H}_L, \mathcal{H}_{L'}$ are conjugate in $O(n)$.*

Corollary 2.2.5. *Holohedry is a coarser equivalence relation on $\mathcal{L}_n$ than homothety.*

We have joined together homothety classes to make holohedral classes. Unfortunately this equivalence relation is now too coarse for our geometric classification. We also need to consider how the holohedral group acts on the lattice. For example the following two lattices have the exact same holohedral group despite their different geometric appearance.

$$\begin{pmatrix} 4 & 0 \\ 0 & 2 \end{pmatrix} \mathbb{Z}^2 \subset \begin{pmatrix} 2 & 2 \\ 1 & -1 \end{pmatrix} \mathbb{Z}^2$$

This holohedral group is generated by the reflections about the x-axis and y-axis. The smaller lattice is known as the rectangular type while the bigger lattice is known as the rhombic type or also as the face-centered rectangular type.
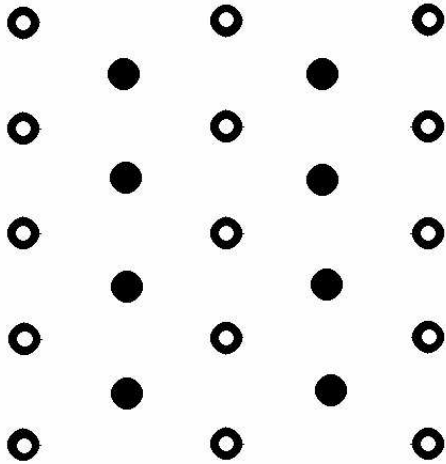
Figure 2.2: The open circles form a rectangular lattice, the open circles joined with the closed circles form a rhombic lattice

The way the holohedral group acts on these two lattices is different. In particular this is exhibited by the effect the reflection about the x-axis has on a particular basis. For the smaller lattice the reflection about the x-axis takes a basis member and replaces it with its negative, while for the larger lattice it permutes the basis members

$$\begin{pmatrix} 1 & 0 \\ 0 & -1 \end{pmatrix} \begin{pmatrix} 4 & 0 \\ 0 & 2 \end{pmatrix} = \begin{pmatrix} 4 & 0 \\ 0 & -2 \end{pmatrix}$$

$$\begin{pmatrix} 1 & 0 \\ 0 & -1 \end{pmatrix} \begin{pmatrix} 2 & 2 \\ 1 & -1 \end{pmatrix} = \begin{pmatrix} 2 & 2 \\ -1 & 1 \end{pmatrix}$$

This is analogous to the way the symmetries of a rectangle are reflections about lines parallel to the edges of the rectangle while the symmetries of a rhombus are reflections about the diagonals of the rhombus.

Given two lattices L, L' and their corresponding holohedral groups $\mathcal{H}_L, \mathcal{H}_{L'}$ we want the way the holohedral groups act on their respective lattices to be the same.

Definition 2.2.4. Let $L, L' \in \mathcal{L}_n$ with $L' = TL$ for some $T \in GL(n, \mathbb{R})$, then L, L' are in the same

bravais class if and only if $\mathcal{H}_{L'} = T\mathcal{H}_L T^{-1}$

Another way to think of bravais classes uses the integral representations of the holohedral

groups.

$$Q \in \mathcal{H}_L \Leftrightarrow Q \in O(n) \quad \text{and} \quad U^{-1}QU \in GL(n, \mathbb{Z})$$

Therefore $U^{-1}\mathcal{H}_L U \subset GL(n, \mathbb{Z})$. In other words if we express the isometries of $\mathcal{H}_L$ in a basis of

the lattice they form a finite subgroup of $GL(n, \mathbb{Z})$. This is known as an integral representation

of the holohedral group. The group $\mathcal{H}_L$ is the isotropy subgroup in $O(n)$ of a point $L \in \mathcal{L}_n$ while

$U^{-1}\mathcal{H}_L U$ is the isotropy subgroup in $GL(n, \mathbb{Z})$ of a point in $\mathcal{M}_n$. The integral representation of a

holohedral group associated to a lattice is not unique, but all of them are conjugate in $GL(n, \mathbb{Z})$.

This is because all of the matrices for a lattice $U\mathbb{Z}^n$ have the form UG for some $G \in GL(n, \mathbb{Z})$. In

fact the conjugacy class of an integral representation is an invariant associated to a bravais class.

Proposition 2.2.6. *Let $L, L' \in \mathcal{L}_n$, the integral representations of the holohedral groups of L, L'*

are conjugate in $GL(n, \mathbb{Z})$ if and only if L, L' are in the same bravais class

Proof. Let $L = U\mathbb{Z}^n, L' = V\mathbb{Z}^n$, and $L' = TL$ where $T, U, V \in GL(n, \mathbb{R})$. The following proof is an

elegant diagram chasing exercise.

Given that the top, bottom, left, and right sides of the diagram commute then the commu-

tativity of the front of the diagram is logically equivalent to the commutativity of the back of the

diagram. Commutativity of the front diagram is the condition that L, L' are in the same bravais

class. Commutativity of the back diagram is the statement that the integral representations of the

holohedral groups are conjugate in $GL(n, \mathbb{Z})$. □

It is not entirely trivial that we have split apart the holohedral classes to obtain the bravais

classes. The following theorem shows us that this is the case.

Proposition 2.2.7. *The bravais classes form a finer equivalence relation on $\mathcal{L}_n$ than holohedry*
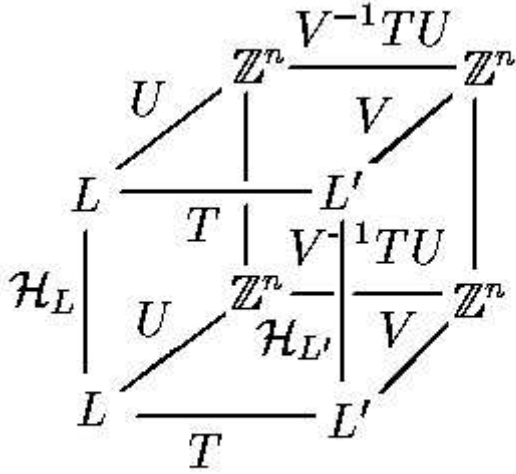
Figure 2.3: Cubic commutative diagram

Proof. Let $U, V \in GL(n, \mathbb{R}), L = U\mathbb{Z}^n, L' = V\mathbb{Z}^n$ and suppose L, L' are in the same bravais class so that $U^{-1}\mathcal{H}_L U, V^{-1}\mathcal{H}_{L'} V$ are conjugate in $GL(n, \mathbb{Z})$. Therefore $\mathcal{H}_L, \mathcal{H}_{L'}$ are conjugate in $GL(n, \mathbb{R})$ as well. But any two finite subgroups of $O(n)$ that are conjugate in $GL(n, \mathbb{R})$ must be conjugate in $O(n)$ [29]. Thus L, L' must be in the same holohedral class. $\qquad\square$

Propositions (2.2.6) and (2.2.7) are original work by the author. However the literature on Crystallography is vast and so no claim to the primacy of these results is made. It is easy to show that

Proposition 2.2.8. *The bravais classes form a coarser equivalence relation on $\mathcal{L}_n$ than the homothety classes.*

Proof. Follows from Proposition 2.2.3 $\qquad\square$

2.3   Lattices in $\mathbb{R}^2$

To obtain the homothety classes of lattices, $\mathcal{N}_2$, it is convenient to treat $\mathbb{R}^2$ as the complex plane $\mathbb{C}$. We consider lattices in $\mathbb{C}$ with two generators. The space of ordered pairs of generators is $\mathbb{C}^2$. Once again we shall need to identify those pairs that generate the same lattice. We need to turn the action of $GL(2, \mathbb{Z})$ on $M(2, \mathbb{R})$ to an action on $\mathbb{C}^2$. There is a convenient way to do this. Let $\begin{pmatrix} u_1 & u_2 \\ v_1 & v_2 \end{pmatrix} \in GL(2, \mathbb{R})$ be an ordered pair of generators for a planar lattice. We map the column vector $\begin{pmatrix} u_n & v_n \end{pmatrix}^T$ to the complex number $z_n = u_n + iv_n$ where $n = 1, 2$. This is a vector space isomorphism. The lattice associated to (z_1, z_2) is all of the integer combinations of z_1, z_2, i.e $(z_1, z_2)\mathbb{Z}^2$. Let $\begin{pmatrix} a & b \\ c & d \end{pmatrix} \in GL(2, \mathbb{Z})$, it is a simple computation to see that the following diagram commutes.

$$\begin{pmatrix} u_1 & u_2 \\ v_1 & v_2 \end{pmatrix}\begin{pmatrix} a & b \\ c & d \end{pmatrix} =\!=\!= \begin{pmatrix} au_1 + cu_2 & bu_1 + du_2 \\ av_1 + cv_2 & bv_1 + dv_2 \end{pmatrix}$$

$$\downarrow \qquad\qquad\qquad\qquad\qquad \downarrow$$

$$\begin{pmatrix} z_1 & z_2 \end{pmatrix}\begin{pmatrix} a & b \\ c & d \end{pmatrix} =\!=\!= \begin{pmatrix} az_1 + cz_2 & bz_1 + dz_2 \end{pmatrix}$$

Therefore the lattice generated by $\mathbf{z} \in \mathbb{C}^2$ is the same as the lattice generated by $\mathbf{z}G$ for any $G \in GL(2, \mathbb{Z})$. The group $GL(2, \mathbb{Z})$ acts on $\mathbb{C}^2$ by multiplying vectors on the right. The collection of group orbits gives the space of lattices $\mathcal{L}_2$.

2.3.1   Homothety Classes $\mathcal{M}_2$

However we go through $\mathcal{M}_2$ rather than $\mathcal{L}_2$ to get $\mathcal{N}_2$. Rotations of the plane can be represented by multiplication by members of $\mathbb{U}(1)$ and scaling can be represented by multiplication by members of $\mathbb{R}^+$. Now $\mathbb{C}\backslash\{0\} = \mathbb{C}^* = \mathbb{U}(1)\mathbb{R}^+$. Thus $\mathbb{C}^*$ is a representation of the group of orientation preserving homotheties of $\mathbb{R}^2$. Moding out by the orbits in $\mathbb{C}^2$ under the action of $\mathbb{C}^*$ gives us the complex projective space $\mathbb{CP}^1$ a.k.a the Riemann sphere.

To obtain $\mathcal{M}_2$ we need to consider the action of the full group of homotheties which is generated by the orientation preserving homotheties along with any orientation reversing homothety.

The orbit of the orientation reversing homothety (such as reflection about the real axis) acting on $\mathbb{CP}^1$ contains exactly two points, $[z, 1]$ and $[\bar{z}, 1]$. We can let points in the upper half plane of $\mathbb{C}$ be representative elements of the homothety classes of ordered basis for discrete lattices. Denote the upper half plane by $\mathbb{H}$ and identify it with $\mathcal{M}_2$. Similarly identify $\overline{\mathbb{H}} = \mathbb{H} \cup \mathbb{R} \cup \{\infty\}$ with $\tilde{\mathcal{M}}_2$

It is fairly well known that $\mathbb{H}$ gives us a model for Hyperbolic geometry. The "lines" in this geometry are semi-circular arcs of circles centered on the real axis together with lines that are orthogonal to the real axis. Note that the real axis is not part of the hyperbolic plane. Points on the real axis are sometimes called the points at infinity of the hyperbolic plane or more briefly as ideal points. The group of isometries for this model of the hyperbolic plane is generated by reflection about the imaginary axis and the Möbius transformations $\frac{az + c}{bz + d}$ where $a, b, c, d \in \mathbb{R}$ and $ad - bc = 1$. We denote a hyperbolic triangle with vertices z_1, z_2, z_3 by $\triangle(z_1, z_2, z_3)$ and a hyperbolic quadrilateral with vertices z_1, z_2, z_3, z_4 by $\square(z_1, z_2, z_3, z_4)$.

Let $G = \begin{pmatrix} a & b \\ c & d \end{pmatrix} \in GL(2, \mathbb{Z})$ and denote the corresponding map acting on $\mathbb{CP}^1$ by g. Using homogeneous coordinates on $\mathbb{CP}^1$ we get the following commutative diagram.

$$
\begin{array}{ccc}
(z_1, z_2) & \xrightarrow{\ G\ } & (az_1 + cz_2, bz_1 + dz_2) \\
\downarrow & & \downarrow \\
[z_1/z_2, 1] & \xrightarrow{\ g\ } & [\frac{az_1 + cz_2}{bz_1 + dz_2}, 1]
\end{array}
$$

Now $\dfrac{az_1 + cz_2}{bz_1 + dz_2} = \dfrac{a\frac{z_1}{z_2} + c}{b\frac{z_1}{z_2} + d}$ so $g([z, 1]) = [\frac{az + c}{bz + d}, 1]$, or for convenience $g(z) = \dfrac{az + c}{bz + d}$.

We can think of the maps on $\mathbb{CP}^1$ as the Möbius transformations $PGL(2, \mathbb{Z})$. However the group operation in $PGL(2, \mathbb{Z})$ is unconventional and slightly awkward. Recall that we multiply members of $\mathbb{C}^2$ on the right by members of $GL(2, \mathbb{Z})$ to obtain generators that generate the same lattice whereas we normally multiply on the left to indicate a transformation. A more conventional diagram looks like

$$
\begin{array}{ccc}
\begin{pmatrix} z_1 \\ z_2 \end{pmatrix} & \xrightarrow{\ G\ } & \begin{pmatrix} az_1 + bz_2 \\ cz_1 + dz_2 \end{pmatrix} \\
\downarrow & & \downarrow \\
[z_1/z_2, 1] & \xrightarrow{\ g\ } & [\frac{az_1 + bz_2}{cz_1 + dz_2}, 1]
\end{array}
$$

In short we would usually write $g(z) = \dfrac{az+b}{cz+d}$. For $g(z) = \dfrac{az+b}{cz+d}$ set $g^t(z) = \dfrac{az+c}{bz+d}$. It follows that $(g_1 \circ g_2)^t = g_2^t \circ g_1^t$ where $\circ$ denotes the usual composition of Möbius transformations. Our maps are of the form g^t. Let g_1^t, g_2^t be two such maps and apply the map g_1^t to $z \in \mathbb{C}$ followed by the map g_2^t, i.e.

$$z \mapsto g_1^t(z) \mapsto g_2^t(g_1^t(z)) = (g_2^t \circ g_1^t)(z) = (g_1 \circ g_2)^t(z)$$

For convenience we drop the superscript and write $g_2(g_1(z)) = (g_1 \circ g_2)(z)$ so that the second map is on the right hand side of the composition just as it is for members of $GL(2, \mathbb{Z})$. This is technically defining a new binary operation on the set $PGL(2, \mathbb{Z})$. However this binary operation merely turns $PGL(2, \mathbb{Z})$ into an isomorphic copy of itself. Rather than bother with a new notation for the group we shall simply write $g_2(g_1(z)) = g_1 g_2(z)$.

The group $PSL(2, \mathbb{Z})$ of Möbius transformations $\dfrac{az+c}{bz+d}$ with $ad - bc = 1$ leaves $\overline{\mathbb{H}}$ invariant. The maps in $PGL(2, \mathbb{Z}) \backslash PSL(2, \mathbb{Z})$ leave $\mathbb{R}$ invariant while swapping the upper and lower half planes. However z and $\bar{z}$ correspond to the same homothety class of ordered basis. So to get members of $PGL(2, \mathbb{Z}) \backslash PSL(2, \mathbb{Z})$ to act on $\mathbb{H}$ we send the image from a map in $PGL(2, \mathbb{Z}) \backslash PSL(2, \mathbb{Z})$ to its complex conjugate.

Each member of $PGL(2, \mathbb{Z}) \backslash PSL(2, \mathbb{Z})$ can be factored into a member of $PSL(2, \mathbb{Z})$ and the map $z \mapsto -z$. This is then followed by complex conjugation. So essentially we replace $z \mapsto -z \in PGL(2, \mathbb{Z}) \backslash PSL(2, \mathbb{Z})$ with $z \mapsto -\bar{z}$ in the factorization to get the members of $PGL(2, \mathbb{Z}) \backslash PSL(2, \mathbb{Z})$ to act on $\mathbb{H}$. The group $PSL(2, \mathbb{Z})$ is known as the Unimodular group and when we adjoin the reflection about the imaginary axis we obtain the extended Unimodular group which we denote by Γ. The extended Unimodular group is a discrete subgroup of hyperbolic isometries. This is summarized in the commutative diagram.

$$
\begin{array}{ccc}
\mathbb{C}^2 & \xrightarrow{\ GL(2,\mathbb{Z})\ } & \mathbb{C}^2 \\
\downarrow & & \downarrow \\
\mathbb{CP}^1 & \xrightarrow{\ PGL(2,\mathbb{Z})\ } & \mathbb{CP}^1 \\
\downarrow & & \downarrow \\
\overline{\mathbb{H}} & \xrightarrow{\ \Gamma\ } & \overline{\mathbb{H}}
\end{array}
$$

2.3.2 $\mathcal{N}_2$ as the Fundamental Domain of the Extended Unimodular Group

The fundamental domain of the Extended Unimodular group, Γ provides us with a collection of representative elements for its orbits in $\mathbb{H}$.

A generalization of the Euclidean algorithm proves that $SL(2,\mathbb{Z})$ is generated by $T_1 = \begin{pmatrix} 1 & 1 \\ 0 & 1 \end{pmatrix}, T_2 = \begin{pmatrix} 1 & 0 \\ 1 & 1 \end{pmatrix}$. These project to $t_1 : z \mapsto \dfrac{z}{z+1}$ and $t_2 : z \mapsto \dfrac{z+1}{z}$ which generates the Modular group, $PSL(2,\mathbb{Z}) \cong SL(2,\mathbb{Z})/\{\pm I_2\}$. Adjoining the reflection about the imaginary axis generates the extended Unimodular group, Γ. Reflection about the imaginary axis is reflection about a side of the $\triangle(0,1,\infty)$. Call this map a. Let $s : z \to 1/(1-z)$ and let $r : z \to 1-z$. Then $t_1 = ra, t_2 = rsa$ so $\Gamma = <a,r,s>$.

Since Möbius transformations take any set of 3 points to any other set of 3 points it is straight forward to determine the isotropy group of the 3 point set $\{0,1,\infty\}$ in $PSL(2,\mathbb{Z})$. It has two generators $\{r,s\}$ which generate a copy of D_3. Adjoin the reflection about any side of $\triangle(0,1,\infty)$ and we get the extended Unimodular group. In other words the extended Unimodular group has 3 generators $\{a,r,s\}$ whose geometric meaning is clear. The reflections about the sides of $\triangle(0,1,\infty)$ generates a triangular tessellation of the hyperbolic plane.

We can choose the fundamental domain of the Extended Unimodular group to be any one of six sub-triangles of $\triangle(0,1,\infty)$, say $\triangle(i, e^{i\pi/3}, \infty)$. The orbit of its vertices and edges under the extended Unimodular group is the set of points in $\mathbb{H}$ which have non-trivial isotropy groups. We can identify $\triangle(i, e^{i\pi/3}, \infty)$ with the collection of homothety classes of lattices $\mathcal{N}_2$. The action of the extended Unimodular group on $\triangle(i, e^{i\pi/3}, \infty)$ generates a triangular tessellation of $\mathbb{H}$.

2.3.3 Isotropy Groups and the Bravais Stratification

Recall that the isotropy subgroups of a point in $\tilde{\mathcal{M}}_2$ is an integral representation of the holohedral group [see section (2.2.2)]. In this case $\tilde{\mathcal{M}}_2 = \overline{\mathbb{H}}$. The group $GL(2,\mathbb{Z})$ acts on $\overline{\mathbb{H}}$ as Γ.
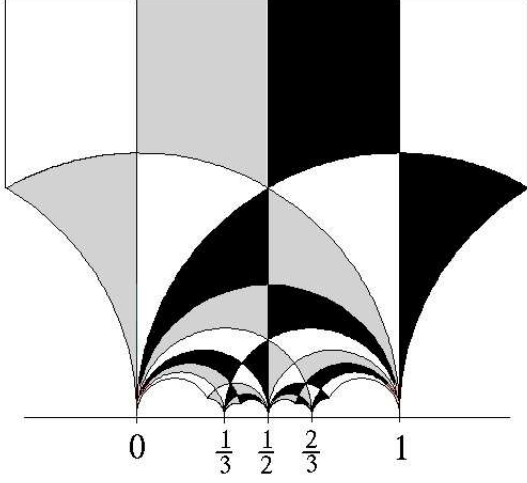
Figure 2.4: Tessellation by the fundamental region of the extended Unimodular group

$$\mathbb{C}^2 \xrightarrow{\;GL(2,\mathbb{Z})\;} \mathbb{C}^2$$
$$\downarrow \qquad\qquad \downarrow$$
$$\overline{\mathbb{H}} \xrightarrow{\;\;\Gamma\;\;} \overline{\mathbb{H}}$$

According to Proposition 2.2.1 $\{\pm I_2\} \subset \mathcal{H}_L$ for any lattice. Since $\{\pm I_2\}$ sits in the center of $GL(2,\mathbb{R})$ the group $\{\pm I_2\}$ must be in the integral representation of $\mathcal{H}_L$. Consequently the isotropy subgroup of a point $z \in \overline{\mathbb{H}}$ is isomorphic to $\mathcal{H}_L/\{\pm I_2\}$ where $L = z\mathbb{Z}^2$. The conjugacy class in $GL(2,\mathbb{Z})$ of an integral representation of a holohedral group becomes the conjugacy class in Γ of an isotropy subgroup of a point in $\mathbb{H}$.

$$\mathbb{C}^2 \xrightarrow{\;H^{-1}\;} \mathbb{C}^2 \xrightarrow{\;G\;} \mathbb{C}^2 \xrightarrow{\;H\;} \mathbb{C}^2$$
$$\downarrow \qquad\quad \downarrow \qquad\quad \downarrow \qquad\quad \downarrow$$
$$\overline{\mathbb{H}} \xrightarrow{\;h^{-1}\;} \overline{\mathbb{H}} \xrightarrow{\;g\;} \overline{\mathbb{H}} \xrightarrow{\;h\;} \overline{\mathbb{H}}$$

Thus the points in $\overline{\mathbb{H}}$ have conjugate isotropy subgroups if and only if the lattices associated to those points are in the same Bravais class. We determine the isotropy subgroups in the fundamental domain of the extended Unimodular group. The isotropy subgroups on the rest of $\overline{\mathbb{H}}$ are then obtained by conjugation.

There are 5 bravais classes of planar lattices. Points in the interior of the fundamental domain of the extended Unimodular group have trivial isotropy subgroups. This bravais class is called oblique. Points on the edges of the fundamental domain have the reflection about their respective edges as their isotropy subgroups. Points on the imaginary axis bounding the fundamental domain have the isotropy subgroup generated by the reflection $z \mapsto -\overline{z}$ which is isomorphic to $\mathbb{Z}_2$. This bravais class is called rectangular. Points on the unit circle bounding the fundamental domain have the isotropy subgroup generated by the reflection $z \mapsto 1/\overline{z}$ and points on the line $Re(z) = 1/2$ bounding the fundamental domain have the isotropy subgroup generated by the reflection $z \mapsto 1 - \overline{z}$. These are conjugate subgroups isomorphic to $\mathbb{Z}_2$ and correspond to the same bravais class. This class is called rhombic. Lattices corresponding to points on the unit circle bounding the fundamental domain are called explicitly rhombic while those corresponding to points on the line $Re(z) = 1/2$ are called implicitly rhombic. For explicitly rhombic lattices the symmetry permutes two of the smallest non-zero members of the lattice while for implicitly rhombic lattices the symmetry permutes two of the second smallest non-zero members of the lattice. The point i has the isotropy subgroup generated by the reflections $z \mapsto -\overline{z}$ and $z \mapsto 1/\overline{z}$. This is isomorphic to $\mathbb{Z}_2 \oplus \mathbb{Z}_2$ and the bravais class is called square. The point $e^{i\pi/3}$ has the isotropy subgroup generated by the reflections $z \mapsto 1/\overline{z}$ and $z \mapsto 1 - \overline{z}$. This is isomorphic D_3 and the bravais class is called hexagonal.

2.3.4 Canonical Bases and a Tessellation of $\mathbb{H}$ by Quadrilaterals

Associated to a lattice is a particular set of bases called the canonical bases. The following proposition is used to define canonical bases.

Proposition 2.3.1. *Let L be a lattice in $\mathbb{C}$ and let l_1 be one of the smallest non-zero members of L and let l_2 be one of the smallest members of the lattice L outside of the sub-lattice generated by l_1. Then $\{l_1, l_2\}$ is a bases for L. For a proof see [6, 52].*

Definition 2.3.1. Let $l_1, l_2,$ and L be defined as in Theorem (2.3.1), then the ordered bases (l_1, l_2) and (l_2, l_1) are called *canonical bases*

Given a point $z \in \mathbb{H}$ we want to determine a canonical basis for a lattice in the equivalence class represented by z. We begin in $\mathbb{H}$ with the fundamental domain of the extended Unimodular group and its image under reflection about the imaginary axis.

Proposition 2.3.2. *The points ± 1 are the smallest non-zero members of the lattice $(z,1)\mathbb{Z}^2$ and $\pm z$ are the smallest members of $(z,1)\mathbb{Z}^2$ outside of the sub-lattice $\mathbb{Z}$ if and only if $|z| > 1$ and $-1/2 < Re(z) < 1/2$.*

Proof. ± 1 are the smallest non-zero members of the lattice implies that $|z| > 1$. And $\pm z$ are the smallest members of $(z,1)\mathbb{Z}^2 \backslash \mathbb{Z}$ implies $-1/2 < Re(z) < 1/2$. Suppose otherwise, then for some non-zero $k \in \mathbb{Z}$ we have $Re(z-k) \leq Re(z)$ while $Im(z-k) = Im(z)$ so that $|z-k| \leq |z|$ which contradicts $\pm z$ are the smallest members of $(z,1)\mathbb{Z}^2 \backslash \mathbb{Z}$.

Now suppose $|z| > 1$ and $-1/2 < Re(z) < 1/2$ and let $\zeta \in (z,1)\mathbb{Z}^2$ with $|\zeta| \leq |z|$. We now show that $|\zeta| \geq 1$ so that ± 1 are the shortest generators and $\pm \zeta$ the second shortest. We can write $\zeta = az + b$ for some $a, b \in \mathbb{Z}$.

Case $a = 0$ implies $\zeta \in \mathbb{Z}$

For the following cases we use the fact $|az + b|^2 \leq |z|^2$ and $z = x + iy$ for real x, y.

$$(ax + b)^2 + (ay)^2 \leq |z|^2 \Leftrightarrow$$

$$a^2(x^2 + y^2) + 2abx + b^2 \leq |z|^2 \Leftrightarrow$$

$$2abx + b^2 \leq (1 - a^2)|z|^2$$

Case $a = \pm 1$ implies $\pm 2bx + b^2 \leq 0$. When $b = 0$ we have $\zeta = \pm z$. When $b \neq 0$ the fact that $-1/2 < x < 1/2$ gives

$$-|b| < \pm 2bx \Leftrightarrow$$

$$b^2 - |b| < \pm 2bx + b^2 \Leftrightarrow$$

$$b^2 - |b| < 0 \Leftrightarrow$$

$$|b| < 1 \Leftrightarrow$$

$$b = 0$$

which is a contradiction.

Case $|a| > 1$. By assumption $|z| > 1$ and $1 - a^2 < 0$ so that $(1 - a^2)|z|^2 < 1 - a^2$. When $b = 0$ we have $0 < 1 - a^2$ which implies $a = 0$ which is a contradiction. When $b \neq 0$ the fact that $-1/2 < x < 1/2$ gives

$$-|ab| < \pm 2abx \Leftrightarrow$$

$$b^2 - |ab| < \pm 2abx + b^2 \Leftrightarrow$$

$$b^2 - |ab| < 1 - a^2 \Leftrightarrow$$

$$a^2 + b^2 < 1 + |ab|$$

Now suppose $ab > 0$, then

$$a^2 + b^2 < 1 + ab \Leftrightarrow$$

$$a^2 - 2ab + b^2 < 1 - ab < 1 \Leftrightarrow$$

$$(a - b)^2 < 1 \Leftrightarrow$$

$$a - b = 0 \Leftrightarrow$$

$$a = b$$

So $|\zeta| = |a||z + 1|$ Now suppose $ab < 0$, then

$$a^2 + b^2 < 1 - ab \Leftrightarrow$$

$$a^2 + 2ab + b^2 < 1 + ab < 1 \Leftrightarrow$$

$$(a + b)^2 < 1 \Leftrightarrow$$

$$a + b = 0 \Leftrightarrow$$

$$a = -b$$

So $|\zeta| = |a||z - 1|$. Since $-1/2 < x < 1/2$ we have $Re(z + 1) > Re(z)$ and $Re(z - 1) < Re(z)$ while $Im(z + 1) = Im(z) = Im(z - 1)$ so that $|z + 1| > |z|$ and $|z - 1| > |z|$. Since $|a| > 1$ we get $|\zeta| > |z|$

which is a contradiction.

Therefore $\zeta \in \{\pm z\} \cup \mathbb{Z}$. The smallest non-zero members of $\{\pm z\} \cup \mathbb{Z}$ are ± 1 and the smallest members of $\{\pm z\}$ are $\pm z$. $\qquad \square$

The reflection about the unit circle, $z \mapsto 1/\overline{z}$, is a member of the extended Unimodular group that comes from the matrix $\begin{pmatrix} 0 & 1 \\ 1 & 0 \end{pmatrix}$ which just permutes the two members of an ordered bases for a lattice. Therefore the lattices associated to corresponding points on each side of the unit circle have the same canonical bases. This gives the following corollary

Corollary 2.3.3. *If $|z| > 1$ and $-1/2 < Re(z) < 1/2$ or if $|z| < 1$ and $-1/2 < Re(1/z) < 1/2$ then $(z, 1)$ is a canonical basis for the lattice $(z, 1)\mathbb{Z}^2$.*

The intersection of the set $\{z : |z| > 1$ and $-1/2 < Re(z) < 1/2\} \cup \{z : |z| < 1$ and $-1/2 < Re(z) < 1/2\}$ with $\mathbb{H}$ forms a hyperbolic quadrilateral. Its vertices are $0, e^{i\pi/3}, \infty$, and $e^{i2\pi/3}$. It contains four copies of the fundamental region of the extended Unimodular group that are obtained by reflecting the fundamental region about the imaginary axis and the unit circle. The action of the extended Unimodular group on this quadrilateral generates a tessellation of the hyperbolic plane by quadrilaterals.

This tessellation is closely related to the Farey tessellation which is generated by the action of $PSL(2, \mathbb{Z})$ on the imaginary axis, see figure (2.3.2). The Farey tessellation is a tessellation by ideal triangles of which $\triangle(0, 1, \infty)$ is an example. The Farey tessellation gets its name from its relationship to the Farey tree. The endpoints of each edge of a triangle are rational numbers that are connected in the Farey tree. The Farey sum of these two rational numbers is the third vertex of a triangle having the first two rational numbers as vertices.

The imaginary axis is a diagonal of the quadrilateral with ideal vertices $0, \infty$. The image of this quadrilateral by a member of the extended Unimodular group has ideal vertices that are rational numbers and that are connected in the Farey tree. The edges in the Farey tessellation are the diagonals of the quadrilaterals. The lattices associated to points on these diagonals are in the rectangular bravais class.
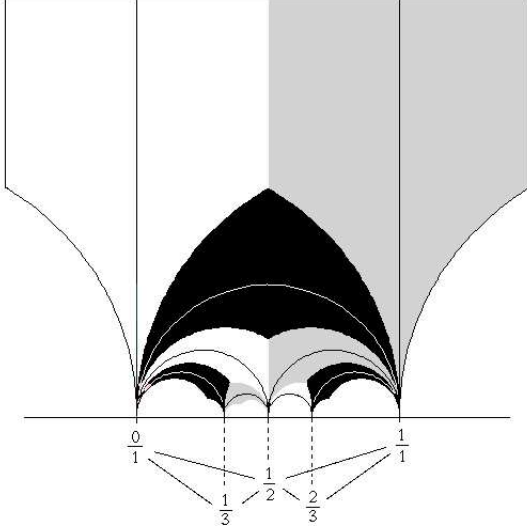
Figure 2.5: Tessellation by quadrilaterals

We are also interested in the other diagonal of the quadrilaterals. The lattices associated to points on these diagonals are in the rhombic bravais class, in particular they are the explicitly rhombic lattices.

The members of $PSL(2, \mathbb{Z})$: $a : z \rightarrow \overline{-z}$, $b : z \rightarrow \overline{2 - z}$, and $c : z \rightarrow \overline{z/(2z - 1)}$ map $\triangle(0, 1, \infty)$ to its adjacent triangles in the Farey tessellation. These members of $PSL(2, \mathbb{Z})$ are induced by the members of $SL(2, \mathbb{Z})$:

$$\begin{pmatrix} 1 & 0 \\ 0 & -1 \end{pmatrix}, \begin{pmatrix} 1 & -2 \\ 0 & -1 \end{pmatrix}, \begin{pmatrix} 1 & 0 \\ 2 & -1 \end{pmatrix}$$

We can factor these matrices

$$\begin{pmatrix} 1 & -2 \\ 0 & -1 \end{pmatrix} = \begin{pmatrix} 1 & 1 \\ 0 & 1 \end{pmatrix} \begin{pmatrix} 1 & 1 \\ 0 & 1 \end{pmatrix} \begin{pmatrix} 1 & 0 \\ 0 & -1 \end{pmatrix}$$

$$\begin{pmatrix} 1 & 0 \\ -2 & -1 \end{pmatrix} = \begin{pmatrix} 1 & 0 \\ 1 & 1 \end{pmatrix} \begin{pmatrix} 1 & 0 \\ 1 & 1 \end{pmatrix} \begin{pmatrix} 1 & 0 \\ 0 & -1 \end{pmatrix}$$

The group generated by the squares of t_1 and t_2 (see section 2.3.2) is known as the Level 2 Congruence Subgroup of $PSL(2, \mathbb{Z})$. If we adjoin the map a to the Level 2 Congruence Subgroup we get the same group as generated by $\{a, b, c\}$ whose geometric meaning is clear. This is the extended level

2 Congruence subgroup. Geometrically the extended Level 2 Congruence subgroup is generated by reflecting about the sides of $\triangle(0, 1, \infty)$. While the extended Modular group is generated by the symmetries of the $\triangle(0, 1, \infty)$ along with a reflection about any of the triangle's sides.

We can construct a Cayley graph for the extended level 2 Congruence subgroup. We start with the point $e^{i\pi/3}$ and act on it with the three generators a, b, c of the extended level 2 Congruence subgroup. We connect the images of $e^{i\pi/3}$ to $e^{i\pi/3}$ with hyperbolic lines. These hyperbolic lines are the diagonals of quadrilaterals and points on them correspond to the explicitly rhombic lattices. The union of all these diagonals is the Cayley graph of the extended level 2 Congruence subgroup.

In chapter 3 we will see that the Cayley graph of the extended level 2 Congruence subgroup is closely related to the bifurcation diagram for the dynamical system.

Figure 2.6: Cayley graph of the extended level 2 congruence subgroup.

2.4   Spiral lattices in $\mathcal{C}$

We begin with some definitions.

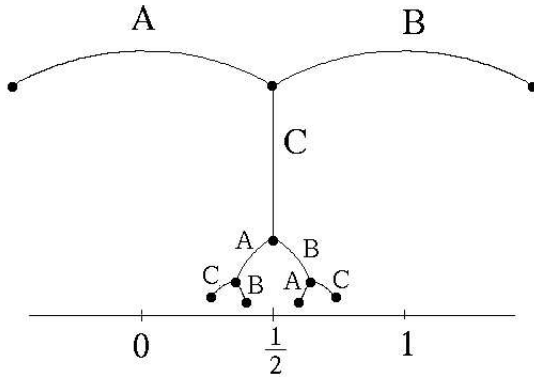**Definition 2.4.1.** The space $\mathcal{C}$ is the set of points $z \in \mathbb{C}$ whose real part is between $-1/2$ and $1/2$ with the lines $Re(z) = -1/2$ and $Re(z) = 1/2$ identified. The space $\mathcal{C}'$ is the set of points $z \in \mathbb{H}$ whose real part is between $-1/2$ and $1/2$ with the lines $Re(z) = -1/2$ and $Re(z) = 1/2$ identified. The space $\partial\mathcal{C}'$ is the set of points $z \in \mathbb{R}$ between $-1/2$ and $1/2$ with the points $-1/2$ and $1/2$ identified.

The spaces $\mathcal{C}$ and $\mathcal{C}'$ are topologically cylinders and $\partial\mathcal{C}'$ is topologically a circle. A convenient metric to use on $\mathcal{C}$ is obtained by projecting down the Euclidean metric on $\mathbb{C}$.

Definition 2.4.2. Let $z = x + iy \in \mathbb{C}$ and $j \in \mathbb{Z}$. We define the following functions. $\Delta_j : \mathbb{C} \to \mathbb{Z}$ takes z to the nearest integer to jx. This is known as the *jth encyclic number* after Bravais [8]. The function $\delta_j : \mathbb{C} \to \partial\mathcal{C}'$ takes z to the fractional part of jx i.e. $\delta_j(z) = jx - \Delta_j(z)$. The function $\lambda_j : \mathbb{C} \to \mathcal{C}$ takes z to $\delta_j(z) + ijy$. We will drop the argument z when convenient.

The function $\lambda_1 : \mathbb{C} \to \mathcal{C}$ is a homomorphism with kernel $\mathbb{Z}$. Therefore for any $z \in \mathbb{H}$ the image of a lattice $L = (z, 1)\mathbb{Z}^2$ is a lattice in $\mathcal{C}$ with a single generator $\lambda_1(z)$ i.e. a spiral lattice. The spiral lattice associated to z is denoted by $\Lambda(z)$ or simply Λ. We can write $\Lambda = \lambda_1(L)$. Conversely let $z \in \mathcal{C}$ be the generator of a spiral lattice, then since $z = \lambda_1(z)$ the spiral lattice is the image of the planar lattice $(z, 1)\mathbb{Z}^2$ under λ_1.

Clearly $\Lambda(z) = \Lambda(-z)$ and if z, w both have positive imaginary part then $\Lambda(z) = \Lambda(w)$ if and only if $z - w$ is an integer. Hence the space of spiral lattices can be identified with points in $\mathbb{H}$ with real part between 0 and 1.

Definition 2.4.3. The space $\mathbb{H}^*$ is the set of points in $z \in \mathbb{H}$ whose real part is between 0 and 1 with the lines $Re(z) = 0$ and $Re(z) = 1$ identified.

It is convenient to project the hyperbolic metric down to $\mathbb{H}^*$. In particular any polygon in $\mathbb{H}$ whose real part is contained in an interval of width less than 1 is projected down to an isometric polygon in $\mathbb{H}^*$.

Definition 2.4.4. Let (m, n) be coprime and choose integers D_m, D_n such that

$$0 \leq D_m < m, 0 \leq D_n < n, and D_n m - D_m n = 1.$$

This choice for D_m, D_n is unique. Note that although there is only one subscript they both depend on m, n. Define the maps

$$g_{mn}^+(z) = \frac{D_m z - D_n}{mz - n}$$

$$g_{mn}^-(z) = \frac{(m - D_m)z - (n - D_n)}{mz - n}$$

These maps take the quadrilateral with ideal vertices $0, \infty$ to a quadrilateral with ideal vertices $D_m/m, D_n/n$ and $1 - D_m/m, 1 - D_n/n$ respectively.

Definition 2.4.5. The quadrilateral with ideal vertices $\{0, \infty\}$ is called a *fundamental quadrilateral* its image under g_{mn}^+ called a *positive (m, n) quadrilateral* and it is denoted by $\square_{mn}^+$. The map $g_{mn}^-(z)$ takes the fundamental quadrilateral to a quadrilateral with vertices $(m - D_m)/m, (n - D_n)/n$. This is called a *negative (m, n)-quadrilateral* and is denoted by $\square_{mn}^-$. It is the image of the positive (m, n)-quadrilateral under the map $z \mapsto 1 - z$. The union of the positive and negative quadrilaterals is denoted by $\square_{mn}^\pm$.

By our choice of D_m, D_n we know these quadrilaterals lie in $\mathbb{H}^*$.

Proposition 2.4.1. $z \in (m, n)$-*quadrilateral* $\Leftrightarrow (\lambda_n(z), \lambda_m(z))$ *is a canonical basis for the lattice associated to z.*

Proof. Let w be in the fundamental quadrilateral with $z = g_{mn}^+(w)$. The lift of the map g_{mn}^+ is $\begin{pmatrix} -D_m & -m \\ D_n & n \end{pmatrix}$. The pre-image of $(z, 1)$ under this automorphism is $(nz - D_n, mz - D_m)$. Hence these points become the canonical basis for the lattice under the automorphism. We apply the homothety $\zeta \mapsto \zeta/(mz - D_m)$ to the canonical basis. To get $(\dfrac{nz - D_n}{mz - D_m}, 1)$ This is homothetic to the basis $(w, 1)$ so $\dfrac{nz - D_n}{mz - D_m} = w = \dfrac{nz - \Delta_n(z)}{mz - \Delta_m(z)}$ (since $|Re(w)| < 1/2$) and

$$(nz - D_n)(mz - \Delta_m) = (nz - \Delta_n)(mz - D_m)$$

$$(1 - (\Delta_n m - \Delta_m n))z = \Delta_m D_n - \Delta_n D_m$$

The functions $\Delta_m(z), \Delta_n(z)$ are piecewise constant so the equality must hold for more than one value of $z \in \square_{mn}^+$. Therefore

$$1 = \Delta_n m - \Delta_m n$$

$$0 = \Delta_m D_n - \Delta_n D_m$$

which together implies $\Delta_m = D_m$ and $\Delta_n = D_n$ so that $(\lambda_n, \lambda_m) = (nz - D_n, mz - D_m)$ is the canonical basis.

The proof for the negative quadrilaterals is essentially the same replacing D_m with $m - D_m$ and D_n with $n - D_n$.

Conversely suppose $(\lambda_n(z)\lambda_m(z))$ is a canonical basis and z is in an (j, k)-quadrilateral. From above the pair $(\lambda_k(z), \lambda_j(z))$ is canonical basis. Then either $(\lambda_j(z) = \lambda_n(z))$ and $(\lambda_k(z) = \lambda_m(z))$ or $(\lambda_j(z) = \lambda_m(z))$ and $(\lambda_k(z) = \lambda_n(z))$. So the (j, k)-quadrilateral is an (m, n)-quadrilateral.

$\square$

2.4.1 The Three Types of Quadrilaterals

It is useful to classify the quadrilaterals according to their shape. The issue that will be important is whether the vertical lines passing through the ideal vertices of a quadrilateral also pass through the quadrilateral. Recall that a hyperbolic line has two ideal points that constitute its boundary in $\overline{\overline{\mathbb{H}}}$. Two edges of the quadrilateral meet at an ideal vertex. If the ideal points at the other end of these two lines is on the same side of the ideal vertex then the vertical line passing through the vertex will not pass through the quadrilateral, otherwise it will. The two ideal points associated to the ideal vertex D_m/m of $\square_{mn}^+$ are $\dfrac{2D_n + D_m}{2n + m}, \dfrac{2D_n - D_m}{2n - m}$. These points are on the same side of D_m/m when

$$\left(\frac{D_m}{m} - \frac{2D_n + D_m}{2n + m}\right)\left(\frac{D_m}{m} - \frac{2D_n - D_m}{2n - m}\right) = \frac{2}{mn^2(2m - n)} > 0$$

For the other vertex we get

$$\left(\frac{D_n}{n} - \frac{2D_m + D_n}{2m + n}\right)\left(\frac{D_n}{n} - \frac{2D_m - D_n}{2m - n}\right) = \frac{2}{nm^2(2m - n)}$$

At most one ideal vertex can have its associated ideal points on opposite sides itself or else the top edges of the quadrilateral would never meet. Therefore the product $(2m - n)(2n - m)$ is positive if both pairs of ideal points associated to the two ideal vertices of the quadrilateral are on the same side of their respective vertices. Otherwise one of the vertices is in between its associated pair of ideal points. Since the negative quadrilaterals are isometric to the positive quadrilaterals the formula applies to them as well.

Definition 2.4.6. If $m > 2$ or $n > 2$ then $\square_{mn}^{\pm}$ is a *regular* quadrilateral if and only if $(2m-n)(2n-m) > 0$ else it is an *irregular* quadrilateral. The fundamental quadrilateral, the $(1, 1)$-quadrilateral, and the $(1, 2)$ quadrilaterals are the *exceptional quadrilaterals* (see figure (2.10) at the end of the chapter.

Definition 2.4.7. We say that a quadrilateral is *below* a second quadrilateral when the ideal vertices of the first quadrilateral are between the ideal vertices of the second quadrilateral

Proposition 2.4.2. *The two adjacent quadrilaterals below either a regular or an irregular quadrilateral is a pair of regular and irregular quadrilaterals*

Proof. Since the ideal vertices of the quadrilaterals follow the Farey tree the two adjacent quadrilaterals beneath an (m, n)-quadrilateral are the $(m, m+n)$-quadrilateral and the $(m+n, n)$-quadrilateral. Computation gives

$$(2(m + n) - m)(2m - (m + n)) \quad = \quad (m + 2n)(m - n) \tag{2.1}$$

$$(2(m + n) - n)(2n - (m + n)) \quad = \quad (2m + n)(n - m) \tag{2.2}$$

and these must have opposite signs. Therefore one is regular and one is irregular $\qquad \square$

Hexagons

It is not always the case that the smallest and second smallest non-zero members of a planar lattice form a bases. The second smallest non-zero member of a lattice can be the smallest

non-zero member added to itself. For z in the fundamental quadrilateral this occurs when $|z| > 2$

or $|z| < 1/2$. These two circles truncate the quadrilateral to produce a hyperbolic hexagon.
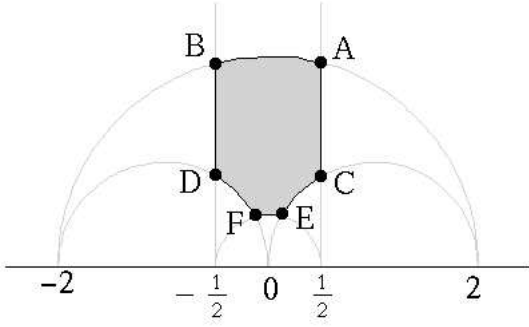
Figure 2.7: Fundamental Hexagon

The vertices of this hexagon are

$$A = \frac{1}{2} + i\frac{\sqrt{15}}{2} \quad B = -\frac{1}{2} + i\frac{\sqrt{15}}{2} \tag{2.3}$$

$$C = \frac{1}{2} + i\frac{\sqrt{3}}{2} \quad D = -\frac{1}{2} + i\frac{\sqrt{3}}{2} \tag{2.4}$$

$$E = \frac{1}{8} + i\frac{\sqrt{15}}{8} \quad F = -\frac{1}{8} + i\frac{\sqrt{15}}{8} \tag{2.5}$$

Definition 2.4.8. The hexagon with the vertices given in equation (2.4.2) is called the *fundamental hexagon*. The images of the fundamental hexagon under the maps $g_{mn}(z)$ give the (m,n)-*hexagons*. The vertices of these hexagons are

$$g_{mn}(A) = \frac{(2D_n n - D_m n - D_n m + 8D_m m) + i\sqrt{15}}{2(n^2 - mn + 4m^2)} \tag{2.6}$$

$$g_{mn}(B) = \frac{(2D_n n + D_m n + D_n m + 8D_m m) + i\sqrt{15}}{2(n^2 + mn + 4m^2)} \tag{2.7}$$

$$g_{mn}(C) = \frac{(2D_n n - D_m n - D_n m + 2D_m m) + i\sqrt{3}}{2(n^2 - mn + m^2)} \tag{2.8}$$

$$g_{mn}(D) = \frac{(2D_n n + D_m n + D_n m + 2D_m m) + i\sqrt{3}}{2(n^2 + mn + m^2)} \tag{2.9}$$

$$g_{mn}(E) = \frac{(2D_m m - D_n m - D_m n + 8D_n n) + i\sqrt{15}}{2(m^2 - mn + 4n^2)} \tag{2.10}$$

$$g_{mn}(F) \;=\; \frac{(2D_m m + D_n m + D_m n + 8D_n n) + i\sqrt{15}}{2(m^2 + mn + 4n^2)}. \tag{2.11}$$

We say a hexagon is regular, irregular, or exceptional according to the type of quadrilateral containing it.

Proposition 2.4.3. *If z is in a (m,n)-hexagon then neither member of the canonical basis $(\lambda_n(z), \lambda_m(z))$ has more than twice the length of the other.*

Proof. Let w be in the fundamental hexagon with $z = g_{mn}^+(w)$. The proposition follows from Proposition (2.4.1) and the fact that the basis $(w, 1)$ is homothetic to the basis $(\lambda_n(z), \lambda_m(z))$ $\qquad\square$
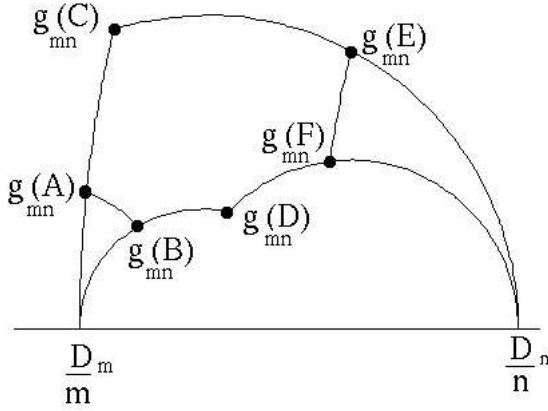
Figure 2.8: (m,n)-Hexagon

Regular regions

We can use the hexagons to define regions that will be important in understanding the dynamical systems of this thesis. By Equation (2.2) when $m < n$ the regular quadrilateral adjacent and below the (m,n)-quadrilateral is the $(n, m+n)$-quadrilateral. The pair (m,n) generates a sequence of pairs of successive generalized Fibonacci numbers $(m,n), (n, m+n), (m+n, m+2n), \ldots$. Each of these pairs corresponds to a regular quadrilateral adjacent and below the quadrilateral corresponding to the previous pair.
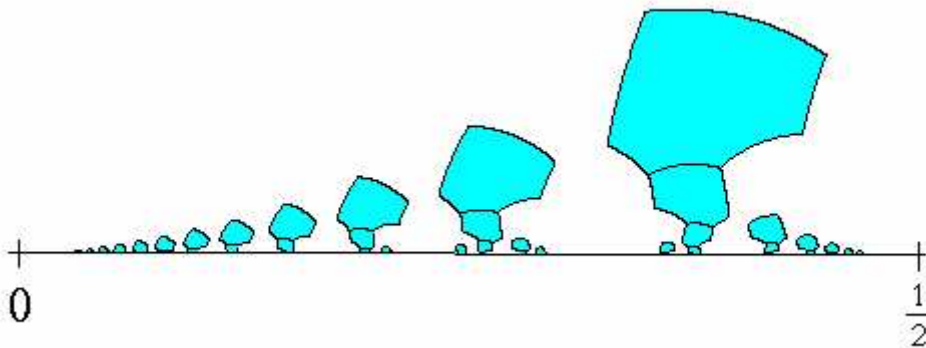
Figure 2.9: Regular Regions

Definition 2.4.9. Let $m < n$ and let the regular (m, n)-quadrilateral be adjacent and under an irregular quadrilateral. The union of the hexagons corresponding to the sequence of pairs of successive generalized Fibonacci sequence $(m, n), (n, m + n), (m + n, m + 2n), \ldots$ is called the *regular region* which we denote by R_{mn}.

The vertices of the quadrilaterals containing the hexagons making up a regular region form a sequence of a rational approximations for a noble number. The part of the boundary of a regular region lying on the real axis is this noble number.

2.4.2 The Fundamental Theorem of Phyllotaxis

We begin this section with a definition.

Definition 2.4.10. The cosets of the group generated by λ_m in in the group Λ are called the *m-parastichies. There are m m-parastichies. When λ_n, λ_m are two of the smallest non-zero members of Λ and neither one of λ_n, λ_m is twice the length of the other then we say the lattice has parastichy numbers (m, n)*

This definition is motivated by the fact that when λ_n, λ_m are two of the smallest non-zero members of Λ and neither one of λ_n, λ_m is twice the length of the other then the m-parastichies and the n-parastichies of a spiral lattice are readily visible. In particular the parastichy numbers

are observed in spiral phyllotaxis.

In 1988 Jean [25] proved what is known as the "Fundamental Theorem of Phyllotaxis". Briefly stated this theorem relates the divergence angle of a spiral lattice to its parastichy numbers. In particular it implies that for coprime m, n with $D_m n - D_n m = \pm 1$ where $0 \leq D_m < m$ and $0 \leq D_n < n$ the divergence angle must be between D_m/m and D_n/n. These are the ideal vertices of a (m, n)-quadrilateral. Using the hexagons we obtain a new version of the "Fundamental Theorem of Phyllotaxis". This version gives both a narrower interval for the divergence angle a well as giving bounds on the parameter y.

Theorem 1. *(m, n) are the parastichy numbers of a spiral lattice $\Lambda(z)$ if and only if z is in a (m, n)-hexagon.*

Proof. By Proposition (2.4.3) z is in a (m, n)-hexagon if and only if $(\lambda_n(z), \lambda_m(z))$ is a canonical basis and neither member has twice the length of the other. $\qquad\square$

From this theorem we can place bounds on the real and imaginary parts of z when the lattice associated to z has parastichy numbers (m, n).

Corollary 2.4.4. *If $\Lambda(z)$ has parastichy numbers (m, n) then the imaginary part of z is less than* $\max\{Im(g_{mn}^+(A)), Im(g_{mn}^+(C)), Im(g_{mn}^+(E))\}$ *and greater than* $\min\{Im(g_{mn}^+(B)), Im(g_{mn}^+(D)), Im(g_{mn}^+(F))\}$ *and the real part of z is less than* $\max\{Re((g_{mn}^+(A)), Re(g_{mn}^+(C)), Re(g_{mn}^+(E))\}$ *and greater than* $\min\{Re((g_{mn}^+(A)), Re(g_{mn}^+(C)), Re(g_{mn}^+(E))\}$
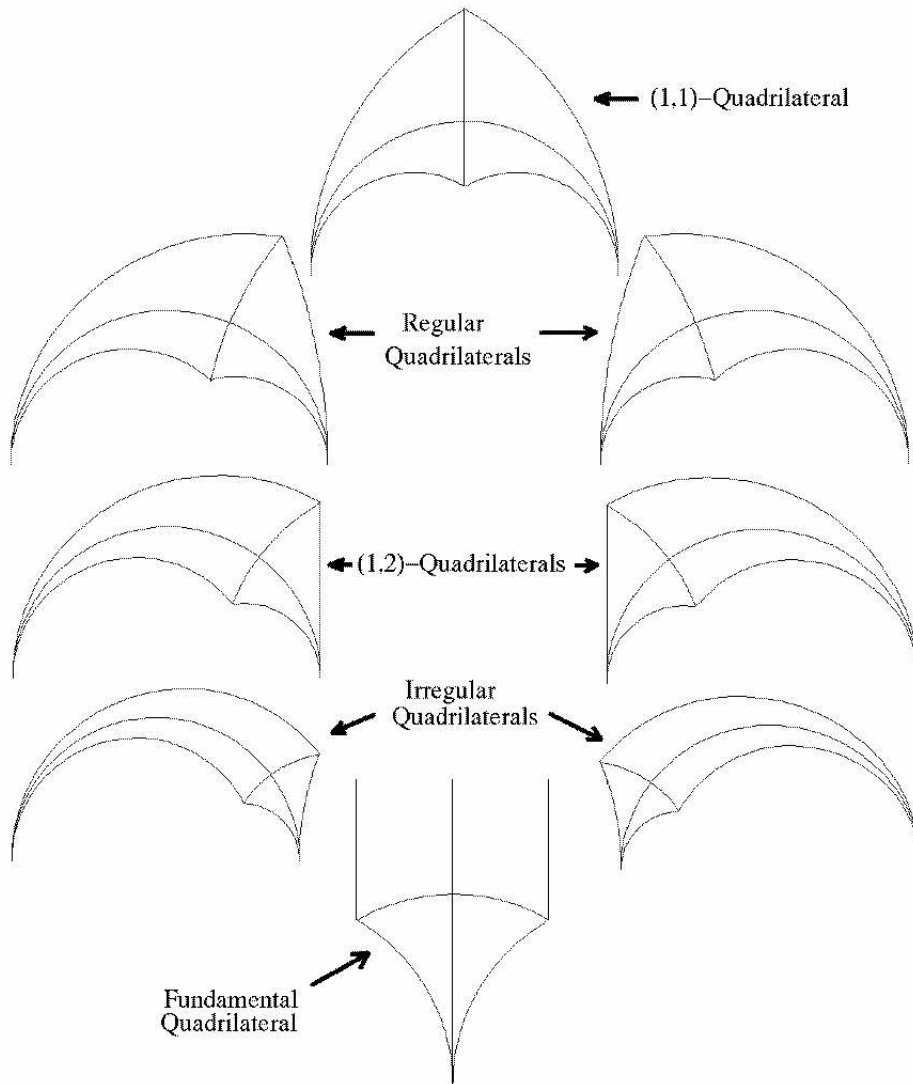
Figure 2.10: The Regular and Irregular Quadrilaterals.

Chapter 3

The First Family of Dynamical Systems

3.1 Definition of $P : \mathbb{T}^\infty \to \mathbb{T}^\infty$

We represent the apex of plant with the flat cylinder $\mathcal{C}'$. The interior of $\mathcal{C}'$ stands for the region where primordia have already formed and the boundary $\partial \mathcal{C}'$ stands for the apical ring where new primordia form. The primordia themselves are represented as particles in $\mathcal{C}'$. We assume one new primordium is produced periodically in time on the apex. As time progresses the apex grows leaving the previously formed primordia behind. This is represented by translating the particles upward (so in a sense the shoot is pointing upside down in the model). We let y denote the distance the points are translated by. This is a parameter of the system and it stands for the relative growth rate of the plant, i.e the rate of growth of plant tissue relative to the rate of primordia production.

In order to avoid changing the dimension of the state space over time we use an infinite dimensional system which means that there are an infinite number of particles in our system. This allows us to add new particles one at a time without altering the total. Of course actual plants only have a finite number of primordia. Later we will consider finite dimensional systems. We denote

the location of the jth particle by r_j. This particle lies on a circle which is parallel to $\partial\mathcal{C}'$ and at distance jy above it.

The angle between the jth particle and the $(j-1)$th particle is denoted by d_j which represents the divergence angle between primordia. Given a value for the parameter $y > 0$ we associate a particular configuration in the cylinder $\mathcal{C}'$ to the sequence of divergence angles $\{d_j \mid j \in \mathbb{N}\}$. Let θ_j be the angular position of r_j. Specifically we choose $\theta_0 = 0$ and $\theta_j = \sum_{k=0}^{j-1} d_j \bmod 1$. The starting configuration is $\{r_j = \theta_j + ijy \mid j \in \mathbb{N}\}$. Then we translate this up by distance y so that the particles lie at $\{r_j + iy = \theta_j + i(j+1)y \mid j \in \mathbb{N}\}$.

Denote the space of sequences of angles by $\mathbb{T}^\infty$. This is our state space and the sequence of angles $\{d_j\} \in \mathbb{T}^\infty$ represents the state of the developing apex. We want to use the following assumption derived from experimental evidence: The primordia produce a repulsive potential that causes the new primordium to form in the apical ring where that potential is lowest (recall Section 1.5.1). This is implemented as follows. We let each particle in the configuration produce a potential that dies off as a power of the distance from the particle. This is known as an homogeneous central potential. At any point $\zeta \in \mathcal{C}'\backslash\{r_j + iy\}$ we can define

$$X_p(\{d_j\}, \zeta) = \sup_{j \in \mathbb{N}}\{|r_j + iy - \zeta|^{-p}\} \quad p > 1$$

Since the configuration is a discrete set for any $\zeta \in \mathcal{C}'$ there is some $m \in \mathbb{N}$ such that $|r_m + iy - \zeta|^{-p} = X_p(\{d_j\}, \zeta)$. The point $r_m + iy$ is the location of a particle in the configuration that's closest to ζ. This point need not be unique. Essentially the point ζ only "feels" the repulsion of its nearest neighbor(s). The Voronoi cell of a particle at $r_j + iy$ is the set of all points in $\mathcal{C}'$ that are closer to $r_j + iy$ than to any other particle in the configuration. The value that the potential X_p takes on at any point ζ of $\mathcal{C}'$ is determined by which Voronoi cell ζ lies in. In the case where ζ lies on the boundary of a Voronoi cell we have a choice of more than one particle which controls the value of X_p, but of course the value of X_p is still uniquely determined.

We are particularly interested in the potential on the apical ring. Let $\phi \in \partial\mathcal{C}'$, when $X_p(\{d_j\}, \phi)$ has a unique absolute minimum on $\partial\mathcal{C}'$ denote it by ϕ^* (there is always at least one

absolute minima). The divergence angle is then $0 - \phi^* = -\phi^*$. Our dynamical system is given by the map $P : \mathbb{T}^\infty \to \mathbb{T}^\infty$ defined as

$$
\begin{aligned}
P_0(\{d_j\}) &= -\phi^* \\
P_j(\{d_j\}) &= d_{j-1} \qquad j \in \mathbb{Z}^+
\end{aligned}
$$

The map P is not defined on all of $\mathbb{T}^\infty$ because not every configuration leads to a unique absolute minimum on $\partial \mathcal{C}'$. One could make a choice between absolute minima when the situation arises. However no choice will make the map continuous. For that reason we refer to the points where the map is undefined as points of discontinuity.

3.2   Fixed Points of P

We now look at the fixed points of P. The condition $P(\{d_j\}) = \{d_j\}$ gives $d_j = -\phi^*$ $j \in \mathbb{N}$. In other words the divergence angles are all the same. The corresponding configuration $\{r_j\}$ is a half lattice Λ' and after translating the configuration up and adding the new particle the resulting configuration is just a copy of Λ' rotated by $-\phi^*$. To iterate again we rotate the configuration back so that $\theta_0 = 0$. Thus a necessary (but not sufficient) condition for a configuration to correspond to a fixed point of P is that it be a half spiral lattice. When $-\phi^* = \delta_1$ then the half spiral lattice will be a fixed point. To find the fixed points we focus on the space of spiral lattices $\mathbb{H}^*$ and make use of the notation from chapter 2. In particular the parameter y of the dynamical system, P, corresponds to the imaginary part of a point $z \in \mathbb{H}^*$ and $r_j = \lambda_j(z)$.

The Voronoi cells of $\Lambda + iy$ are convex polygons whose edges are the orthogonal bisectors of points in $\Lambda + iy$. For z in a fundamental quadrilateral or in a $(1,1)$-quadrilateral there is a single Voronoi cell that intersects $\partial \mathcal{C}'$ and the intersection is all of $\partial \mathcal{C}'$. The value of X_p has a single maximum at 0 which is the closest point of $\partial \mathcal{C}'$ to the particle at iy which generates the Voronoi cell. And X_p has a single minimum at $1/2$ which is the furthest point of $\partial \mathcal{C}'$ to iy. Points on the set of implicitly rhombic lattices in the fundamental quadrilateral are fixed points of P. For z in the

remaining quadrilaterals the intersection of a convex polygon with $\partial\mathcal{C}'$ is an arc and the collection of Voronoi cells intersects $\partial\mathcal{C}'$ in a finite collection of arcs. On each arc the value of X_p increases going inward from the end points and achieves a unique local maximum in the arc at the point closest to the particle generating the Voronoi cell. The local minima are therefore the end points of the arcs.

Proposition 3.2.1. *Let m be the largest integer such that the Voronoi cell of $\lambda_m + iy$ intersects $\partial\mathcal{C}'$. A tie for the absolute minimum of X_p on $\partial\mathcal{C}'$ can only occur at the end points of the arc where the Voronoi cell of λ_m intersects $\partial\mathcal{C}'$.*

Proof. If the Voronoi cell of $\lambda_k + iy$ intersects $\partial\mathcal{C}'$ then for $j \leq k$ the Voronoi cell of $\lambda_j + iy$ must intersect $\partial\mathcal{C}'$. This follows from the translational symmetry of the collection of Voronoi cells and the fact that $\lambda_j + iy$ is closer to $\partial\mathcal{C}'$ than $\lambda_k + iy$ when $j < k$. The Voronoi cells that intersect $\partial\mathcal{C}'$ form a contiguous collection of Voronoi cells, let the last one be generated by the particle at $\lambda_m + iy$. The absolute minima of X_p on $\partial\mathcal{C}'$ must must be an end point of the arc where this Voronoi cell intersects $\partial\mathcal{C}'$. A tie for the absolute minimum can only occur with the two end points of this arc. $\qquad\square$

We assume for the rest of Section (3.2) that m is the largest integer such that the Voronoi cell of λ_m intersects $\partial\mathcal{C}'$. Let $\lambda_n + iy$ be the starting location of a particle within $\Lambda + iy$ such that the shared boundary of the Voronoi cells for $\lambda_m + iy, \lambda_n + iy$ contains ϕ^*. For calculational purposes it is convenient to work with the untranslated lattice. We think of X_p as being generated by particles at the points $\{\lambda_j \mid j \in \mathbb{Z}^+\}$. Let φ_n denote the intersection of the orthogonal bisector of λ_m, λ_n with $\partial\mathcal{C}'$. When $\varphi_n = 0$ then the half lattice configuration, Λ', corresponds to a fixed point of P. We are also interested in the other end point of the arc where the Voronoi cell of λ_m intersects $\partial\mathcal{C}'$. When $(m, n) = (2, 1)$ this is $1 - \varphi_1$ and for $m > n$ with $(m, n) \neq (2, 1)$ this is on the shared boundary of the Voronoi cells for λ_{m-n} and λ_m. Denote this point by φ_{m-n}. If a tie for the absolute minimum of X_p occurs it is between the two intersection points, either φ_1 and $1 - \varphi_1$ or φ_n and φ_{m-n}.

φ_n is the intersection point of the orthogonal bisector of λ_m, λ_n with $\partial\mathcal{C}'$ and φ_{m-n} is the intersection point of the orthogonal bisector of λ_m, λ_{m-n} with $\partial\mathcal{C}'$. Writing this out we have the

pair of equations

$$\varphi_n = \frac{|\lambda_m|^2 - |\lambda_n|^2}{2(\delta_m - \delta_n)}$$

$$\varphi_{m-n} = \frac{|\lambda_m|^2 - |\lambda_{m-n}|^2}{2(\delta_m - \delta_{m-n})}$$

We can substitute $\delta_{m-n} = \delta_m - \delta_n$ to obtain

$$\varphi_n = \frac{|\lambda_m|^2 - |\lambda_n|^2}{2\delta_{m-n}} \tag{3.1}$$

$$\varphi_{m-n} = \frac{|\lambda_m|^2 - |\lambda_{m-n}|^2}{2\delta_n} \tag{3.2}$$

Proposition 3.2.2. *The configuration corresponding to a fixed point of P is an explicitly rhombic lattice*

Proof. If $\varphi_n = 0$ then $|\lambda_m| = |\lambda_n|$ and therefore the lattice Λ must be of the explicitly rhombic type within a (m, n)-quadrilateral. $\square$

So the set of fixed points of P is a subset of the set of explicitly rhombic lattices (see Figure 2.6 at the end of Section (2.3)).

3.2.1 The Discontinuities of P in $\mathbb{H}^*$

We now determine the points of discontinuity of the map P in the space of lattices $\mathbb{H}^*$.

Proposition 3.2.3. *The points of discontinuity in the $(2, 1)$-quadrilaterals lie on the intersection of the line $x = 1/2$ with the $(2, 1)$-quadrilateral.*

Proof. In the case $(m, n) = (2, 1)$ we get a tie when φ_1 and $1 - \varphi_1$ are equidistant to λ_2. This happens when λ_1 is on the opposite side of $\mathcal{C}'$ from λ_2, i.e. when the divergence angle is $1/2$ $\square$

When $m > n$ and $(m, n) \neq (2, 1)$ a discontinuity occurs when φ_n, φ_{m-n} tie for being the absolute minimum of X_p on $\partial \mathcal{C}'$. This happens when φ_n, φ_{m-n} are equidistant from λ_m. This condition leads to the following lemma.

Lemma 3.2.4. *If φ_n, φ_{m-n} are equidistant from λ_m then the projection of λ_m on $\partial \mathcal{C}'$ is exactly halfway between φ_n and φ_{m-n}.*

Proof.

$$\mid \lambda_m - \varphi_n \mid^2 \;=\; \mid \lambda_m - \varphi_{m-n} \mid^2 \Leftrightarrow$$

$$(\delta_m - \varphi_n)^2 + m^2 y^2 \;=\; (\delta_m - \varphi_{m-n})^2 + m^2 y^2 \Leftrightarrow$$

$$\delta_m^2 - 2\delta_m \varphi_n + \varphi_n^2 \;=\; \delta_m^2 - 2\delta_m \varphi_{m-n} + \varphi_{m-n}^2 \Leftrightarrow$$

$$\varphi_n^2 - \varphi_{m-n}^2 \;=\; 2\delta_m(\varphi_n - \varphi_{m-n}) \Leftrightarrow$$

$$\varphi_n + \varphi_{m-n} \;=\; 2\delta_m \tag{3.3}$$

Consequently the projection of λ_m onto $\partial \mathcal{C}'$ lies exactly halfway in between φ_n and φ_{m-n}. $\qquad\square$

We can use this lemma to determine points of discontinuity. This is done in the following proposition.

Proposition 3.2.5. *For each m, n with $m > n$ and $(m, n) \neq (2, 1)$ the map P is discontinuous in $\mathbb{H}^*$ at the intersection of the (m, n)-quadrilaterals with the cubic curves:*

$$(3mn(m-n)x - 3mn(\Delta_m - \Delta_n) \pm (m+n)) y^2 =$$

$$(mx - \Delta_m)(nx - \Delta_n)((m-n)x - (\Delta_m - \Delta_n)) \tag{3.4}$$

Proof. Equation (3.3) determines an algebraic curve in $\mathbb{H}^*$ as follows. When we are in a (m, n)-quadrilateral we can use Equations (3.1) and (3.2) to get

$$\varphi_n + \varphi_{m-n} \;=\; \frac{\mid \lambda_m \mid^2 - \mid \lambda_n \mid^2}{2\delta_{m-n}} + \frac{\mid \lambda_m \mid^2 - \mid \lambda_{m-n} \mid^2}{2\delta_n} \Leftrightarrow$$

$$\varphi_n + \varphi_{m-n} \;=\; \frac{(\delta_n + \delta_{m-n}) \mid \lambda_m \mid^2 - \delta_n \mid \lambda_n \mid^2 - \delta_{m-n} \mid \lambda_{m-n} \mid^2}{2\delta_n \delta_{m-n}}$$

Using $\delta_m = \delta_n + \delta_{m-n}$ we get

$$\varphi_n + \varphi_{m-n} \;=\; \frac{\delta_m \mid \lambda_m \mid^2 - \delta_n \mid \lambda_n \mid^2 - \delta_{m-n} \mid \lambda_{m-n} \mid^2}{2\delta_n \delta_{m-n}}$$

which we can then substitute into Equation (3.3) to obtain the equation

$$\frac{\delta_m \mid \lambda_m \mid^2 - \delta_n \mid \lambda_n \mid^2 - \delta_{m-n} \mid \lambda_{m-n} \mid^2}{2\delta_n \delta_{m-n}} = 2\delta_m$$

Multiplying the denominator times both sides gives

$$\delta_m \mid \lambda_m \mid^2 -\delta_n \mid \lambda_n \mid^2 -\delta_{m-n} \mid \lambda_{m-n} \mid^2 = 4\delta_m \delta_n \delta_{m-n}$$

Writing the moduli of the λ's in terms of their real and imaginary parts gives

$$\delta_m(\delta_m^2 + m^2 y^2) - \delta_n(\delta_n^2 + n^2 y^2) - \delta_{m-n}(\delta_{m-n}^2 + (m-n)^2 y^2) = 4\delta_m \delta_n \delta_{m-n} \quad \Leftrightarrow$$

$$\left(\delta_m m^2 - \delta_n n^2 - \delta_{m-n}(m-n)^2\right) y^2 = 4\delta_m \delta_n \delta_{m-n} - \delta_m^3 + \delta_n^3 + \delta_{m-n}^3 \quad \Leftrightarrow$$

$$\left(\delta_m m^2 - \delta_n n^2 - \delta_{m-n}(m-n)^2\right) y^2 = 4\delta_m \delta_n (\delta_m - \delta_n) - \delta_m^3 + \delta_n^3 + (\delta_m - \delta_n)^3 \quad \Leftrightarrow$$

$$\left(2\delta_m mn - \delta_m n^2 + \delta_n m^2 - 2\delta_n mn\right) y^2 = \delta_m \delta_n \delta_{m-n}$$

Now recall from section 2.4 that $\delta_m = mx - \Delta_m$, $\delta_n = nx - \Delta_n$ and $\delta_{m-n} = (m-n)x - (\Delta_m - \Delta_n)$ which we can substitute in

$$\left(2(mx - \Delta_m)mn - (mx - \Delta_m)n^2 + (nx - \Delta_n)m^2 - 2(nx - \Delta_n)mn\right) y^2 =$$

$$(mx - \Delta_m)(nx - \Delta_n)((m-n)x - (\Delta_m - \Delta_n)) \Leftrightarrow$$

$$\left(3mn(m-n)x - 3mn(\Delta_m - \Delta_n) + (m+n)(\Delta_m n - \Delta_n m)\right) y^2 =$$

$$(mx - \Delta_m)(nx - \Delta_n)((m-n)x - (\Delta_m - \Delta_n))$$

Therefore we have a tie with φ_n and φ_{m-n} if and only if $x + iy$ sits in a (m,n)-quadrilateral and satisfies the above equation Recall from the proof of Proposition (2.4.1) that either $\Delta_m = D_m$ and $\Delta_n = D_n$ or $\Delta_m = m - D_m$ and $\Delta_n = n - D_n$ according to whether we are in positive or negative (m,n)-quadrilateral. Therefore $\Delta_m n - \Delta_n m = \pm 1$ and we get Equation (3.4). $\qquad \square$

A brute force computer generated plot of the points of discontinuity in $\mathbb{H}^*$ is shown in Figure 3.1.

3.2.2 Bifurcation Diagram for P

A half spiral lattice corresponds to a fixed point of P when φ_n is zero and is further from λ_m than φ_{m-n} is. We know from Proposition (3.2.2) that $\varphi_n = 0$ when the lattice is explicitly rhombic.
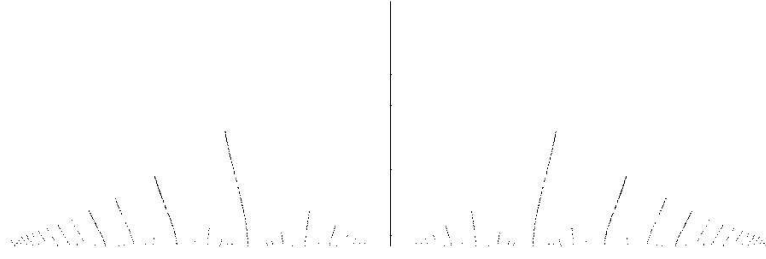
Figure 3.1: The Curves of Discontinuity for the Map P

We want to determine where on the set of explicitly rhombic lattices there are discontinuities in the map P.

Proposition 3.2.6. *If the diagonal of explicitly rhombic lattices in a (m, n)-quadrilateral intersects the curve of discontinuity in the (m, n)-quadrilateral it must be at the point*

$$x + iy = \frac{m(2\Delta_m + \Delta_n) - n(2\Delta_n + \Delta_m)}{2(m^2 - n^2)} + i\frac{\sqrt{3}}{2(m^2 - n^2)}$$

Proof. We are interested in the intersection of the curve where λ_m and λ_n are equal distant to 0 (i.e. the diagonal of explicitly rhombic lattices) with the curve where φ_n and φ_{m-n} are equidistant to λ_m (i.e. Equation (3.4)). At the intersection point of these two curves $\varphi = 0$ and φ_{m-n} are equidistant to λ_m. So the curve where 0 and φ_{m-n} are equidistant to λ_m must also pass through this point. Therefore to find this intersection point we intersect the curve where 0 and φ_{m-n} are equidistant to λ_m with the diagonal of explicitly rhombic lattices.

The set of points where 0 and φ_{m-n} are equal distant to λ_m is given by the equality

$$
\begin{aligned}
\mid \lambda_m - \varphi_{m-n} \mid^2 &= \mid \lambda_m - 0 \mid^2 \Leftrightarrow \\
(\delta_m - \varphi_{m-n})^2 + m^2 y^2 &= \delta_m^2 + m^2 y^2 \Leftrightarrow \\
-2\delta_m \varphi_{m-n} + \varphi_{m-n}^2 &= 0 \Leftrightarrow \\
\varphi_{m-n} &= 2\delta_m
\end{aligned}
$$

Now substitute in Equation (3.2)

$$\frac{\mid \lambda_m \mid^2 - \mid \lambda_{m-n} \mid^2}{2\delta_n} = 2\delta_m \Leftrightarrow$$

$$| \lambda_m |^2 - | \lambda_{m-n} |^2 = 4\delta_m\delta_n \Leftrightarrow$$

$$\delta_m^2 - (\delta_m - \delta_n)^2 + (m^2 - (m - n)^2)y^2 = 4\delta_m\delta_n \Leftrightarrow$$

$$2\delta_m\delta_n - \delta_n^2 + (2mn - n^2)y^2 = 4\delta_m\delta_n$$

Adding $\delta_n^2 - 2\delta_m\delta_n$ to both sides

$$n(2m - n)y^2 = \delta_n^2 + 2\delta_m\delta_n \Leftrightarrow$$

$$n(2m - n)y^2 = \delta_n(2\delta_m + \delta_n)$$

Now we substitute $\delta_m = mx - \Delta_m$ and $\delta_n = nx - \Delta_n$

$$n(2m - n)y^2 = (nx - \Delta_n)((2m + n)x - (2\Delta_m + \Delta_n)) \Leftrightarrow$$

$$\frac{2m - n}{2m + n}y^2 = (x - \frac{\Delta_n}{n})(x - \frac{2\Delta_m + \Delta_n}{2m + n}) \tag{3.5}$$

This is the equation for a hyperbola. We want to find the intersection of this hyperbola with the diagonal of explicitly rhombic lattices. From Section (2.4) we know that this is the image of the corresponding diagonal of the fundamental quadrilateral under either g_{mn}^+ or g_{mn}^-. The diagonal of explicitly rhombic lattices in the fundamental quadrilateral is the unit circle which has equation $0 = y^2 + (x - 1)(x + 1)$. Applying g_{mn}^+ to the ideal vertices gives $\frac{D_m - D_n}{m - n}$ and $\frac{D_m + D_n}{m + n}$ while applying g_{mn}^- to the ideal vertices gives $\frac{(m - D_m) - (n - D_n)}{m - n}$ and $\frac{(m - D_m) + (n - D_n)}{m + n}$. Recall the proof of Proposition (2.4.1) once again. In a positive (m, n)-quadrilateral $\Delta_m = D_m$ and $\Delta_n = D_n$. In a negative (m, n)-quadrilateral $\Delta_m = m - D_m$ and $\Delta_n = n - D_n$ so we can write the equation for the diagonal of explicitly rhombic lattices in a positive or negative (m, n)-quadrilateral as

$$0 = y^2 + (x - \frac{\Delta_m - \Delta_n}{m - n})(x - \frac{\Delta_m + \Delta_n}{m + n})$$

We can rewrite these two equations

$$0 = -(2m - n)y^2 + (2m + n)(x - \frac{\Delta_n}{n})(x - \frac{2\Delta_m + \Delta_n}{2m + n})$$

$$0 = (2m - n)y^2 + (2m - n)(x - \frac{\Delta_m - \Delta_n}{m - n})(x - \frac{\Delta_m + \Delta_n}{m + n})$$

Adding these two equations together gives

$$
\begin{aligned}
0 &= (2m+n)(x - \frac{\Delta_n}{n})(x - \frac{2\Delta_m + \Delta_n}{2m+n}) + (2m-n)(x - \frac{\Delta_m - \Delta_n}{m-n})(x - \frac{\Delta_m + \Delta_n}{m+n}) \Leftrightarrow \\
0 &= 4mx^2 - \frac{2\Delta_m n + 2\Delta_n m + 2\Delta_n n}{n}x + \frac{\Delta_n}{n}(2\Delta_m + \Delta_n) \\
&\quad -(2m-n)\frac{2\Delta_m m - 2\Delta_n n}{m^2 - n^2}x + (2m-n)\frac{\Delta_m^2 - \Delta_n^2}{m^2 - n^2}
\end{aligned}
$$

Multiplying through by $n(m^2 - n^2)$ gives

$$
\begin{aligned}
0 &= 4mn(m^2 - n^2)x^2 - (m^2 - n^2)(2\Delta_m n + 2\Delta_n m + 2\Delta_n n)x + \Delta_n(2\Delta_m + \Delta_n)(m^2 - n^2) \\
&\quad -n(2m-n)(2\Delta_m m - 2\Delta_n n)x + n(2m-n)(\Delta_m^2 - \Delta_n^2) \Leftrightarrow \\
0 &= 4mn(m^2 - n^2)x^2 - (2\Delta_m m^2 n + 2\Delta_n m^3 + 2\Delta_n m^2 n - 2\Delta_m n^3 - 2\Delta_n m^2 n - 2\Delta_n n^3)x \\
&\quad + (2\Delta_m^2 mn - 2\Delta_n^2 mn - \Delta_m^2 n^2 + \Delta_n^2 n^2) - (4\Delta_m m^2 n - 4\Delta_n mn^2 - 2\Delta_m mn^2 + 2\Delta_n n^3)x \\
&\quad + (2\Delta_m \Delta_n m^2 - 2\Delta_m \Delta_n n^2 + \Delta_n^2 m^2 - \Delta_n^2 n^2) \Leftrightarrow \\
0 &= 4mn(m^2 - n^2)x^2 - (6\Delta_m m^2 n - 2\Delta_m mn^2 - 2\Delta_m n^3 + 2\Delta_n m^3 + 2\Delta_n m^2 n - 6\Delta_n mn^2)x \\
&\quad + (2\Delta_m^2 mn - \Delta_m^2 n^2 + 2\Delta_m \Delta_n m^2 - 2\Delta_m \Delta_n n^2 + \Delta_n^2 m^2 - 2\Delta_n^2 mn) \\
0 &= 4mn(m^2 - n^2)x^2 - (2(m^2 - n^2)(\Delta_m n + \Delta_n m) + 2mn(2\Delta_m m - \Delta_m n - 2\Delta_n n + \Delta_n m))x \\
&\quad + (\Delta_m n + \Delta_n m)(2\Delta_m m - \Delta_m n - 2\Delta_n n + \Delta_n m) \Leftrightarrow \\
0 &= (2mnx - (\Delta_m n + \Delta_n m))(2(m^2 - n^2)x - (2\Delta_m m - \Delta_m n - 2\Delta_n n + \Delta_n m))
\end{aligned}
$$

Substituting

$$
x = \frac{\Delta_m n + \Delta_n m}{2mn}
$$

into either Equation (3.5) or (3.6) gives an imaginary value for y. Substituting

$$
x = \frac{m(2\Delta_m + \Delta_n) - n(2\Delta_n + \Delta_m)}{2(m^2 - n^2)}
$$

into either Equation (3.5) or (3.6) gives

$$
y^2 = \frac{3(\Delta_m n - \Delta_n m)^2}{4(m^2 - n^2)^2}
$$

We know $\Delta_m n - \Delta_n m = \pm 1$ so

$$
y = \frac{\sqrt{3}}{2(m^2 - n^2)}
$$

This can be substituted back into Equation (3.4) to verify that it is indeed a point of discontinuity of P. $\qquad\square$

These points of discontinuity were derived by Douady [11] using a disk packing argument. These points are a good approximation of the discontinuity seen in numerical simulations. However Douady left open the possibility that other points of discontinuity could exist. For example he conjectured Lemma (3.2.1). Now we want to see if this intersection point actually lies in the (m, n)-quadrilateral.

Proposition 3.2.7. *The point*

$$x + iy = \frac{m(2\Delta_m + \Delta_n) - n(2\Delta_n + \Delta_m)}{2(m^2 - n^2)} + i\frac{\sqrt{3}}{2(m^2 - n^2)}$$

lies in a (m, n)-quadrilateral if and only if the quadrilateral is irregular.

Proof. The vertices $g_{mn}^{\pm}(C), g_{mn}^{\pm}(D)$ of the (m, n)-quadrilateral are the end points of the diagonal of explicitly rhombic lattices in the (m, n)-quadrilateral. From Equations (2.8) and (2.9) the real parts of these vertices are

$$Re(g_{mn}(C)) = \frac{2\Delta_n n - \Delta_m n - \Delta_n m + 2\Delta_m m}{2(n^2 - mn + m^2)}$$

$$Re(g_{mn}(D)) = \frac{2\Delta_n n + \Delta_m n + \Delta_n m + 2\Delta_m m}{2(n^2 + mn + m^2)}$$

The point

$$x + iy = \frac{m(2\Delta_m + \Delta_n) - n(2\Delta_n + \Delta_m)}{2(m^2 - n^2)} + i\frac{\sqrt{3}}{2(m^2 - n^2)}$$

will lie in the (m, n) quadrilateral if and only if if the real part of this point is between the real parts of the vertices $g_{mn}^{\pm}(C), g_{mn}^{\pm}(D)$. This happens when $Re(g_{mn}^{\pm}(C)) - x$ and $Re(g_{mn}^{\pm}(D)) - x$ have opposite signs so we compute these quantities.

$$Re(g_{mn}^{\pm}(C)) - x = \frac{2\Delta_n n - \Delta_m n - \Delta_n m + 2\Delta_m m}{2(n^2 - mn + m^2)} - \frac{m(2\Delta_m + \Delta_n) - n(2\Delta_n + \Delta_m)}{2(m^2 - n^2)} \Leftrightarrow$$

$$Re(g_{mn}^{\pm}(C)) - x =$$

$$\frac{(2\Delta_n n - \Delta_m n - \Delta_n m + 2\Delta_m m)(m^2 - n^2) - (m(2\Delta_m + \Delta_n) - n(2\Delta_n + \Delta_m))(n^2 - mn + m^2)}{2(n^2 - mn + m^2)(m^2 - n^2)}$$

Expanding the numerator of this we get

$$2\Delta_n m^2 n - \Delta_m m^2 n - \Delta_n m^3 + 2\Delta_m m^3$$

$$-2\Delta_n n^3 + \Delta_m n^3 + \Delta_n mn^2 - 2\Delta_m mn^2$$

$$-2\Delta_m mn^2 - \Delta_n mn^2 + 2\Delta_n n^3 + \Delta_m n^3$$

$$+2\Delta_m m^2 n + \Delta_n m^2 n - 2\Delta_n mn^2 - \Delta_m mn^2$$

$$-2\Delta_m m^3 - \Delta_n m^3 + 2\Delta_n m^2 n + \Delta_m m^2 n$$

$$= +2\Delta_m m^2 n - 5\Delta_m mn^2 + 2\Delta_m n^3 - 2\Delta_n m^3 + 5\Delta_n m^2 - 2\Delta_n mn^2$$

$$= -\Delta_m n(2m - n)(2n - m) + \Delta_n m(2m - n)(2n - m)$$

$$= -(2m - n)(2n - m)(\Delta_m n - \Delta_n m)$$

For $Re(g_{mn}^{\pm}(D)) - x$ we get

$$Re(g_{mn}^{\pm}(D)) - x = \frac{2\Delta_n n + \Delta_m n + \Delta_n m + 2\Delta_m m}{2(n^2 + mn + m^2)} - \frac{m(2\Delta_m + \Delta_n) - n(2\Delta_n + \Delta_m)}{2(m^2 - n^2)} \Leftrightarrow$$

$$Re(g_{mn}^{\pm}(D)) - x =$$

$$\frac{(2\Delta_n n + \Delta_m n + \Delta_n m + 2\Delta_m m)(m^2 - n^2) - (m(2\Delta_m + \Delta_n) - n(2\Delta_n + \Delta_m)(n^2 + mn + m^2)}{2(n^2 + mn + m^2)(m^2 - n^2)}$$

Expanding the numerator again we get

$$2\Delta_n m^2 n + \Delta_m m^2 n + \Delta_n m^3 + 2\Delta_m m^3$$

$$-2\Delta_n n^3 - \Delta_m n^3 - \Delta_n mn^2 - 2\Delta_m mn^2$$

$$-2\Delta_m mn^2 - \Delta_n mn^2 + 2\Delta_n n^3 + \Delta_m n^3$$

$$-2\Delta_m m^2 n - \Delta_n m^2 n + 2\Delta_n mn^2 + \Delta_m mn^2$$

$$-2\Delta_m m^3 - \Delta_n m^3 + 2\Delta_n m^2 n + \Delta_m m^2 n$$

$$= -3\Delta_m mn^2 + 3\Delta_n m^2 n$$

$$= -3mn(\Delta_m n - \Delta_n m)$$

The quantities $Re(g_{mn}^{\pm}(C)) - x$ and $Re(g_{mn}^{\pm}(D)) - x$ have opposite signs when their product is

negative.

$$(Re(g_{mn}(C)) - x)(Re(g_{mn}(D)) - x) = \frac{3mn(2m - n)(2n - m)(\Delta_m n - \Delta_n m)^2}{4(n^2 - mn + m^2)(n^2 + mn + m^2)(m^2 - n^2)^2}$$

The factors $n^2 - mn + m^2$ is a positive definite quadratic forms in m, n so it is positive when m, n are not zero. The factors that are squared are all positive and since m, n are positive both mn and $n^2 + mn + m^2$ are positive. So the whole product is negative if and only if $(2m - n)(2n - m)$ is negative which means that the (m, n)-quadrilateral is irregular. $\qquad\square$

From this proposition we can conclude that 0 is the absolute minimum of X_p on $\partial \mathcal{C}'$ for either all points or none of the points on the diagonal of explicitly rhombic lattices in a regular or $(1, 1)$-quadrilateral. On the other hand in a irregular quadrilateral 0 is the absolute minimum of X_p on $\partial \mathcal{C}'$ for part of the diagonal but it is not clear at this point which part. We now resolve these ambiguities.

Theorem 2. *The diagonal of explicitly rhombic lattices of regular quadrilaterals and the $(1, 1)$- quadrilateral are fixed points of P. That portion of the diagonal of explicitly rhombic lattices of irregular quadrilaterals below the intersection point with Equation (3.4) are also fixed points.*

Proof. We want to check when φ_n is closer to λ_m than φ_{m-n}. The point of discontinuity on the diagonal is at the intersection point of Equations (3.4) and (3.5). As we move along the diagonal away from the intersection point $\varphi_n = 0$ and so either $\varphi_n = 0$ gets closer or further away from λ_m than φ_{m-n}. So we determine on which side of the intersection point we have 0 closer to λ_m than φ_{m-n}. Writing this conditions out we have

$$| \lambda_m - 0 |^2 > | \lambda_m - \varphi_{m-n} |^2 \Leftrightarrow$$

$$\delta_m^2 + m^2 y^2 > (\delta_m - \varphi_{m-n})^2 + m^2 y^2 \Leftrightarrow$$

$$\delta_m^2 > \delta_m^2 - 2\delta_m \varphi_{m-n} + \varphi_{m-n}^2 \Leftrightarrow$$

$$2\delta_m \varphi_{m-n} > \varphi_{m-n}^2$$

Now when $\varphi_{m-n} > 0$ we get

$$2\delta_m \quad > \quad \varphi_{m-n}$$

We can substitute in Equation (3.2) to get

$$2\delta_m > \frac{\mid \lambda_m \mid^2 - \mid \lambda_{m-n} \mid^2}{2\delta_n}$$

Since φ_{m-n} and δ_n are on opposite sides of 0 we get

$$4\delta_m\delta_n \quad < \quad \mid \lambda_m \mid^2 - \mid \lambda_{m-n} \mid^2$$

Since φ_{m-n} and δ_n are on opposite sides we get the same result when $\varphi_{m-n} < 0$ as when $\varphi_{m-n} > 0$.

Expanding this result gives

$$4\delta_m\delta_n \quad < \quad \delta_m^2 + m^2y^2 - \delta_{m-n}^2 - (m-n)^2y^2 \Leftrightarrow$$

$$4\delta_m\delta_n \quad < \quad \delta_m^2 - (\delta_m - \delta_n)^2 + (m^2 - (m-n)^2)y^2 \Leftrightarrow$$

$$4\delta_m\delta_n \quad < \quad 2\delta_m\delta_n - \delta_n^2 + (2mn - n^2)y^2$$

Adding $\delta_n^2 - 2\delta_m\delta_n$ to both sides

$$\delta_n^2 + 2\delta_m\delta_n \quad < \quad n(2m - n)y^2 \Leftrightarrow$$

$$\delta_n(2\delta_m + \delta_n) \quad < \quad n(2m - n)y^2$$

Now we substitute $\delta_m = mx - \Delta_m$ and $\delta_n = nx - \Delta_n$ in

$$(nx - \Delta_n)((2m + n)x - (2\Delta_m + \Delta_n)) \quad < \quad n(2m - n)y^2$$

$$(x - \frac{\Delta_n}{n})(x - \frac{2\Delta_m + \Delta_n}{2m + n}) \quad < \quad \frac{2m - n}{2m + n}y^2 \tag{3.6}$$

Also recall from section 2.4.1 that the Equation for the bottom edge of a (m, n)-quadrilateral is

$$0 = y^2 + (x - \frac{\Delta_n}{n})(x - \frac{2\Delta_m + \Delta_n}{2m + n}) \tag{3.7}$$

Inequality (3.6) is the region between two branches of a hyperbola which intersects $\partial\mathcal{C}'$ in the same points as the circle in Equation (3.6). For a regular quadrilateral or a $(1, 1)$-quadrilateral the

projection of the diagonal of rhombic lattices is between these two points. Consequently $\varphi^* = 0$ is an absolute minimum. For an irregular quadrilateral only the bottom end point of the diagonal lies in this region. Therefore $\varphi_n = 0$ is an absolute minimum for lattices corresponding to points between the intersection of Equation (3.4) with the diagonal and the bottom end point of the diagonal. $\quad\square$
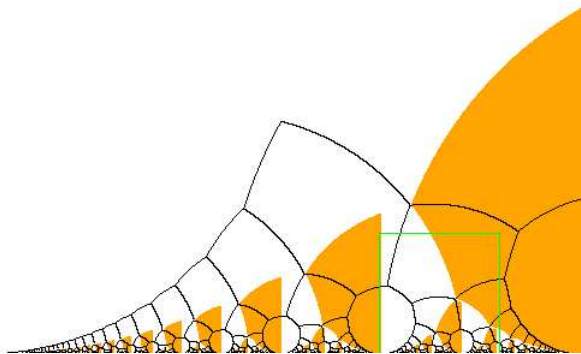
Figure 3.2: The Local Extrema of X_p and the (m, n)-Hexagons

We are now prepared to describe the bifurcation diagram in $\mathbb{H}^*$. In Figure (2) we see the (m, n)-hexagons in the "left half" of $\mathbb{H}^*$. The shaded regions of the diagram correspond to lattices such that the potential function X_p is positive at 0. The lattices such that X_p has a local minimum at 0 lie on the boundary of the shaded regions. From Theorem (2) we know that the points on the diagonals of the regular hexagons are fixed points. The union of these diagonals forms a continuous curve inside a regular region. Above each regular region is either an irregular quadrilateral or a $(2, 1)$-quadrilateral. In the irregular quadrilateral we know from Theorem (2) that the points on the lower portion of the diagonal are fixed points. These join up with the curve of fixed points in the regular regions to form an entire branch of fixed points of P. For a $(2, 1)$-quadrilateral the points of discontinuity lie on the edge of the quadrilateral (see proposition (3.2.3)). This intersects the

diagonal at the top vertex of the quadrilateral. This diagonal joins the curve of fixed points in the regular region below the $(2, 1)$-quadrilateral to form another branch of fixed points of P. This is shown in Figure (2) for the "left half" of $\mathbb{H}^*$.
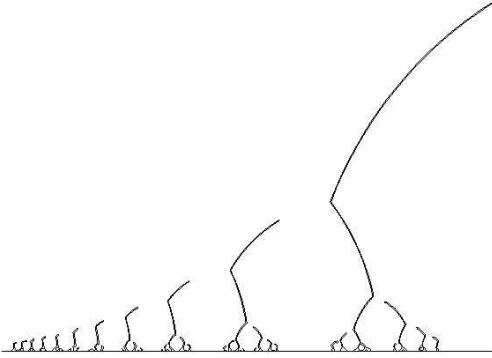
Figure 3.3: The Bifurcation Diagram of P

Recall from the beginning of this chapter that the edge of implicitly rhombic lattices in the fundamental quadrilateral are fixed points. There are no points of discontinuity in the fundamental quadrilateral because there is only one local minimum for X_p on $\partial \mathcal{C}'$. The edge of implicitly rhombic lattices in the fundamental quadrilateral are fixed points. These join up with the diagonal of explicitly rhombic fixed points in the $(1, 1)$-quadrilateral. This in turn meets the point of discontinuity at the top vertex of the $(2, 1)$-quadrilaterals. This superficially resembles a pitchfork bifurcation but in fact it is just three branches of fixed points that share an endpoint at a point of discontinuity. In conclusion we have a branch of fixed points corresponding to each regular region and one more branch of fixed points contained in the line $x = 1/2$.

3.3 Spectral Stability of the Fixed Points

The spiral configurations are well known in plants and they emerge naturally from the dynamical system. Plant development in nature is somewhat exposed to the environment so we also need to show that the fixed points of the dynamical system are stable. This is done in the following

theorem.

Theorem 3. *The fixed points of P are spectrally stable*

Proof. Let $\lambda_m, \lambda_n \in \mathcal{C}'$ with $m > n$ be the starting location of a pair of particles within $\Lambda + iy$ such that the boundaries of their Voronoi cells contain ϕ^*. So ϕ^* is the intersection point of the orthogonal bisector of $\lambda_m + iy, \lambda_n + iy$ with $\partial\mathcal{C}'$.

For $j > 0$ the partial derivatives are $\dfrac{\partial P_j}{\partial d_k} = \dfrac{\partial d_{j-1}}{\partial d_k}$ which is 1 when $k = j - 1$ and 0 otherwise. For $\dfrac{\partial P_0}{\partial d_k}$ we have to consider how ϕ^* varies with d_k.

Recall that $\lambda_m = \delta_m + imy, \lambda_n = \delta_n + iny$. The intersection point of the orthogonal bisector of $\lambda_m + iy, \lambda_n + iy$ with $\partial\mathcal{C}'$ is

$$\phi^* = \frac{\mid \lambda_m + iy \mid^2 - \mid \lambda_n + iy \mid^2}{2(\delta_m - \delta_n)}$$

To compute $\dfrac{\partial\phi^*}{\partial d_j}$ it is convenient to rewrite this as

$$\begin{aligned}
\phi^* &= \frac{\delta_m^2 + (m+1)^2 y^2 - \delta_n^2 - (n+1)^2 y^2}{2(\delta_m - \delta_n)} \\
&= \frac{\delta_m^2 - \delta_n^2}{2(\delta_m - \delta_n)} + \frac{((m+1)^2 - (n+1)^2) y^2}{2(\delta_m - \delta_n)} \\
&= \frac{1}{2}(\delta_m + \delta_n) + \frac{(m-n)(m+n+2) y^2}{2(\delta_m - \delta_n)} \\
&= \frac{1}{2}\left(\sum_{k=0}^{m-1} d_k + \sum_{k=0}^{n-1} d_k\right) + \frac{(m-n)(m+n+2) y^2}{2\sum_{k=n}^{m-1} d_k}
\end{aligned}$$

There are three cases for $\dfrac{\partial\phi^*}{\partial d_j}$ according to whether $j < n$, $n \leq j < m$, or $m \leq j$. When $j < n$ we have $\dfrac{\partial\phi^*}{\partial d_j} = \dfrac{1}{2}(1+1) = 1$ and therefore $\dfrac{\partial P_0}{\partial d_j} = -1$. This also follows from the fact that when we change d_j for $j < n$ we rotate λ_m, λ_n by equal amounts so that ϕ^* is rotated by the same amount. When $m \leq j$ the $\dfrac{\partial P_0}{\partial d_j} = -\dfrac{\partial\phi^*}{\partial d_j} = 0$. This also follows from the fact that changing d_j for $j \geq m$ has no effect on the location of λ_m, λ_n.

When $n \leq j < m$

$$\begin{aligned}
\frac{\partial\phi^*}{\partial d_j} &= \frac{1}{2}(1) - \frac{(m-n)(m+n+2) y^2}{2\left(\sum_{k=n}^{m-1} d_k\right)^2} \\
&= \frac{1}{2} - \frac{(m-n)(m+n+2) y^2}{2(\delta_m - \delta_n)^2}
\end{aligned}$$

This value is the same for any j satisfying inequality $n \leq j < m$ so we denote this value by a. As we rotate λ_m with respect to λ_n ϕ^* will follow so a is positive and it is less than $1/2$ since $m > n$. In other words rotating λ_m with respect to λ_n rotates ϕ^* less than half the amount.

So the differential of the map P is a matrix of the form:

$$\begin{pmatrix} -1 & \cdots & \cdots & -1 & -a & \cdots & -a & 0 & \cdots & 0 \\ 1 & 0 & \cdots & \cdots & \cdots & \cdots & \cdots & \cdots & \cdots & 0 \\ 0 & 1 & 0 & \cdots & \cdots & \cdots & \cdots & \cdots & \cdots & 0 \\ 0 & 0 & 1 & 0 & \cdots & \cdots & \cdots & \cdots & \cdots & 0 \\ & & & \ddots & \ddots & \ddots & & & & \\ & & & & \ddots & \ddots & \ddots & & & \\ & & & & & \ddots & \ddots & \ddots & & \\ & & & & & & \ddots & \ddots & \ddots & \\ & & & & & & & \ddots & \ddots & \ddots \\ & & & & & & & 0 & 1 & 0 \end{pmatrix}$$

where the first $-a$ term occurs at column $n - 1$ and the last $-a$ term appears at column $m - 1$.

The first $m - 1$ columns of the matrix representing the linearized map determine the non-zero members of its spectrum. This upper $m - 1 \times m - 1$ block of the matrix has the form of a rational canonical matrix with the entries reflected about the non-main diagonal. This type of reflection does not change the characteristic polynomial of the matrix. The characteristic Equation is

$$\sigma^{m-1} + \sigma^{m-2} + \ldots \sigma^{m-n} + a\sigma^{m-n-1} + a\sigma^{m-n-2} + \ldots + a = 0 \tag{3.8}$$

Note that since all the coefficients are positive none of the roots of the polynomial can be positive real numbers. We want to show that the roots of the characteristic polynomial have modulus less than 1. We do this in two steps. First by showing that the modulus of the roots are not greater than 1 and then by showing that the modulus of the roots are not equal to 1. First multiply both

sides of Equation (3) by $\sigma - 1$ to get

$$\sigma^m + (a-1)\sigma^{m-n} - a = 0$$

which we can rewrite as

$$\sigma^m - a = (1-a)\sigma^{m-n}$$

The set $S_1 = \{\sigma^m - a : \mid \sigma \mid = s\}$ where s is a positive real number is a circle of radius s^m about the point $-a$ and the set $S_2 = \{(1-a)\sigma^{m-n} : \mid \sigma \mid = s\}$ is a circle of radius $(1-a)s^{m-n}$ about 0. The intersection of these two circles is a necessary (but not sufficient) condition for a root with modulus s to exist.

We want to show that when $s > 1$ all the points on the circle S_1 have larger modulus than the points on the circle S_2. From this we can conclude there are no roots with modulus greater than 1. The point on the circle S_1 with the smallest modulus is $s^m - a$ while all the points on the circle S_2 have modulus $(1-a)s^{m-n}$. So we want to show

$$s^m - a > (1-a)s^{m-n}$$

$$s^m + (a-1)s^{m-n} - a > 0$$

$$(s^{m-1} + s^{m-2} + \ldots s^{m-n} + as^{m-n-1} + as^{m-n-2} + \ldots + a)(s-1) > 0$$

The first factor is positive when $s > 0$ and the second is positive when $s > 1$. Thus when $s > 1$ the product is indeed positive. Therefore the two circles don't intersect and there are no roots with modulus greater than 1.

Now suppose $s = 1$, then the point on the circle S_1 with the smallest modulus is $1 - a$ while all the points on the circle S_2 have modulus $1 - a$. Thus the two circles intersect at exactly one point $1 - a$. We have to check now if this intersection point actually yields a root for the characteristic polynomial. So we look for some σ such that

$$\sigma^m - a = 1 - a = (1-a)\sigma^{m-n}$$

$$\sigma^m = 1 \text{ and } \sigma^{m-n} = 1$$

When $m, m-n$ are coprime (or equivalently when m, n are coprime) $\sigma = 1$ is the only solution. When the configuration is a half lattice m, n are coprime. But we already know that there are no positive real roots for the characteristic polynomial. Therefore all the roots of the polynomial have modulus less than 1 and the spectrum of the fixed points lies in the unit disk of $\mathbb{C}$. The fixed points are spectrally stable. $\qquad\square$

3.4 Periodic Points of P

We consider periodic orbits of P. A periodic orbit is a sequence $\{d_j\}$ that returns to itself after a certain number (say η) of iterations of the map. The condition $P^{(\eta)}(\{d_j\}) = \{d_j\}$ gives $d_j = d_{j+\eta}$. In other words the sequence of divergence angles are themselves periodic with period η. The corresponding configuration $\{r_j\}$ is half of a regular point set in a cylinder.

Several periodic orbits have been found numerically. The following examples used the ambient metric of $\mathbb{C}^*$ for the cylinder. In phyllotaxis this is known as the centric representation. The points of the configuration lie on concentric circles about the origin with radii increasing exponentially. The unit circle in $\mathbb{C}$ represents the apex. The radii of the circles are powers of the radius of the first circle beyond the unit circle. This radius is a parameter of the system which we denote by R.

When $R = 7/6$ the period 4 orbit $\{257.211^o, 170.505^o, 76.601^o, 170.505^o, 257.211^o, \ldots\}$ was observed. When $R = 5/4$ the period 6 orbit, $\{213.825^o, 80.546^o, 131.704^o, 91.665^o, 192.991^o, 253.733^o, 213.825^o, \ldots\}$ was observed. One of the more interesting periodic orbits was observed at $R = 1.066$. This is the period 8 orbit whose angles are roughly $\{130^o, 89^o, 89^o, 130^o, 89^o, 89^o, 130^o, 315^o, 130^o, \ldots\}$. This orbit matches up fairly well with the one which has been observed by Tucker [51] in the development of magnolia carpels. This orbit is $\{134^o, 94^o, 83^o, 138^o, 92^o, 86^o, 136^o, 310^o, 134^o, \ldots\}$.

The ability of this dynamical system to explain both the prevalence of the Fibonacci numbers as well as this less well known type of phyllotaxis suggests that the door has been opened to a greater unification of phyllotactic forms.

Chapter 4

The Second Family of Dynamical Systems

4.1   Definition of the Potential

The Dynamical System defined in Chapter 3 assumed that the repulsive potential generated by a primordia only exerted an influence around that primordium. Another possibility is that all of the primordia exert an influence so that the repulsion experienced is a sum of the repulsion generated by all of the primordia. This leads us to define

$$W_p(\{d_j\}, \zeta) = \sum_{j \in \mathbb{N}} |r_j + iy - \zeta|^{-p} \quad p > 1$$

for $\zeta \in \mathcal{C}'$. As before we are interested in the potential on the apical ring $\partial C'$. We parameterize $\partial \mathcal{C}'$ with ϕ. When $W_p(\{d_j\}, \phi)$ has a unique absolute minimum on $\partial \mathcal{C}'$ denote it by ϕ^*. The map $P : \mathbb{T}^\infty \to \mathbb{T}^\infty$ is defined as before

$$
\begin{aligned}
P_0(\{d_j\}) &= -\phi^* \\
P_j(\{d_j\}) &= d_{j-1} \quad j \in \mathbb{Z}^+
\end{aligned}
$$

Like before the map P is not not defined on all of $\mathbb{T}^\infty$ because not every configuration leads to a

unique absolute minimum on $\partial \mathcal{C}'$.

4.2 Equivalence of Bifurcation Diagrams

Once again we seek the fixed points of P. The condition $P(\{d_j\}) = \{d_j\}$ gives $d_j =$

$-\phi^*$ $j \in \mathbb{N}$ like before and the configurations fixed by P are half spiral lattices $\Lambda' \in \mathcal{C}'$. After

translating the configuration up and adding the new particle the resulting configuration is just a

copy of Λ' rotated by $-\phi^*$. To iterate again we rotate the configuration back so that $\theta_0 = 0$. As in

Chapter 3 we focus on the space of spiral lattices $\mathbb{H}^*$ and make use of the notation from chapter 2.

The parameter y of the dynamical system, P, corresponds to the imaginary part of a point $z \in \mathbb{H}^*$

and $r_j = \lambda_j(z)$. As in Chapter 3 it is convenient to work with the untranslated lattice. We think of

W_p as being generated by particles at the points $\{\lambda_j \mid j \in \mathbb{Z}^+\}$. We are now interested having the

absolute minimum at 0.

The potential is smooth on $\partial \mathcal{C}'$. A necessary (but not sufficient) condition for 0 to be an

absolute minimum is that it be a zero of $\frac{\partial W_p}{\partial \phi}$. Thus we compute the partial derivative.

$$\frac{\partial}{\partial \phi}|\lambda_j - \phi|^{-p} = \frac{\partial}{\partial \phi}(|\lambda_j - \phi|^2)^{-p/2}$$

$$= p(\delta_j - \phi)|\lambda_j - \phi|^{-p-2}$$

Differentiating the series term by term gives

$$\frac{\partial W_p}{\partial \phi} = p\sum_{j=0}^{\infty}(d_j - \phi)|\lambda_j - \phi|^{-p-2} \tag{4.1}$$

$$\left.\frac{\partial W_p}{\partial \phi}\right|_{\phi=0} = p\sum_{j=0}^{\infty}\delta_j|\lambda_j|^{-p-2} \tag{4.2}$$

The zero set of this function contains the set of fixed points for the map P.

Definition 4.2.1. We denote the zero set of $\left.\dfrac{\partial W_p}{\partial \phi}\right|_{\phi=0}$ by Z_0.

The ultimate goal is to show show that the bifurcation diagram for this map is Topologically

the same as that obtained with the potential X_p and that the branches go through regular regions

just as with X_p, i.e. that the two bifurcation diagrams are essentially equivalent. The following theorem brings us closer to this result by showing that Z_0 does just that. What remains to be done is to estimate the variation in curves of discontinuity for the map defined with W_p from the curves of discontinuity for the map defined with X_p. Computer simulations indicate this variation is small and that the curves of discontinuity continue to lie in the irregular quadrilaterals. Therefore that part of Z_0 that lies in the regular regions would indeed be fixed points.

Theorem 4. *For each m, n defining a regular region, R_{mn}, and for $p \geq 23$ the intersection of $\mathcal{Z}_0$ with R_{mn} and a horizontal line consists of a single point*

This theorem is like one proved by Kunz [33]. This result goes beyond it in three ways. First Kunz only establishes the existence of a value for K_0 (he uses K where we use p) such for $K > K_0$ his theorem holds. While we have established a specific value, i.e. 23, such that Theorem (4) holds for all $p > 23$. Second Theorem (4) holds for all regular regions while Kunz's theorem is only established for some of the regular regions (he uses the term regular branches and doesn't make use of Hyperbolic tessellations). And third he does not establish the uniqueness of his branches leaving the topology of the diagram in question.

This theorem will be proved through a sequence of lemmas. We begin by defining a tubular-like neighborhood about the bifurcation diagram for the X_p potential. There are two main steps in the proof. First we show that Z_0 lies inside of this tubular-like neighborhood and that there must be at least one branch inside the intersection of this tubular-like neighborhood with each regular region. Second we show that there is at most one branch inside the intersection of this neighborhood with a regular region.

4.2.1 Hyperbolic Tubular-like Neighborhood of the X_p Bifurcation Diagram

It is fairly easy to define a tubular neighborhood around the set of explicitly rhombic lattices in $\mathbb{H}$. Let ϵ be some small positive number and set $\alpha = 1 + \epsilon$. Take the intersection of the

fundamental quadrilateral with the (Euclidean) circle about the origin with radius α. Reflect this arc about the unit circle to obtain a second arc in the fundamental quadrilateral with radius $1/\alpha$. These arcs are segments of hyperbolic lines. The union of these two lines are invariant under the isotropy group of the fundamental quadrilateral. We now act on these hyperbolic lines with the extended Level 2 congruence subgroup to produce lines surrounding the set of explicitly rhombic lattices in $\mathbb{H}$. The set of points in each quadrilateral between these lines forms a tubular like neighborhood around the line of explicitly rhombic lattices. Note that while these lines are parallel in the hyperbolic plane the width between them is not fixed. This is of course a characteristic feature of hyperbolic geometry. Denote this tubular like neighborhood by $\mathcal{T}_\epsilon$.

Recall that the canonical bases for lattices associated to the points z in the fundamental quadrilateral is made up of ± 1 and $\pm z$. For z between the two arcs in the fundamental quadrilateral the ratio between the lengths of 1 and z is between $1/\alpha$ and α. When z is outside of this region the ratio of the lengths is outside the interval $[1/\alpha, \alpha]$. It remains the case that for the lattices associated to points in $\mathcal{T}_\epsilon$ the ratio between the lengths of the members of the canonical bases is in the interval $[1/\alpha, \alpha]$ regardless of which quadrilateral we are in. While for lattices associated to points outside of $\mathcal{T}_\epsilon$ the ratio of the lengths of the members of a canonical bases is outside of the interval $[1/\alpha, \alpha]$.

This tubular like neighborhood contains the Cayley graph of the extended Level 2 congruence subgroup but we only want a neighborhood of the branches of the fixed points of the dynamical system defined using the potential X_p. To get a neighborhood of the branches in the regular regions we begin by taking the intersection of $\mathcal{T}_\epsilon$ with the union of the regular regions. However the branches pass through the triple points and any neighborhood of a triple point must intersect an irregular quadrilateral. Consequently we want to include some part of $\mathcal{T}_\epsilon$ in the irregular quadrilaterals.

Let G be the intersection point of the circle with radius *alpha* about the origin with the line $x = 1/2$. Explicitly $G = \dfrac{1 + i\sqrt{4\alpha^2 - 1}}{2}$. The image of G under the map $z \mapsto 1/\bar{z}$ is G/α^2. We can draw an Euclidean line through the origin, G/α^2 and G. The segment of this line inside the fundamental quadrilateral bounds a wedge of $\mathcal{T}_\epsilon$.
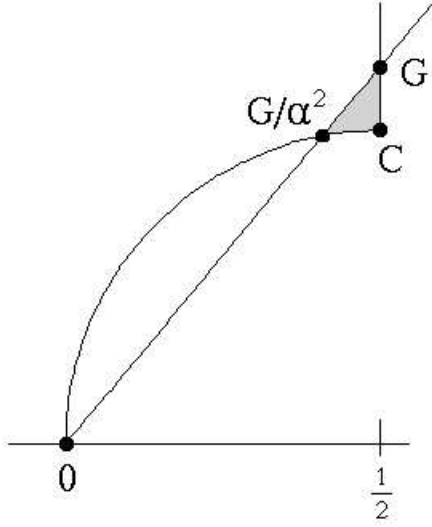
Figure 4.1: Fundamental wedge

Definition 4.2.2. The region in the fundamental quadrilateral bounded by the Euclidean line segment connecting G to G/α^2, the hyperbolic line segment connecting G/α^2 to $(1+\sqrt{3})/2$, and the line segment connecting $(1+\sqrt{3})/2$ to G is called the *fundamental wedge*. The image of this wedge under the map $g_{mn}(z)$ is called a (m,n)-*wedge*

Note that the image of the Euclidean line passing through the origin and G under the Möbius transformation $g_{mn}(z)$ is a circle containing the ideal vertices of the (m,n)-quadrilateral. These wedges are contained in $\mathcal{T}_\epsilon$. To obtain the neighborhood of the branches in the regular regions we want to include the (m,n)-wedges from the irregular quadrilaterals. Note that since the imaginary part of $g_{mn}(C)$ is always larger than the imaginary part of $g_{mn}(D)$ these wedges only contain the top vertices of the irregular quadrilaterals.

Definition 4.2.3. The set Σ_ϵ is the intersection of $\mathcal{T}_\epsilon$ with the union of the regular regions joined with the (m,n)-wedges of the irregular quadrilaterals.

$$g_{mn}(G/\alpha^2)$$

$$g_{mn}(C)$$

$$g_{mn}(G)$$

$$\frac{D_m}{m} \qquad \frac{D_n}{n}$$
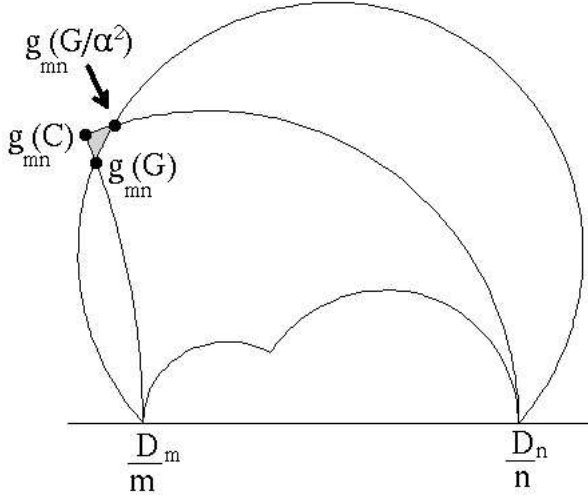
Figure 4.2: (m, n)-wedge

4.2.2 Regular quadrilaterals

For sufficient stiffness the branches must lie in Σ_ϵ

We begin by showing that we can compare $\left.\dfrac{\partial W_p(z, \phi)}{\partial \phi}\right|_{\phi=0}$ with $\left.\dfrac{\partial X_p(z, \phi)}{\partial \phi}\right|_{\phi=0}$ outside of Σ_ϵ.

Lemma 4.2.1. *Given $\alpha \in (1, 2]$ and p such that $p > 2 + \sqrt{3}$ and $32(\alpha + 1) < \alpha^p$ then for z in a regular (m, n)-hexagon and $z \notin \Sigma_\epsilon$, the functions $\left.\dfrac{\partial W_p(z, \phi)}{\partial \phi}\right|_{\phi=0}$ and $\left.\dfrac{\partial X_p(z, \phi)}{\partial \phi}\right|_{\phi=0}$ have the same sign.*

Proof. For some $m \in \mathbb{N}$ depending on $z = x + iy \in \mathbb{H}^*$

$$
\begin{aligned}
X_p(\{\delta_j\}, \phi) &= \sup_{j \in \mathbb{N}}\{|\lambda_j - \phi|^{-p}\} = |\lambda_m - \phi|^{-p} \\
\left.\frac{\partial X_p}{\partial \phi}\right|_{\phi=0} &= p\delta_m|\lambda_m|^{-p-2}
\end{aligned}
$$

The quantity m is unique in the interior of a half of a quadrilateral. The zero set of $\left.\dfrac{\partial X_p}{\partial \phi}\right|_{\phi=0} = p$ is $\delta_m = 0 \Leftrightarrow mx \in \mathbb{Z} \Leftrightarrow x \in \frac{1}{m}\mathbb{Z}$. This line is only contained in a (m, n)-quadrilateral when it is irregular. So $\left.\dfrac{\partial X_p}{\partial \phi}\right|_{\phi=0}$ is not zero outside of Σ_ϵ.

Since $\delta_m(z) \neq 0$ for z in a regular quadrilateral we can compute the ratio of the two potentials.

$$\frac{\frac{\partial W_p}{\partial \phi}\Big|_{\phi=0}}{\frac{\partial X_p}{\partial \phi}\Big|_{\phi=0}} = \frac{p\sum_{j=0}^{\infty}\delta_j|\lambda_j|^{-p-2}}{p\delta_m|\lambda_m|^{-p-2}} = \sum_{j=0}^{\infty}\left|\frac{\lambda_j}{\lambda_m}\right|^{-p-2}\frac{\delta_j}{\delta_m} = 1 + \sum_{\substack{j=0\\j\neq m}}^{\infty}\left|\frac{\lambda_j}{\lambda_m}\right|^{-p-2}\frac{\delta_j}{\delta_m}$$

$$\frac{\frac{\partial W_p}{\partial \phi}\Big|_{\phi=0}}{\frac{\partial X_p}{\partial \phi}\Big|_{\phi=0}} - 1 = \frac{|\lambda_m|}{\delta_m}\sum_{\substack{j=0\\j\neq m}}^{\infty}\left|\frac{\lambda_j}{\lambda_m}\right|^{-p-1}\frac{\delta_j}{|\lambda_j|}$$

We want to show that for a given ϵ there is a N such that for $p > N$ the functions $\frac{\partial W_p}{\partial \phi}\Big|_{\phi=0}$ and $\frac{\partial X_p}{\partial \phi}\Big|_{\phi=0}$ have the same sign in a (m,n)-hexagon outside of the ϵ tubular neighborhood. We will proceed through a series of lemmas. Define

$$S_p = \frac{\frac{\partial W_p}{\partial \phi}\Big|_{\phi=0}}{\frac{\partial X_p}{\partial \phi}\Big|_{\phi=0}} - 1$$

When $|S_p| < 1$ the functions $\frac{\partial W_p}{\partial \phi}\Big|_{\phi=0}$ and $\frac{\partial X_p}{\partial \phi}\Big|_{\phi=0}$ must have the same sign.

$$|S_p| \leq \left|\frac{\lambda_m}{\delta_m}\right|\sum_{\substack{j=0\\j\neq m}}^{\infty}\left|\frac{\lambda_j}{\lambda_m}\right|^{-p-1}\left|\frac{\delta_j}{\lambda_j}\right| \leq \left|\frac{\lambda_m}{\delta_m}\right|\sum_{\substack{j=0\\j\neq m}}^{\infty}\left|\frac{\lambda_j}{\lambda_m}\right|^{-p-1}$$

since $\left|\frac{\delta_j}{\lambda_j}\right| \leq 1$. The sum $\sum_{\substack{j=0\\j\neq m}}^{\infty}\left|\frac{\lambda_j}{\lambda_m}\right|^{-p-1}$ is like taking the W_{p+1} potential on a half lattice obtained from Λ' by scaling by a factor of $|\lambda_m|^{-1}$.

We use a density argument to bound $\sum_{\substack{j=0\\j\neq m}}^{\infty}\left|\frac{\lambda_j}{\lambda_m}\right|^{-p-1}$. We count the points of $\Lambda'/|\lambda_m|$ by applying the density argument to the planar lattice $L/|\lambda_m|$. This will be an over count of the points in $\Lambda'/|\lambda_m|$.

Lemma 4.2.2. *Given $\alpha \in (1,2]$ and $p > 2 + \sqrt{3}$ then for any z in a regular (m,n)-hexagon and $z \notin \Sigma_\epsilon$ we have* $\sum_{\substack{j=0\\j\neq m}}^{\infty}\left|\frac{\lambda_j}{\lambda_m}\right|^{-p-1} < \frac{8(\alpha+1)}{\alpha^p}$

Proof. Define the annulus

$$A_k = \{z \in \mathbb{C} \mid (k-1)\alpha \leq |z| < k\alpha\}$$

where α is defined in Section (4.2.1). We seek an upper bound on the number of points in $L/\lambda_m \cap A_k$.

All of the points of $L/|\lambda_m|$— are at least distance 1 apart. So $L/|\lambda_m|$— can be covered by disjoint

open disks of radius 1/2 centered on the lattice points. The union of the disks covering the points in $L/|\lambda_m| \cap A_k$ is contained in the annulus

$$B_k = \{z \in \mathbb{C} \mid (k-1)\alpha - \frac{1}{2} < |z| \le k\alpha + \frac{1}{2}\}$$

This has area

$$m(B_k) = \pi(k\alpha + \frac{1}{2})^2 - \pi((k-1)\alpha - \frac{1}{2})^2 = \pi\alpha(\alpha+1)(2k-1)$$

We can divide this in half since $\Lambda'/|\lambda_m|$ is contained in $\mathbb{H}$ we only look at the area of $B_k \cap \mathbb{H}$. This still over counts the points of $\Lambda'/|\lambda_m|$. The area of a disk is $\pi/4$ so there is at most $2\alpha(\alpha+1)(2k-1)$ disks in B_k and therefore at most that many lattice points in A_k.

The norm on the lattice points of A_k is bounded from below by $(k-1)\alpha$ so the potential any of then generates is bounded from above by $(k-1)^{-p-1}\alpha^{-p-1}$. The total potential generated by the lattice points of A_k is bounded from above by

$$\frac{2\alpha(\alpha+1)(2k-1)}{\alpha^{p+1}(k-1)^{p+1}} = \frac{2(\alpha+1)(2k-1)}{\alpha^p(k-1)^{p+1}}$$

Now we sum over all of the annuli. Note that by the definition of α the set $\Lambda'/\lambda_m \cap A_1$ only contains λ_m/λ_m. Since were summing over $j \ne m$ the annulus A_1 contributes nothing.

$$\begin{aligned}
\sum_{k=2}^{\infty} \frac{2(\alpha+1)(2k-1)}{\alpha^p(k-1)^{p+1}} &= \frac{2(\alpha+1)}{\alpha^p} \sum_{k=2}^{\infty} \frac{2k-1}{(k-1)^{p+1}} \\
&= \frac{2(\alpha+1)}{\alpha^p} \sum_{k=1}^{\infty} \frac{2k+1}{k^{p+1}} \\
&\le \frac{2(\alpha+1)}{\alpha^p} \frac{3p^2-1}{p^2-p}
\end{aligned}$$

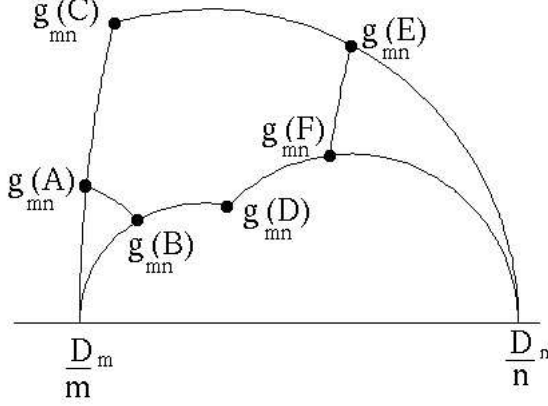When $p > 2 + \sqrt{3}$ the fraction $\dfrac{3p^2-1}{p^2-p} < 4$. So we have

$$\sum_{k=2}^{\infty} \frac{2(\alpha+1)(2k-1)}{\alpha^p(k-1)^{p+1}} \le 8\frac{\alpha+1}{\alpha^p}$$

$\square$

Using this result we have

$$|S_p| \le 8\frac{\alpha+1}{\alpha^p}\left|\frac{\lambda_m}{\delta_m}\right|$$

Now we seek bounds on $\left|\frac{\lambda_m}{\delta_m}\right|$.

Figure 4.3: (m, n)-Hexagon

Lemma 4.2.3. *For z in a (m, n)-hexagon $\left| \dfrac{\lambda_m(z)}{\delta_m(z)} \right| < 4$*

Proof. We can rewrite the ratio

$$\left| \frac{\lambda_m}{\delta_m} \right|^2 = \frac{\delta_m^2 + m^2 y^2}{\delta_m^2} = 1 + \left(\frac{my}{\delta_m} \right)^2$$

Let z be a point in the m side of a (m, n)-hexagon.

The slope of a (Euclidean) line through the ideal vertex D_m/m and the point z is

$$\frac{y - 0}{x - D_m/m} \frac{m}{m} = \frac{my}{mx - D_m} = \frac{my}{\delta_m}$$

Where we have used the fact that we are in a (m, n)-quadrilateral in the denominator. Thus $\left| \dfrac{\lambda_m}{\delta_m} \right|^2$ is an increasing function of the slope of this line. As the slope increases the last point of intersection of the line with the hexagon is $g_{mn}(A)$. So evaluating the slope of the line connecting D_m/m with $g_{mn}(A)$ will give us an upper bound on $\left| \dfrac{\lambda_m}{\delta_m} \right|$. Using Equation (2.6) we compute the slope.

$$\frac{\frac{\sqrt{15}}{2(n^2 - mn + 4m^2)} - 0}{\frac{2D_n n - D_m n - D_n m + 8D_m m}{2(n^2 - mn + 4m^2)} - \frac{D_m}{m}} = \frac{\sqrt{15}m}{m(2D_n n - D_m n - D_n m + 8D_m m) - 2D_m(n^2 - mn + 4m^2)}$$

$$= \frac{\sqrt{15}m}{2n + m} \qquad (4.3)$$

where we use the fact that $D_n m - D_m n = 1$ to simplify the denominator. Thus $\left| \dfrac{my}{\delta_m} \right| < 15$. This gives $\left| \dfrac{\lambda_m(A)}{\delta_m(A)} \right|^2 = 1 + \dfrac{15m^2}{(2n + m)^2} \leq 16$. Therefore $\left| \dfrac{\lambda_m}{\delta_m} \right| \leq 4$

□

Using the result of Lemma (4.2.3) we can complete the proof of Lemma (4.2.1). We know that

$$|S_p| \leq 8\frac{\alpha+1}{\alpha^p}4 = 32\frac{\alpha+1}{\alpha^p}$$

The right hand side is less than 1 if $32(\alpha+1) < \alpha^p$.

Consequently $\left.\dfrac{\partial W_p(z,\phi)}{\partial\phi}\right|_{\phi=0}$ and $\left.\dfrac{\partial X_p(z,\phi)}{\partial\phi}\right|_{\phi=0}$ have the same sign for z in a regular (m,n)-hexagon and $z \notin \Sigma_\epsilon$. □

We know that for z in a regular (m,n)-hexagon and outside of Σ_ϵ the function $\left.\dfrac{\partial X_p(z,\phi)}{\partial\phi}\right|_{\phi=0}$ is never zero and so therefore $\left.\dfrac{\partial W_p(z,\phi)}{\partial\phi}\right|_{\phi=0}$ is never zero on these regions. Now we want to show that no branches go through the wedges of Σ_ϵ.

Lemma 4.2.4. *Given $\alpha \in (1,2]$ and p such that $p > 2 + \sqrt{3}$ and $16(\alpha^2+1) < \alpha^{p-2}$ then for z in a $(m+n,m)$-wedge, the functions $\left.\dfrac{\partial W_p(z,\phi)}{\partial\phi}\right|_{\phi=0}$ and $\left.\dfrac{\partial X_p(z,\phi)}{\partial\phi}\right|_{\phi=0}$ have the same sign.*

Proof. Recall from equation (4.2) that

$$\left.\frac{\partial W_p}{\partial\phi}\right|_{\phi=0} = p\sum_{j=0}^{\infty}\delta_j|\lambda_j|^{-p-2}$$

Let

$$A = 1 + \frac{\delta_m}{\delta_{m+n}}\left|\frac{\lambda_m}{\lambda_{m+n}}\right|^{-p-2} + \frac{\delta_n}{\delta_{m+n}}\left|\frac{\lambda_n}{\lambda_{m+n}}\right|^{-p-2}.$$

We rewrite the sum as

$$\left.\frac{\partial W_p}{\partial\phi}\right|_{\phi=0} = p\delta_{m+n}|\lambda_{m+n}|^{-p-2}\left(A + \sum_{j\neq m,n,m+n}^{\infty}\frac{\delta_j}{\delta_{m+n}}\left|\frac{\lambda_j}{\lambda_{m+n}}\right|^{-p-2}\right)$$

We want to show that $A > 1$. Since $|\lambda_m| < |\lambda_n|$ we know that $\left|\dfrac{\lambda_m}{\lambda_{m+n}}\right|^{-p-2} > \left|\dfrac{\lambda_n}{\lambda_{m+n}}\right|^{-p-2}$.

Since the wedge is in an irregular quadrilateral its projection onto $\partial\mathbb{H}^*$ is outside the interval $[D_{m+n}/(m+n), D_m/m]$ the m and $m+n$ parastichies are not opposed so that δ_m and δ_{m+n} must have the same sign. The actual bound on α to assure this still needs to be determined. Since the

$(m + n, m)$-wedge is on the side of a regular region the m and n parastichies are opposed. Because $\delta_{m+n} = \delta_m + \delta_n$ we know that $|\delta_m| > |\delta_n|$ and that $\dfrac{\delta_m}{\delta_{m+n}} > \dfrac{\delta_n}{\delta_{m+n}}$. Therefore

$$\frac{\delta_m}{\delta_{m+n}}\left|\frac{\lambda_m}{\lambda_{m+n}}\right|^{-p-2} + \frac{\delta_n}{\delta_{m+n}}\left|\frac{\lambda_n}{\lambda_{m+n}}\right|^{-p-2} > 0$$

and $A > 1$. Now we want to bound the absolute value of the sum

$$\sum_{j \neq m,n,m+n}^{\infty} \frac{\delta_j}{\delta_{m+n}}\left|\frac{\lambda_j}{\lambda_{m+n}}\right|^{-p-2}$$

When this bound is below 1 we know that $\left.\dfrac{\partial W_p}{\partial \phi}\right|_{\phi=0}$ has the same sign as $p\delta_{m+n}|\lambda_{m+n}|^{-p-2}$ which has the same sign as $p\delta_m|\lambda_m|^{-p-2} = \left.\dfrac{\partial X_p}{\partial \phi}\right|_{\phi=0}$ since δ_m and δ_{m+n} have the same sign.

$$\left|\sum_{j \neq m,n,m+n}^{\infty} \frac{\delta_j}{\delta_{m+n}}\left|\frac{\lambda_j}{\lambda_{m+n}}\right|^{-p-2}\right| = \left|\frac{\lambda_{m+n}}{\delta_{m+n}}\right| \sum_{j \neq m,n,m+n}^{\infty} \left|\frac{\lambda_j}{\lambda_{m+n}}\right|^{-p-1}\left|\frac{\delta_j}{\lambda_j}\right|$$

$$\leq \left|\frac{\lambda_{m+n}}{\delta_{m+n}}\right| \sum_{j \neq m,n,m+n}^{\infty} \left|\frac{\lambda_j}{\lambda_{m+n}}\right|^{-p-1}$$

As with Lemma (4.2.3) we bound the factors of the above expression separately.

Lemma 4.2.5. *Given $\alpha \in (1,2]$ and $p > 2 + \sqrt{3}$ then for z in a $(m+n, m)$- wedge with $|\lambda_m(z)| < |\lambda_{m+n}(z)|$ we have* $\displaystyle\sum_{j \neq m,n,m+n}^{\infty} \left|\frac{\lambda_j}{\lambda_{m+n}}\right|^{-p-1} \leq \frac{8(\alpha^2 + 1)}{\alpha^{p-1}}$

Proof. We use a density argument as in Lemma (4.2.2). We over count the points of $\Lambda'/|\lambda_{m+n}|$ by working with $L/|\lambda_{m+n}|$. We define the annuli A_k like before:

$$A_k = \{z \in \mathbb{C} \mid (k-1)\alpha \leq |z| < k\alpha\}$$

We seek an upper bound on the number of points in $L/|\lambda_{m+n}| \cap A_k$. All the points of the lattice $L/|\lambda_{m+n}|$ are at least distance $\left|\dfrac{\lambda_m}{\lambda_{m+n}}\right| = \dfrac{1}{\alpha}$ apart. We can cover the points of $L/|\lambda_{m+n}| \cap A_k$ with disks of radius $1/(2\alpha)$. The union of these disks is contained in

$$B_k = \{z \in \mathbb{C} \mid (k-1)\alpha - \frac{1}{2\alpha} \leq |z| < k\alpha + \frac{1}{2\alpha}\}$$

This is slightly smaller than the B_k in Lemma (4.2.2) and it has area

$$m(B_k) = \pi(k\alpha + \frac{1}{2\alpha})^2 - \pi((k-1)\alpha - \frac{1}{2\alpha})^2 = \pi(\alpha^2 + 1)(2k - 1)$$

We divide this in half because we only want to count those points in $\mathbb{H}$. The area of a disk is $\pi/(4\alpha^2)$ so there is at most $2\alpha^2(\alpha^2+1)(2k-1)$ lattice points in A_k. The potential generated individually by these lattice points is no more than $(k-1)^{-p-1}\alpha^{-p-1}$ and the potential generated by the all lattice points in A_k is

$$\frac{2(\alpha^2+1)(2k-1)}{\alpha^{p-1}(k-1)^{p+1}}$$

We claim that when $\alpha < \sqrt{2}$ the only points of $L/|\lambda_{m+n}|$ in A_1 are $\lambda_n/|\lambda_{m+n}|$, $\lambda_m/|\lambda_{m+n}|$, and $\lambda_{m+n}/|\lambda_{m+n}|$. The point in $L/|\lambda_{m+n}$ with smallest modulus is $\lambda_{m+n}/|\lambda_{m+n}|$, the point with the second smallest modulus is $\lambda_m/|\lambda_{m+n}|$, and the point with the third smallest modulus is $\lambda_n/|\lambda_{m+n}|$. The point $\lambda_n/|\lambda_{m+n}|$ is the difference between $\lambda_m/|\lambda_{m+n}|$ and $\lambda_{m+n}/|\lambda_{m+n}$ so the point of $L/|\lambda_{m+n}|$ with the fourth smallest modulus is the sum of $\lambda_m/|\lambda_{m+n}|$ and $\lambda_{m+n}/|\lambda_{m+n}$. This lattice is homothetic to a lattice corresponding to a point of the fundamental wedge. Two points of this lattice with smallest modulus are 1 and a z in the fundamental wedge. Their sum $1+z$ achieves the smallest modulus over all z in the fundamental wedge when $z = G/\alpha^2$.

When $\alpha < \sqrt{2}$ we have $|1 + G/\alpha^2| > \alpha$. To see this we compute $|1 + G/\alpha^2|$.

$$|1 + G/\alpha^2| > \alpha \Leftrightarrow$$

$$|\alpha^2 + G| > \alpha^3 \Leftrightarrow$$

$$|\alpha^2 + G|^2 > \alpha^6 \Leftrightarrow$$

$$|\alpha^2 + \frac{1}{2} + i\frac{1}{2}\sqrt{4\alpha^2 - 1}|^2 > \alpha^6 \Leftrightarrow$$

$$(\alpha^2 + \frac{1}{2})^2 + \frac{1}{4}(4\alpha^2 - 1) > \alpha^6 \Leftrightarrow$$

$$\alpha^4 + \alpha^2 + \frac{1}{4} + \alpha^2 - \frac{1}{4} > \alpha^6 \Leftrightarrow$$

$$\alpha^4 + 2\alpha^2 > \alpha^6 \Leftrightarrow$$

$$-\alpha^6 + \alpha^4 + 2\alpha^2 > 0 \Leftrightarrow$$

$$(\alpha^2 + 1)(2 - \alpha^2) > 0 \Leftrightarrow$$

$$\alpha < \sqrt{2}$$

So now we sum over all the annuli except A_1, this over counts the points even more than in Lemma (4.2.2).

$$\sum_{k=2}^{\infty} \frac{2(\alpha^2+1)(2k-1)}{\alpha^{p-1}(k-1)^{p+1}} = \frac{2(\alpha^2+1)}{\alpha^{p-1}} \sum_{k=2}^{\infty} \frac{(2k-1)}{(k-1)^{p+1}}$$

$$= \frac{2(\alpha^2+1)}{\alpha^{p-1}} \frac{3p^2-1}{p^2-p}$$

When $p > 2 + \sqrt{3}$ the fraction $\dfrac{3p^2-1}{p^2-p} < 4$ so

$$\sum_{j \neq m,n,m+n}^{\infty} \left| \frac{\lambda_j}{\lambda_{m+n}} \right|^{-p-1} \leq \frac{8(\alpha^2+1)}{\alpha^{p-1}}$$

$\square$

Lemma 4.2.6. *For z in a $(m+n,m)$-wedge* $\left| \dfrac{\lambda_{m+n}(z)}{\delta_{m+n}(z)} \right| < 2\alpha$

Proof. Like before

$$\left| \frac{\lambda_{m+n}(z)}{\delta_{m+n}(z)} \right|^2 = 1 + \left(\frac{(m+n)y}{\delta_{m+n}} \right)^2$$

The point of the wedge that makes the largest slope (in absolute value) with $D_{m+n}/(m+n)$ is $g_{m+n,m}(G)$. See Figure 4.2 We compute $g_{m+n,m}(G)$.

$$g_{m+n,m}(G) = \frac{D_{m+n}\left(\frac{1+i\sqrt{4\alpha^2}}{2\alpha^2} \right) - D_m}{(m+n)\left(\frac{1+i\sqrt{4\alpha^2}}{2\alpha^2} \right) - m}$$

$$= \frac{4\alpha^2(\alpha^2 D_m m + D_{m+n}(m+n)) - 2\alpha^2(D_{m+n}m + D_m(m+n)) + i2\alpha^2\sqrt{4\alpha^2-1}}{4\alpha^2(\alpha^2 m^2 - (m+n)m + (m+n)^2)}$$

The slope this point makes with the point $D_{m+n}/(m+n)$ is

$$-\frac{\sqrt{4\alpha^2-1}(m+n)}{2\alpha^2 m + (m+n)}$$

This is bounded in absolute value by $\sqrt{4\alpha^2-1}$. Therefore

$$\left| \frac{\lambda_{m+n}}{\delta_{m+n}} \right|^2 < 1 + (4\alpha^2-1)$$

$$\left| \frac{\lambda_{m+n}}{\delta_{m+n}} \right| < 2\alpha$$

$\square$

We can now conclude from Lemmas (4.2.5) and (4.2.6) that

$$\left| \sum_{j \neq m,n,m+n}^{\infty} \frac{\delta_j}{\delta_{m+n}} \left| \frac{\lambda_j}{\lambda_{m+n}} \right|^{-p-2} \right| < \frac{16(\alpha^2 + 1)}{\alpha^{p-2}}$$

Thus $A + \sum_{j \neq m,n,m+n}^{\infty} \frac{\delta_j}{\delta_{m+n}} \left| \frac{\lambda_j}{\lambda_{m+n}} \right|^{-p-2} > 1 - \frac{16(\alpha^2 + 1)}{\alpha^{p-2}}$. Given α we can find N such that for

$p > N$ the factor $A + \sum_{j \neq m,n,m+n}^{\infty} \frac{\delta_j}{\delta_{m+n}} \left| \frac{\lambda_j}{\lambda_{m+n}} \right|^{-p-2}$ is bounded away from zero. This concludes the

proof of Lemma (4.2.4). $\qquad\qquad\qquad\qquad\qquad\qquad\qquad\qquad\qquad\qquad\qquad\qquad$ $\square$

From Lemmas (4.2.1) and (4.2.4) we can conclude that $\left. \frac{\partial W_p}{\partial \phi} \right|_{\phi=0}$ is not zero outside of Σ_ϵ.

Furthermore the function $\left. \frac{\partial X_p}{\partial \phi} \right|_{\phi=0}$ has opposite signs in the two halves of a quadrilateral so that

$\left. \frac{\partial W_p}{\partial \phi} \right|_{\phi=0}$ must have opposite signs in the two halves of a quadrilateral outside of Σ_ϵ. Therefore

$\left. \frac{\partial W_p}{\partial \phi} \right|_{\phi=0}$ must be zero somewhere inside of Σ_ϵ.

Uniqueness of Z_0 in Σ_ϵ

We look at how $\left. \frac{\partial W_p}{\partial \phi} \right|_{\phi=0}$ varies as we change x keeping y constant. If this is a monotonic

function it can only have one zero so that W_p can have only one extremal point in the intersection

of a horizontal line with a regular region. This leads to the following lemma.

Lemma 4.2.7. *Given $\alpha \in (1,2]$ and $p > 14 + 256(\alpha + 1)/\alpha^p$ then for $z \in \Sigma_\epsilon$ the function*

$\left. \frac{\partial}{\partial x} \frac{\partial W_p}{\partial \phi} \right|_{\phi=0}$ *is negative*

Proof. Begin by computing the derivative. We take the derivative of both sides of the equation (4.2)

$$\begin{aligned} \left. \frac{\partial}{\partial x} \frac{\partial W_p}{\partial \phi} \right|_{\phi=0} &= \frac{\partial}{\partial x} p \sum_{j=0}^{\infty} \delta_j |\lambda_j|^{-p-2} \\ &= p \sum_{j=0}^{\infty} \left(\left(\frac{\partial}{\partial x} \delta_j \right) |\lambda_j|^{-p-2} + \delta_j \left(\frac{\partial}{\partial x} |\lambda_j|^{-p-2} \right) \right) \end{aligned}$$

Using the facts

$$\begin{aligned} \frac{\partial \delta_j}{\partial x} &= j, \\ \frac{\partial}{\partial x} |\lambda_j|^{-p-2} &= -j(p+2)\delta_j |\lambda_j|^{-p-4}, \end{aligned}$$

we get

$$\frac{\partial}{\partial x} \frac{\partial W_p}{\partial \phi}\bigg|_{\phi=0} = p \sum_{j=0}^{\infty} j|\lambda_j|^{-p-4}(j^2 y^2 - (p+1)\delta_j^2)$$

We want this to be negative or equivalently we want the following inequality to hold.

$$\sum_{j=0}^{m} j|\lambda_j|^{-p-4}((p+1)\delta_j^2 - j^2 y^2) > \sum_{j=m+1}^{\infty} j|\lambda_j|^{-p-4}(j^2 y^2 - (p+1)\delta_j^2)$$

Where λ_m is the smallest nonzero point of the half lattice Λ'. Each of the factors in the terms of the sum on the left hand side is always positive except possibly for $((p+1)\delta_j^2 - j^2 y^2)$. We want to determine p so that each term of the left hand side is positive. This happens when

$$p > \frac{j^2 y^2}{\delta_j^2} - 1$$

for $j \in \{0, \ldots, m\}$. The ratio $\frac{jy}{\delta_j}$ is the slope of λ_j. Now we already have a bound on this slope for the case $j = m$ from equation (4.3). Also recall from section (3.2.1) that for $j < m$ the point λ_j is closer to $\partial \mathcal{C}'$ than λ_m. However λ_m is the point of Λ' with the smallest modulus. Therefore the slopes are even smaller when $j < m$. Consequently

$$\sqrt{15} > \frac{jy}{\delta_j} \quad j \in \{0, \ldots, m\}$$

So when $p > 14$ every term on the left hand side of the inequality is positive. Now since every term on the left hand side of the inequality is positive the inequality holds if only a single term on the left hand side is larger than the right hand side. We can consider the mth term. We want

$$m|\lambda_m|^{-p-4}((p+1)\delta_m^2 - m^2 y^2) > \sum_{j=m+1}^{\infty} j|\lambda_j|^{-p-4}(j^2 y^2 - (p+1)\delta_j^2)$$

Define $T_j^2(z) = \frac{j^2 y^2}{\delta_j^2(z)}$. We can rewrite this inequality as

$$m|\lambda_m|^{-p-4}(p+1 - T_m^2)\delta_m^2 > \sum_{j=m+1}^{\infty} j|\lambda_j|^{-p-4}(T_j^2 - (p+1))\delta_j^2$$

Now using

$$\frac{\delta_j^2}{|\lambda_j|^2} = \frac{1}{1 + \frac{j^2 y^2}{\delta_j^2}} = \frac{1}{1 + T_j^2},$$

we can further rewrite Inequality (4.4).

$$m|\lambda_m|^{-p-2}(p+1-T_m^2)\frac{1}{1+T_m^2} \quad > \quad \sum_{j=m+1}^{\infty} j|\lambda_j|^{-p-2}(\delta_j^2-(p+1))\frac{1}{1+T_j^2}$$

$$m|\lambda_m|^{-p-2}(p+1-T_m^2)\frac{1}{1+T_m^2} \quad > \quad \sum_{j=m+1}^{\infty} j|\lambda_j|^{-p-2}\frac{\delta_j^2}{1+T_j^2} - (p+1)\sum_{j=m+1}^{\infty} \frac{j}{1+T_j^2}|\lambda_j|^{-p-2}$$

The sum $\displaystyle\sum_{j=m+1}^{\infty} \frac{j}{1+T_j^2}|\lambda_j|^{-p-2}$ is positive and so the Inequality (4.4) holds when

$$m|\lambda_m|^{-p-2}(p+1-T_m^2)\frac{1}{1+T_m^2} > \sum_{j=m+1}^{\infty} j|\lambda_j|^{-p-2}\frac{\delta_j^2}{1+T_j^2}$$

This estimate is exceedingly rough. By obtaining a better estimate at this point in the proof of

Theorem (4) there is a good chance of strengthening the result. However we continue on with this

estimate and divide through by $m|\lambda_m|^{-p-2}$ which gives

$$\frac{p+1-T_m^2}{1+T_m^2} > \frac{1}{m}\sum_{j=m+1}^{\infty} j\left|\frac{\lambda_j}{\lambda_m}\right|^{-p-2}\frac{\delta_j^2}{1+T_j^2}$$

And since $\dfrac{\delta_j^2}{1+T_j^2} < 1$ it suffices to show that

$$\frac{p+1-T_m^2}{1+T_m^2} > \frac{1}{m}\sum_{j=m+1}^{\infty} j\left|\frac{\lambda_j}{\lambda_m}\right|^{-p-2}$$

We want to find an upper bound on the right hand side. We can rewrite this as

$$\frac{1}{m}\sum_{j=m+1}^{\infty} j\left|\frac{\lambda_j}{\lambda_m}\right|^{-p-2} = \frac{1}{m}\sum_{j=m+1}^{\infty} j\left|\frac{\lambda_j}{\lambda_m}\right|^{-1}\left|\frac{\lambda_j}{\lambda_m}\right|^{-p-2}$$

We seek an $h > 0$ such that $\left|\dfrac{\lambda_m}{\lambda_j}\right| < \dfrac{j}{m}h$ because with this h the above inequality holds when

$$\frac{p+1-T_m^2}{1+T_m^2} > h^{-1}\sum_{j=m+1}^{\infty} \left|\frac{\lambda_j}{\lambda_m}\right|^{-p-1} \tag{4.4}$$

Let $h_j = Im\left(\dfrac{\lambda_j}{|\lambda_m|}\right)$ where, as before, λ_m is the smallest nonzero member of Λ'. We want to focus

on h_m.

$$h_m^2 = \frac{m^2 y^2}{\delta^2 + m^2 y^2} = \frac{\left(\frac{my}{\delta_m}\right)^2}{1+\left(\frac{my}{\delta_m}\right)^2}$$

So h_m is an increasing function of the slope $\left(\frac{my}{\delta_m}\right)^2$. We can obtain a lower bound on h_m when we have a lower bound on the slope. This is equal to the slope of a line through the point D_m/m and z in regular (m,n)-hexagon. This slope is smallest when $z = g_{mn}(D)$ at which point it is

$$\frac{\sqrt{3}m}{2n+m}$$

Therefore

$$\left(\frac{my}{\delta_m}\right)^2 \geq \frac{3m^2}{(2n+m)^2}$$

$$h_m^2 \geq \frac{\frac{3m^2}{(2n+m)^2}}{1+\frac{3m^2}{(2n+m)^2}} = \frac{3}{4}\frac{m^2}{n^2+mn+m^2}$$

This has no lower bound if we let n grow without bound. However we are in a regular quadrilateral so there is a limit to the value of n for a given m. The (m,n)-quadrilateral is regular when $(2n - m)(2m - n) > 0$ (see Definition 2.4.6). This is equivalent to $\frac{1}{2}m < n < 2m$. So, for a given m, the largest n can be is $2m - 1$. Substituting this into the right hand side gives

$$h_m^2 \geq \frac{3}{4}\frac{m^2}{(7m^2 - 5m + 1)}$$

This function has two critical points $0, 2/5$. The value 0 gives a local minimum and $2/5$ gives a local maximum. Thus the function is decreasing for $m > 2/5$. Therefore it achieves it largest value over the set of positive integers when $m = 1$. Substituting this in gives

$$h_m \geq \frac{1}{2}$$

Since $h_j = \frac{j}{m}h_m$ we get

$$\left|\frac{\lambda_j}{\lambda_m}\right| > Im\left(\frac{\lambda_j}{|\lambda_m|}\right) = h_j > \frac{1}{2}\frac{j}{m}$$

So our h is $1/2$. Substituting into equation (4.4) gives

$$\frac{p+1-T_m^2}{1+T_m^2} > 2\sum_{j=m+1}^{\infty}\left|\frac{\lambda_j}{\lambda_m}\right|^{-p-1}$$

This sum is less than the sum in Lemma (4.2.2). Therefore it is enough to establish that

$$\frac{p+1-T_m^2}{1+T_m^2} > 16\frac{\alpha+1}{\alpha^p} \Leftrightarrow$$

$$\alpha^p(p+1-T_m^2) > 16(\alpha+1)(1+T_m^2)$$

By choosing the largest possible value for T_m we make the the left hand side of the inequality as small as possible and the right hand side as large as possible. From Lemma (4.2.3) we have $T_m^2 < 15$. Substituting in gives

$$\alpha^p(p-14) > 16(\alpha+1)(16) \Leftrightarrow$$

$$p > 14 + 256\frac{\alpha+1}{\alpha^p}$$

$\square$

To prove Theorem (4) we want Lemmas (4.2.1), (4.2.4), and (4.2.7) to hold simultaneously. That is we need:

$$32(\alpha+1) < \alpha^p$$

$$16(\alpha^2+1) < \alpha^{p-2}$$

$$p > 14 + 256\frac{\alpha+1}{\alpha^p}$$

Since $\alpha \leq 2$ we have

$$32\frac{\alpha+1}{\alpha^p} \geq 16\frac{\alpha+1}{\alpha^{p-1}}$$

$$> 16\frac{\alpha+1/\alpha}{\alpha^{p-1}}$$

$$= 16\frac{\alpha^2+1}{\alpha^{p-2}}$$

and so Lemma (4.2.4) holds for α and p such that Lemma (4.2.1) holds. Now suppose $32(\alpha+1) < \alpha^p$, then $256\frac{\alpha+1}{\alpha^p} < 8$ and Lemma (4.2.7) holds when $p > 14+8 = 22$. When $p > 22$ and $\alpha = 2$ all three conditions are satisfied. We seek the smallest α such that for $p > 23$ we can have $32(\alpha+1) < \alpha^{23}$ or equivalently when

$$\alpha^{23} - 32\alpha - 32 > 0$$

This inequality holds for α larger than the largest real root of the polynomial. There is at most one real root larger than the largest critical point. The critical points are roots of $23\alpha^{22} - 32 = 0$. So there is one positive critical point, i.e. $(32/23)^{(1/22)}$. This is approximately 1.015. The polynomial

is negative at $\alpha = 1.015$, it has a root at approximately $\alpha = 1.21$, and it is positive when $\alpha > 1.21$. In the proof of Lemma (4.2.5) we require $\alpha < \sqrt{2}$. Therefore when $0.41 > \epsilon > 0.21$ and $p \geq 23$ Theorem (4) holds.

Bibliography

[1] Adler I., A model of contact pressure in phyllotaxis *J. Theor. Biol.* **45**, (1974) pp. 1-79.

[2] Adler I., *J. Theor. Biol.* **53**, (1975) pp. 435-444

[3] Adler I., *J. Theor. Biol.* **65**, (1977) pp. 29-77

[4] Adler I., Generating Phyllotactic Patterns on a Cylindrical Point Lattice, in *Symmetry in Plants*, World Scientific Publishing (1998) pp. 249-279.

[5] Adler I., Prologue by a Mathematician, in *Symmetry in Plants*, World Scientific Publishing (1998) pp. xiii-xvi.

[6] Ahlfors L.V., *Complex Analysis*, McGraw-Hill (1966)

[7] Bonnet, C., *Recherches sur l'usage des feuilles dans les plantes* Gottingen and Leyden, E. Luzac, fils. (1754)

[8] Bravais, L. & Bravais, A., *Annales des Sciences Naturelles Botanique* **7** (1837) pp. 193-221, pp. 291-348, **8** (1837) pp. 11-42, **12** (1839) pp. 65-77

[9] Coxeter, *J. Algebra* **20** (1972) pp. 167-175

[10] Douady S. & Couder Y., Phyllotaxis as a Self Organizing Iterative Process, Part I, *J. Theor. Biol.* **178**, (1996) pp. 255-274, Part II, *J. Theor. Biol.* **178**, (1996) pp. 275-294, Part III, *J. Theor. Biol.* (1996) **178**, pp. 295-312.

[11] Douady S., The Selection of Phyllotactic Patterns, in *Symmetry in Plants*, World Scientific Publishing (1998) pp. 335-358.

[12] Endress, Peter K. *Diversity and Evolutionary Biology of Tropical Flowers* Cambridge University Press (1994) pg. 95

[13] Farey, J., On a Curious property of vulgar fractions, *Philosophical Magazine J. London* **47** (1816) pp. 385-386

[14] Fibonacci, L., *Liber Abaci* (1202)

[15] Goodwin, Brian, *How the Leopard Changed its Spots* New York, Touchstone of Simon & Schuster (1994)

[16] Green, Havelange, & Bernier, *Planta* **185** (1991) pp. 502-512

[17] Green P.B., *Int. J. Plant Sci.* **153** (1992)(3) pp. 559-575

[18] Green P.B., Steele C.R. & Rennich S.C., Phyllotactic Patterns: a biophysical mechanism for their origin, *Ann. Bot.* (1996).

[19] Hardy H. & Wright E.M, *An Introduction to the Theory of Numbers*, Harvard Univ. Press (1976)

[20] Harrison, Lionel G., Graham, Keith T. & Lakowski, Bernard C., Calcium localization during *Acetabularia* whorl formation: evidence supporting a two-stage hierarchical mechanism, *Development* **104** (1988) pp. 255-262

[21] Hernandez, Havelange, Bernier, & Green, *Planta* **185** (1991) pp. 139-147

[22] Hofmeister W., Allgemeine Morphologie der Gewachse, in *Handbuch der Physiologishcen Botanik*, **1** Engelmann, Leipzig (1868) pp. 405-664.

[23] Jean R.V., *Math. Biosci.* **79** (1986) pp. 127-154

[24] Jean R.V., *J. Theor. Bio.* **129** (1987) pp. 69-90

[25] Jean R.V., Number-theoretic properties of two-dimensional lattices, *J. Number Theory* **29** (1988) pp 206-223.

[26] Jean R.V., *Can. J. Bot.* **67** (1990) pp. 3103-3107

[27] Jean R.V., *Math. Biosci.* **98** (1990) pp. 13-42

[28] Jean R.V., *Phyllotaxis, a Systemic Study in Plant Morphogenesis* (1994)

[29] Lomont, J.S., *Applications of Finite Groups*, Dover, (1987)

[30] Lyndon, Robert F., Phyllotaxis in Flowers and in Flower Reversion, in *Symmetry in Plants*, World Scientific Publishing (1998) pp. 109-124.

[31] Koch A.J., Bernasconi G., & Rothen F., Phyllotaxis as a Geometrical and Dynamical System, in *Symmetry in Plants*, World Scientific Publishing (1998).

[32] Kunz M., *Thèse*, Université de Lausanne, Switzerland (1997).

[33] Kunz M., Some Analytic Results About Two Physical Models of Phyllotaxis, *Communications in Mathematical Physics* **169** (1995) pp. 261-295.

[34] Levitov L.S., *Phys. Rev. lett.* **66** (1991) pp. 224-227.

[35] Levitov L.S., Energetic Approach to Phyllotaxis, *Europhys. Lett.* **14** (1991b), pp. 533-539.

[36] Magnus W., Noneuclidean Tesselations and their Groups, Academic Press (1974)

[37] Marzec, C., & Kappraff, J. Properties of Maximal Spacing on a Circle Relating to Phyllotaxis and to the Golden Mean *J. Theor. Bio.* **103** (1983) pp. 201-226

[38] Richards F.J., *Phil. Trans. R. Soc. Lon.* **235 B** (1951) pp. 509-564

[39] Richards F.J., Phyllotaxis: its quantitative expression and relation to growth in the apex. *Phil. Trans. Roy. Soc.* **237B** (1952) pp. 37-72.

[40] Rothen & Koch, *J. Physique* bf 50 (1989) pp. 633-657

[41] Rothen & Koch, *J. Physique* bf 50 (1989) pp. 1603-1621

[42] Sattler, Rolf, *Organogenesis of Flowers* University of Toronto and Buffalo (1973) pg. 74

[43] Schoute, J.C., *Recueil des Travaux Botaniques Neerlandais* **10** (1913) pp. 153-325

[44] Schoute, J.C., *Recueil des Travaux Botaniques Neerlandais* **19** (1922) pp. 184-218

[45] Schoute, J.C., *Recueil des Travaux Botaniques Neerlandais* **22** (1925) pp. 128-72

[46] Schoute, J.C., *Recueil des Travaux Botaniques Neerlandais* **33** (1936) pp. 670-87

[47] Schwabe W.W. & Clewer A.G., A Simple Computer Model Based on the Theory of a Polarly Translocated Inhibitor, *J. Theor. Bio.* (1984) pp. 595-619.

[48] Schwabe W.W., *Symposium of the Society for Experimental Biology* **25** pp. 301-322

[49] Schwabe W.W., The Role and Importance of Vertical Spacing at the Plant Apex in Dtermining Phyllotactic Pattern, in *Symmetry in Plants*, World Scientific Publishing (1998) pp. 523-535.

[50] Stebbins, Ledyard G., *Flowering Plants: evolution above the species level* Cambridge, Belknap Press of Havard University Press (1974)

[51] Tucker S.C., Phyllotaxis and Vascular Organization of the Carpels of *Michelia Fuscata, Am. J. Bot.* **48** (1961) pp. 60-71.

[52] Turing A.M., The chemical basis of morphogenesis, *Phil. Trans. Roy. Soc.* **237B** (1952) pp. 37-72.

[53] Van Iterson G., *Mathematische und microscopisch-anatamische Studien uber Blattstellungen, nebst Betraschungen uber der Schalenbau der Miliolinen* Gustav-Fischer-Verlag, Jena (1907)